ORNL-TM-4324

EFFECT OF PARTIAL BLOCKAGES IN SIMULATED LMFBR FUEL ASSEMBLIES

M. H. Fontana
T. S. Kress
L. F. Parsly
D. G. Thomas
J. L. Wantland

[redacted]

OAK RIDGE NATIONAL LABORATORY
OPERATED BY UNION CARBIDE CORPORATION • FOR THE U.S. ATOMIC ENERGY COMMISSION

Printed in the United States of America. Available from
the U.S. Atomic Energy Commission, Technical Information Center
P.O. Box 62, Oak Ridge, Tennessee 37830
Price: Printed Copy $5.45 ; Microfiche $1.45

ORNL-TM-4324
UC-79e, UC-79p

Contract No. W-7405-eng-26

REACTOR DIVISION

EFFECT OF PARTIAL BLOCKAGES IN SIMULATED LMFBR FUEL ASSEMBLIES

M. H. Fontana T. S. Kress L. F. Parsly D. G. Thomas J. L. Wantland

DECEMBER 1973

NOTICE

This is a report of research on the effects of idealized blockage configurations on 19-rod simulated LMFBR fuel assemblies; no inferences should be drawn about the credibility of these blockages occurring in a real reactor. The report summarizes some of the work accomplished as part of a continuing program at ORNL and is distributed at this time for comment and to make available existing technical information for which there is a current need.

OAK RIDGE NATIONAL LABORATORY
Oak Ridge, Tennessee 37830
operated by
UNION CARBIDE CORPORATION
for the
U.S. ATOMIC ENERGY COMMISSION

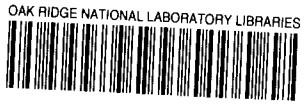

CONTENTS

EFFECT OF PARTIAL BLOCKAGES IN SIMULATED LMFBR FUEL ASSEMBLIES

M. H. Fontana T. S. Kress L. F. Parsly D. G. Thomas J. L. Wantland

ABSTRACT

Experimental data on the effects of partial blockages in simulated LMFBR rod bundles are reviewed and the results presented. Experiments performed in the ORNL Fuel Failure Mockup (FFM) with 13- and 24-channel inlet blockages in 19-rod sodium-cooled electrically heated rod bundles indicate that excessive temperatures do not occur as a result of the blockages. Similar experiments with 6-channel non-heat-generating blockages in the heated zone of the rod bundle indicate local temperature increases of ~100°F at full flow and linear heat ratings of 10 kW/ft. Calculations of temperatures within heat-generating blockages indicate that, with more than one subchannel blocked over an "infinite" length, resulting temperatures are above the cladding limit. Results from experiments with the FFM water mockup showed local heat transfer variations with 6-, 12-, and 24-channel central blockages and with edge blockages extending over one-third of the total area of the rod bundle. For this latter case, reductions in heat transfer coefficient to one-third of the free-stream value were observed. A simple representation of flow recirculation in the wake of a blockage indicates that a small recirculating flow significantly reduces temperatures in the wake zone.

1. INTRODUCTION

Experimental data from the Oak Ridge National Laboratory (ORNL) Liquid-Metal Fast Breeder Reactor (LMFBR) safety and core systems programs were reviewed to evaluate possible effects of hypothetical partial blockages in Fast Flux Test Facility (FFTF) fuel subassemblies. These data were obtained at ORNL as part of the Fuel Failure Mockup (FFM) program. Data from sodium-cooled rod bundles were obtained in the FFM, an engineering-scale sodium-flow loop, and support data using water as the test fluid were obtained in the FFM water mockup, a triple-scale replica of the FFM designed for dynamic similarity.

The sodium loop used 19-rod bundles of electric cartridge heaters assembled to simulate fuel rod bundles having the heat flux and external configuration of the FFTF fuel. Data were obtained with bundle inlet blockages of 13 and 24 channels and with heated-zone internal blockages of 6 channels.

Data from the water mockup included tests with 6, 13, and 24 channels blocked at the bundle inlet; with the central 6, 12, and 24 channels blocked at the bundle midplane; and with blockages of the channels along the two rows of rods nearest two duct flats (constituting a blockage of one-third of the total flow area of the bundle).

Various analytical models were used to support and interpret the data. The ORRIBLE code[1] was used to compute the flow and temperature distributions in the rod bundles downstream of the recirculating wake zones. (ORRIBLE uses a simplified flow formulation and is computationally stable for cases where partial areas of the rod bundle are entirely blocked.) Temperature distributions in the recirculating wake zone immediately behind the blockage were estimated using simple arbitrary representations of the wake flow with varying levels of recirculation velocity and blockage sizes. Temperatures within the blockage itself were calculated using HEATING,[2,3] a three-dimensional heat conduction code. Heat conduction computations were made for heat-generating and non-heat-generating blockages with arbitrary shapes and boundary conditions.

The results are presented in a manner so that the effects of partial blockages can be discerned by comparison with equivalent unblocked cases. Estimates are presented of the behavior of similar blockages in the full-scale FFTF fuel assemblies.

The present review of partial results from a continuing program was made to aid in licensing of the FFTF. It is expected that more definitive conclusions may be drawn after completion of the program objectives.

2. BACKGROUND

2.1 Types of Blockages

Partial blockage of rod bundles may be caused by foreign materials lodging at the inlet to the bundle. Blockages could be caused by single pieces of debris or by buildup of particulate matter. A plate about the size of a dime would be required to produce a blockage of about 13 channels. However, since the Fermi accident, all LMFBRs have had fuel assembly inlet flow paths designed to prevent complete blockage of a subassembly, and presently envisioned inlet configurations would not allow entry of foreign material of this size. The sizes of these entrance flow passages are not likely to be increased in the future because the pressure losses in that region are already small compared with the pressure losses in the fuel rod region.[4]

The smallest flow paths in the system are the fuel subchannels, and buildup of foreign matter in the entrance region of the fuel bundle could conceivably cause excessive blockage. The consequences of such a blockage would depend on whether it is concentrated locally or distributed over the entire frontal surface of the rod bundle. If several contiguous channels were blocked, the temperature of the fuel in the heated zone might be excessive. (Experimental data given later in this report indicate that inlet blockages of less than 10 to 24 subchannels are not likely to cause excessive temperatures in the FFTF fuel.) However, properly designed fuel assembly inlets should cause evenly distributed flow; if the debris follows the flow paths, distributed blockages would result. Under these circumstances, flow would probably be reduced gradually, and low flows might be detected prior to excessive pin damage due to high temperatures.

Estimates made of the reduction of flow as a consequence of partial subassembly blockages[5] show that it is necessary to block about 50% of the total flow area of a subassembly to cause a 5% reduction in flow. This is substantiated by the fact that the increased pressure drop due to partial blockages is small compared with the pressure drop due to the rod bundle itself. Therefore, it is not likely that solid blockages covering a small fraction of flow area could be detected by flow measurements alone. However, distributed debris might be detected prior to fuel failure, because a uniform reduction in flow would cause a detectable general increase in fuel assembly temperature rather than just a hot spot.

Blockage within the heated zone of the rod bundle could conceivably be caused by

1. lodging of debris within fuel channels;
2. broken wire-wrap spacers;
3. swelling of fuel pins due to defects, weak spots, overenriched pellets, or poor heat transfer (caused perhaps by gas release, debris hangup, or distorted pins and adjacent swelling);
4. fuel debris from failed pins; or
5. widespread pin swelling due to power-flow mismatch during a loss-of-flow incident.

All the above items except item 5 are classed as potential accident initiators and are being investigated, particularly with respect to their potential for failure propagation.

2.2 Flow in the Wake Zone behind Blockages

Considerable information is available on flow separation caused by obstructions such as cylinders,[6] disks,[7] steps in a surface of a plate,[8-10] and walls perpendicular to the flow path,[11] in boundary layers[12]

over wedge shapes,[13] and past bluff bodies.[14] An extensive review of flow separation is given by Chang.[15] Some attempts have been made to apply some of this information to the analysis of flow in rod bundles,[16,17] and limited experimental work has been done with water.[18,19]

If a blockage due to an obstruction is such that flow separation does occur, heat transfer in parts of the wake zone may be enhanced. This has been observed in water experiments in rod bundles for four-channel[18] and for six-channel[19] planar blockages. However, if the blockage is large, flow recirculation may only partially mitigate the effect of the flow obstruction. Enhancement of heat transfer would not be expected for longer, relatively streamlined bodies that do not promote flow separation.

Kirsch and Schleisiek[20] made the rather startling prediction that flow recirculation in the separated flow zone behind a blockage would safely remove the heat generated behind a blockage extending to more than 40% of the total full-scale Na-2 reactor bundle flow area. They investigated this effect with sodium flowing in an obstructed annulus having one wall shaped to loosely simulate fuel rods. They also conducted experiments in rod bundles with water, using salt injected into the wake zone. They found that the length of the recirculation zone was relatively independent of velocity, as was the mass interchange between the fluid in the recirculation zone and the "free stream" fluid. Calculations were made for the Na-2 reactor for a blocked area/total flow area ratio of 0.147 at the midplane. A maximum sodium temperature of 190°C (374°F) higher than the coolant temperature immediately ahead of the blockage was predicted, and for a blocked/total flow area ratio of 0.411 (a blockage diameter of ~3 in.), the predicted temperature rise was 292°C (557°F).

Gast[21] predicted that void growth and collapse would serve to remove the heat from the region behind a blockage of 55% of the bundle flow area (4.1 cm radius). He stated, "The analytical results lead to preliminary conclusions that, even at superheat as high as 150°C (270°F) individual vapor bubbles recondense within 35 msec, that the fuel cladding within the bubble is not overheated during this time, and that local boiling is unlikely to cause thermal-hydraulic instability in the affected fuel subassembly. Furthermore, it is shown that in case of considerable superheat, the rapid volume change of individual vapor bubbles causes variations of the coolant flow rate at the subassembly outlet, which may be detected by means of an electromagnetic flowmeter." The calculations were performed on the assumption that the fuel rods had no effect on the hydrodynamics. This analysis must be checked experimentally and, if substantiated, should essentially solve the problem of subassembly blockage (particularly if constituted of non-heat-generating material) with respect to gross heat removal from the blocked zone.

Steifel[22] performed experiments in two parallel channels, one of which was blocked. He found that pressure equalized rapidly downstream of the blockage, but differences in flow persisted. This observation might be of value in the development of detection techniques because the coolant in the channels having lower flow should leave the bundle at higher temperatures.

In practice, it is unlikely that a large blockage will occur that is completely impervious. A slight leakage through a blocked zone might significantly diminish temperature in the blocked region.[23] However, Basmer, Kirsch, and Schultheiss[24] show that slight leakage can destroy the recirculating flow patterns in the wake zone and could actually hinder heat transfer in this region. The relative importance of these effects is not known at this time but will be investigated in the ORNL LMFBR-FFM program.

2.3 Philosophy of Investigations of Flow Blockages

Two approaches could be taken in investigating the problem of heated-zone blockage: (1) the limits of credibility of the size of blockages can be postulated and their damage potential investigated or (2) the consequences of various-sized blockages along with their detectability could be investigated parametrically.

The first approach requires proving a negative postulate, that is, that something cannot happen, and further requires almost continuous investigations as to the credibility of postulated events. The second approach has the advantage of eliminating the question of credibility. If it can be shown that a blockage (of whatever origin) can be detected before significant damage results, it is only necessary to determine the limit of damage that can be accepted before shutdown and repair are required. In the long term, there is a tendency to lean toward the second approach. However, the need for starting with the first approach is recognized because with the second approach, detection methods must be proved for the full-scale reactor. Since the FFTF instrument packages are already designed, sufficiently early detection might not be possible; therefore, with respect to the FFTF the acceptability of a nominally credible blockage was investigated.

Different types of blockages may require different methods of experimental investigation. For example, blockages caused by nonfuel debris may vary in their effect on local and downstream temperature distributions because of variations in their thermal conductance, porosity, and flow leakage through the blockage. Blockages caused by fuel would generate heat. Blockages caused by rod swelling or distortion are not likely to completely block flow channels but are likely to be of streamlined shape and therefore may not promote turbulence or enhance heat transfer.

2.4 Current Investigations at ORNL

The FFM program currently under way at ORNL is investigating these phenomena both experimentally and analytically. Blockages of various sizes have been installed at the inlet of sodium-cooled rod bundles in which the fuel rods are simulated by electric cartridge heaters having heat fluxes and external configurations identical to the FFTF fuel. Temperature profiles downstream of the blockages have been measured by means of thermocouples distributed throughout the bundle. Concurrently, signals generated by pressure sensors, flowmeters, and certain thermocouples have been monitored for comparison with tests of the unblocked bundle and to permit correlation of noise signals from these sources. Supporting tests have been carried out in water systems to supplement the sodium test results and to provide information for extrapolation to large sodium-cooled fuel subassemblies.

This report presents experimental data obtained during only the early stages of a coherent program[25] designed to investigate the blockage question thoroughly and to develop solutions as necessary. Therefore the report is an interim evaluation of the present status of knowledge on blockage effects and is issued at this time to aid in FFTF licensing. As additional information becomes available over the next two years, the blockage question should be better understood.

3. FLOW BLOCKAGE EXPERIMENTS IN THE FUEL FAILURE MOCKUP (FFM)

3.1 Description of the Facility

The FFM is a large-scale sodium facility at ORNL. A flow diagram is shown in Fig. 1. The centrifugal pump has a flow capacity of 600 gpm, which is adequate for testing full-scale 217-rod subassemblies. However, at the present time the power controllers and the heat dump limit the power to 422 kW, which allows 24.5 kW per rod in a 19-rod bundle. Experiments are conducted with rod bundles in which fuel rods are simulated by electrical heaters having the same linear power density (up to 17.5 kW/ft) and external configuration as the FFTF fuel rods. The rods are 0.230 in. in diameter and are spaced by 0.056-in.-diam wires wrapped on a 12-in. pitch. Figure 2 shows a typical heater rod.

The facility has provisions for subdivided control of the individual groups of heaters, so that many combinations of heaters can be operated at any power level up to 24.5 kW/ft each.

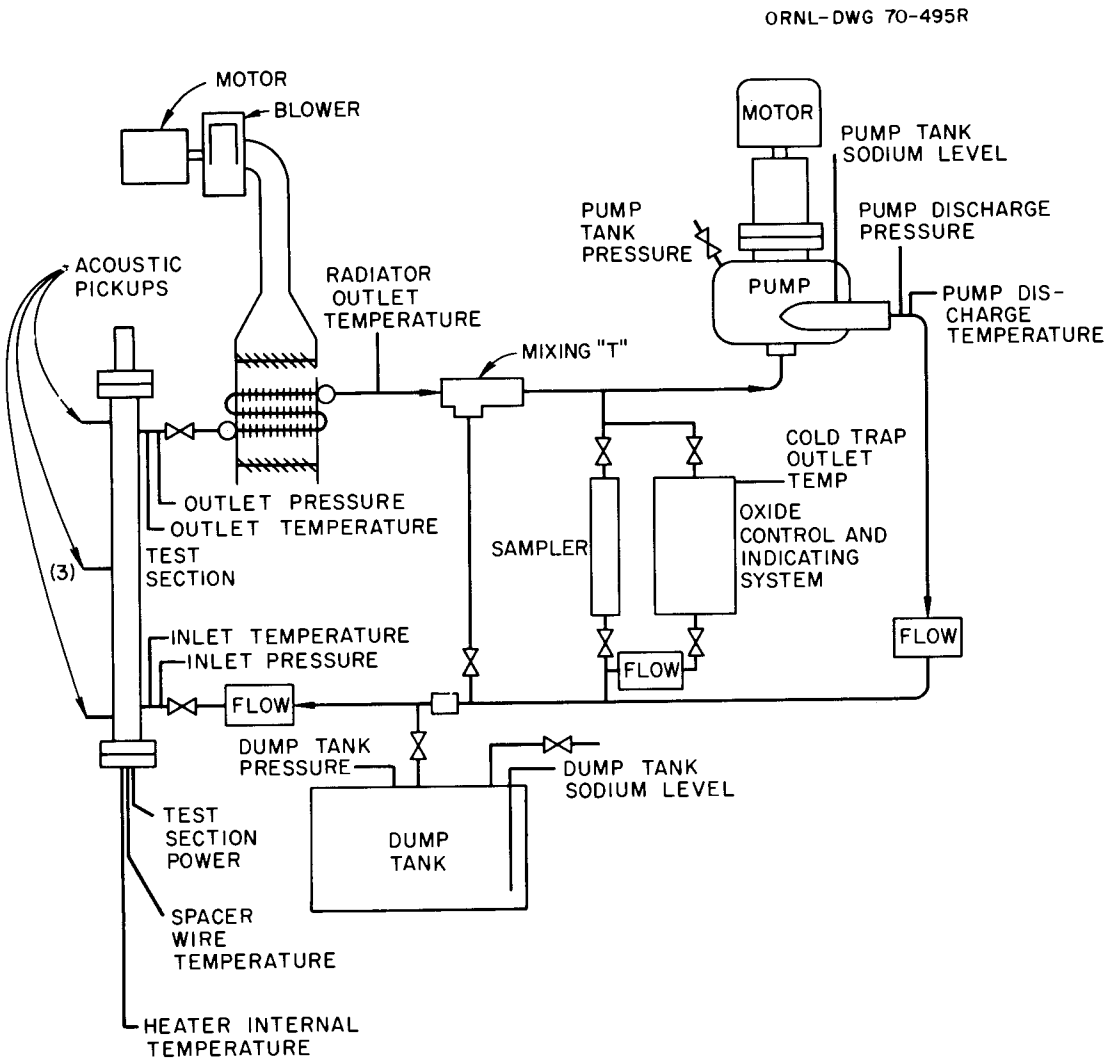

Fig. 1. Flow diagram of the Fuel Failure Mockup (FFM).

Temperatures throughout the rod bundle are measured (without causing flow perturbations) by thermocouples placed within the heater sheath and within the wire-wrap spacers. Detailed descriptions of the instrumentation are given in later sections of this report.

Detailed descriptions of the facility are given in refs. 25 and 26.

3.2 Effect of 13- and 24-Channel Inlet Blockage in FFM Bundle 2B

3.2.1 Description of rod bundle 2. FFM bundle 2 is a 19-rod bundle in a hexagonal duct. The dimensions and configuration of the bundle are similar to those of the FFTF fuel subassembly except that the heated length is 21 in. rather than 36 in. There is a 3-in. unheated length between the heated section and the free end of the bundle.

Bundle 2 was designed for operation in an unblocked condition with most of the instrumentation 18 in. above the inlet to the heated zone simulating the midplane of the FFTF core. The free end of the bundle

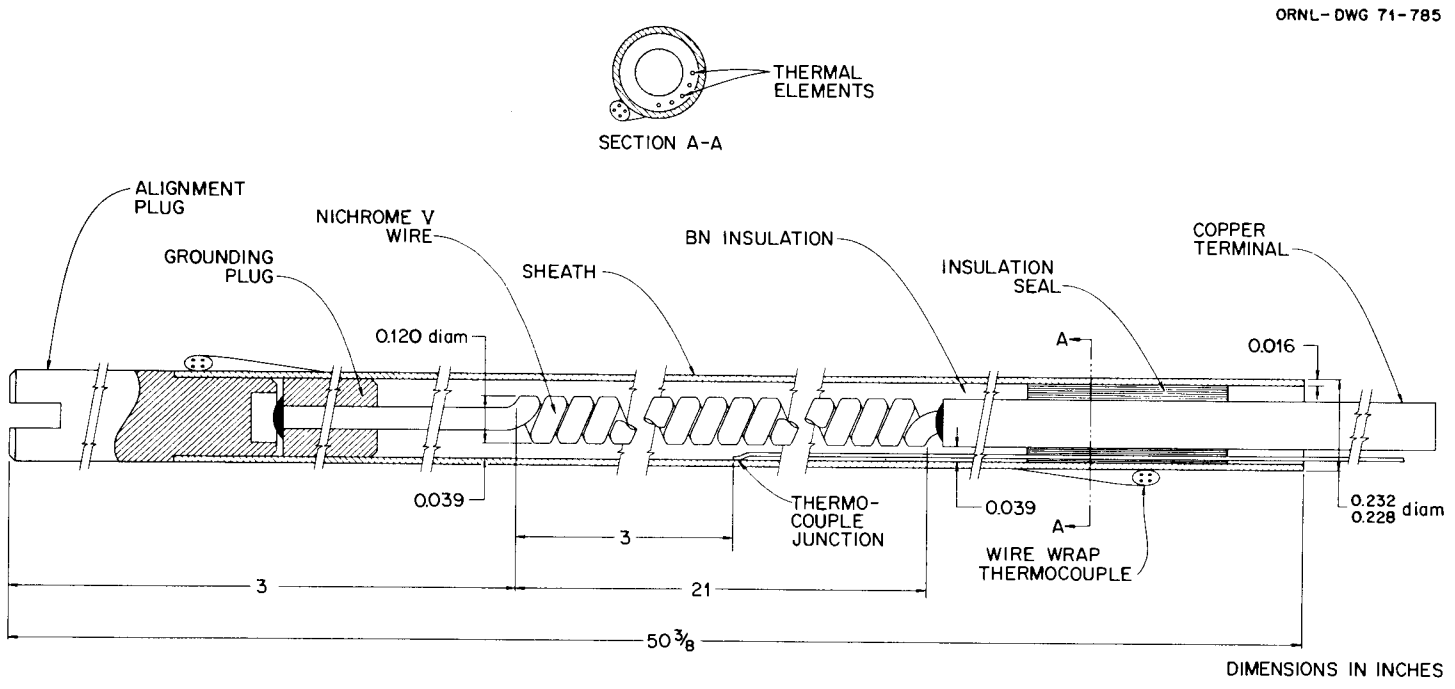

Fig. 2. Heater for LMFBR fuel simulation.

was the downstream end, thus allowing the use of a thermocouple rake for measuring the exit sodium temperature profile. Results of these experiments are presented in refs. 27 and 28.

After the prescribed test program was successfully completed, the still operable bundle was inverted in the test section for testing with inlet blockages. This orientation resulted in a 3-in. unheated entrance length followed by a 21-in. heated length. The heavily instrumented plane (previously at the 18-in. heated level) was now 3 in. above the inlet to the heated zone. Thus most of the instrumentation was well into the heated section but reasonably close (6 in. or less) to the inlet blockage. The orientation of the bundle in the test section for the inlet blockage tests is shown in Fig. 3. The bundle in its original orientation is designated FFM bundle 2A, and in the inverted orientation for inlet blockage tests, it is designated FFM bundle 2B.

The four types of temperature instrumentation in this bundle are described below:

1. Thirteen wire-wrap spacers each contain two ungrounded Chromel-Alumel thermocouples spaced 2 or 12 in. apart axially.
2. Six wire-wrap spacers each contain two grounded Chromel-Alumel thermocouples diametrically opposed in the wrap; in bundle 2B three pairs are at the 2-in. level (19 in. in 2A), and three pairs are at the 3-in. level (18 in. in 2A).
3. Alternate Chromel and Alumel bare wires (10 mils in diameter) are installed in the heater in the 0.039-in. clearance between the heating element and the sheath. These wires are separately joined to the sheath to form an intrinsic thermocouple junction on the inner surface of the heater sheath.
4. Chromel-Alumel thermocouples are installed at intervals along the bundle length to measure the inner wall temperatures of the hexagonal duct.

The locations of the heater internal thermocouples, the grounded wire-wrap thermocouples, and the 3-in.-level duct-wall thermocouples for FFM bundle 2B are shown in Fig. 4, along with the rod and channel numbering convention.

Testing was conducted with (1) no inlet blockage, (2) 13 channels blocked (channels 1 to 6 and 13 to 19; see Fig. 4), and (3) 24 channels blocked (channels 1 to 24 – all but the peripheral channels). The 13- and the 24-channel inlet blockage plates are shown in Figs. 5 and 6 respectively. When the 24-channel inlet blockage plate was installed, a duct-wall extension piece was added to give a more realistic inlet flow distribution; this is shown in Fig. 6. With the 24-channel inlet blockage plate installed, approximately half of the net flow cross-sectional area was covered.

3.2.2 Summary of inlet blockage results. During this series of tests the flow was varied from 10 to 55 gpm with all 19 rods heated at a uniform heat rate of 2 to 8 kW/ft per rod. Over this flow range the total bundle pressure drop did not increase significantly above the unblocked value with the addition of either inlet blockage plate.

The thermal results of these tests are summarized in Tables 1–4 and Figs. 7 and 8. For comparison, the use of the dimensionless temperature rise $(T - T_{in})/(T_{out} - T_{in})$ is convenient, where T is the temperature measured by the thermocouple under consideration, T_{in} is the sodium inlet temperature (~600°F), and T_{out} is the bulk sodium outlet temperature. Results from the duct-wall thermocouples are not considered in this discussion, since they yielded little information with respect to blockages except that, as flow is diverted to the outer channels by centrally located blockages, relative wall temperatures are slightly depressed.

In these presentations all axial measurements are given in inches downstream from the start of the heated section, which is 3 in. downstream from the inlet blockage.

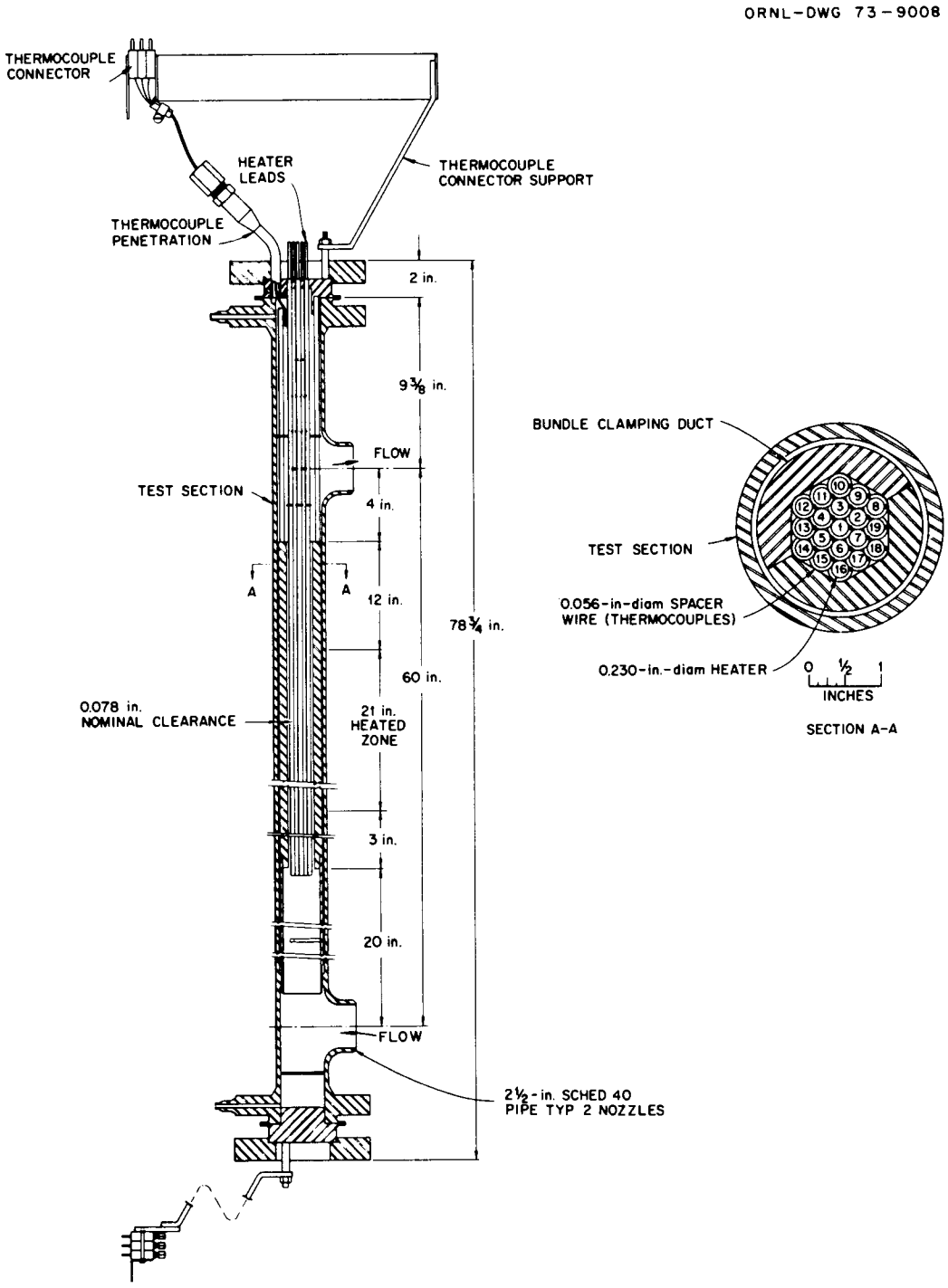

Fig. 3. Test section orientation for FFM bundle 2B.

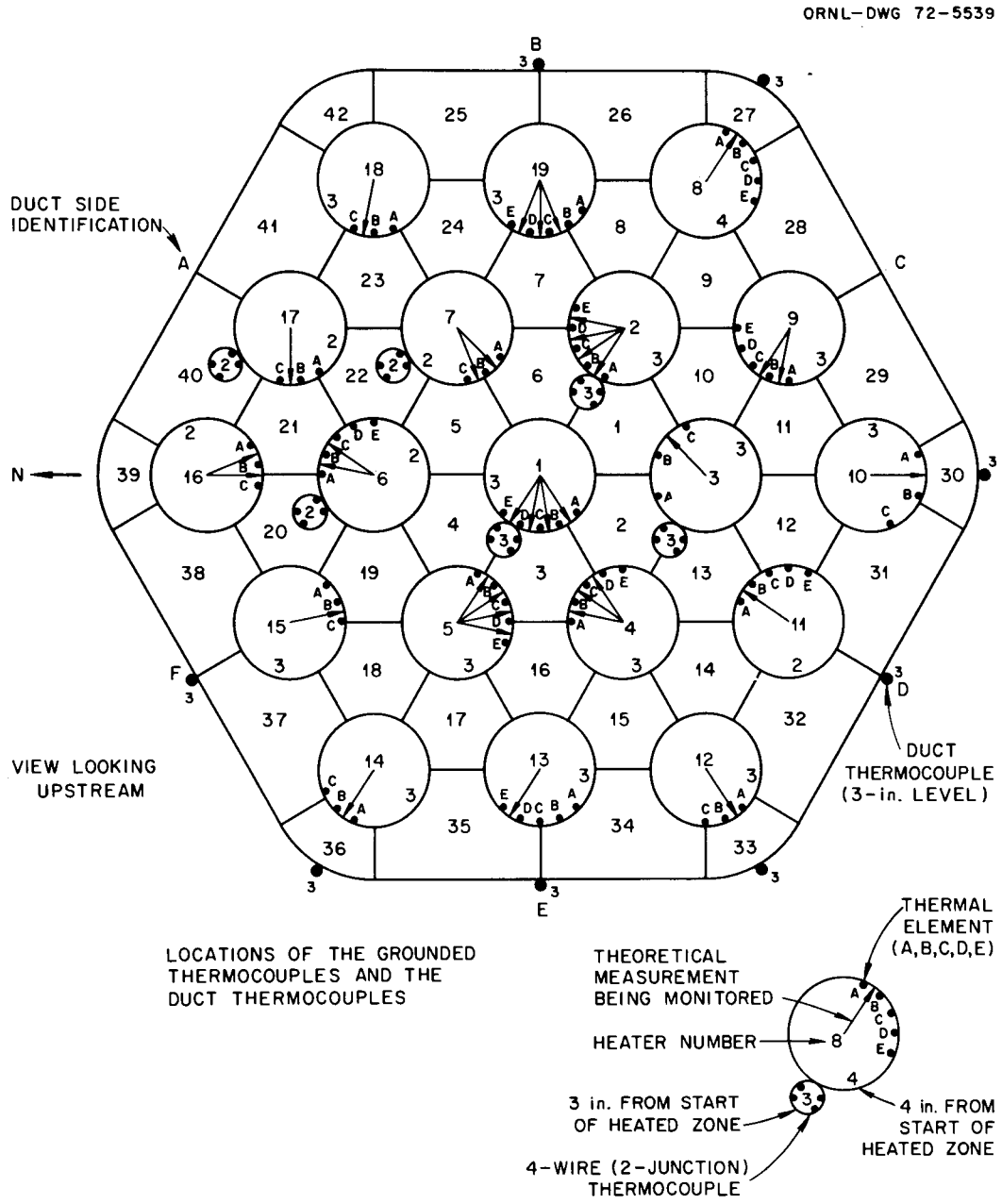

Fig. 4. Locations of heater thermocouples, grounded wire-wrap thermocouples, and 3-in. duct-wall thermocouples in FFM bundle 2B.

Table 1 gives typical temperature rises measured by the wire-wrap and heater internal thermocouples for the 24-channel inlet blockages with a flow of 55 gpm and all 19 rods heated at 5 kW/ft per rod.

Table 2 gives the dimensionless temperature rises at the 3-in. level for no blockage, 13-channel inlet blockage, and 24-channel inlet blockage for various flows and power levels. The effect of flow variation can be seen from this table. For either inlet blockage condition the dimensionless temperatures vary

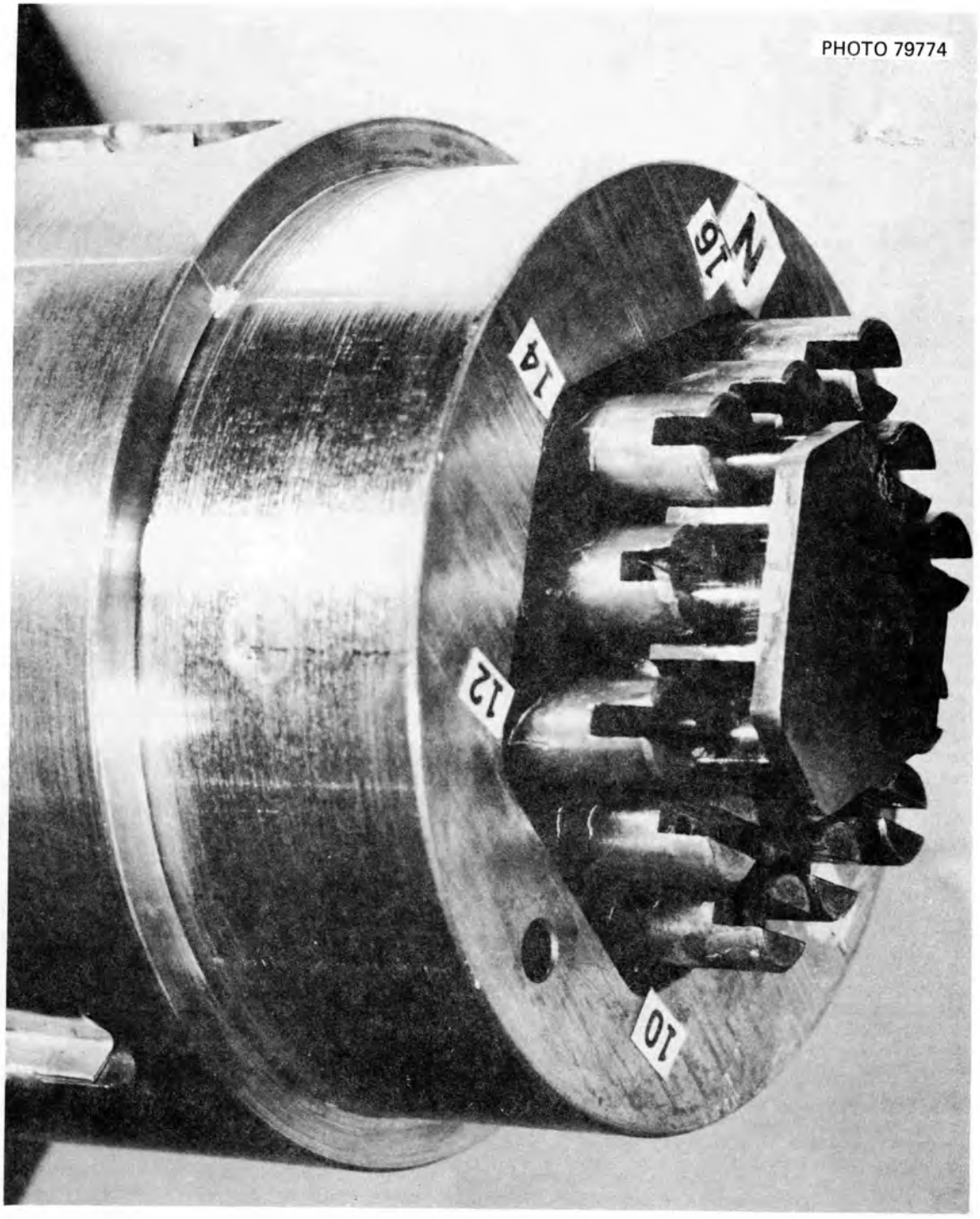

Fig. 5. Inlet end of FFM bundle 2B with the 13-channel inlet blockage plate.

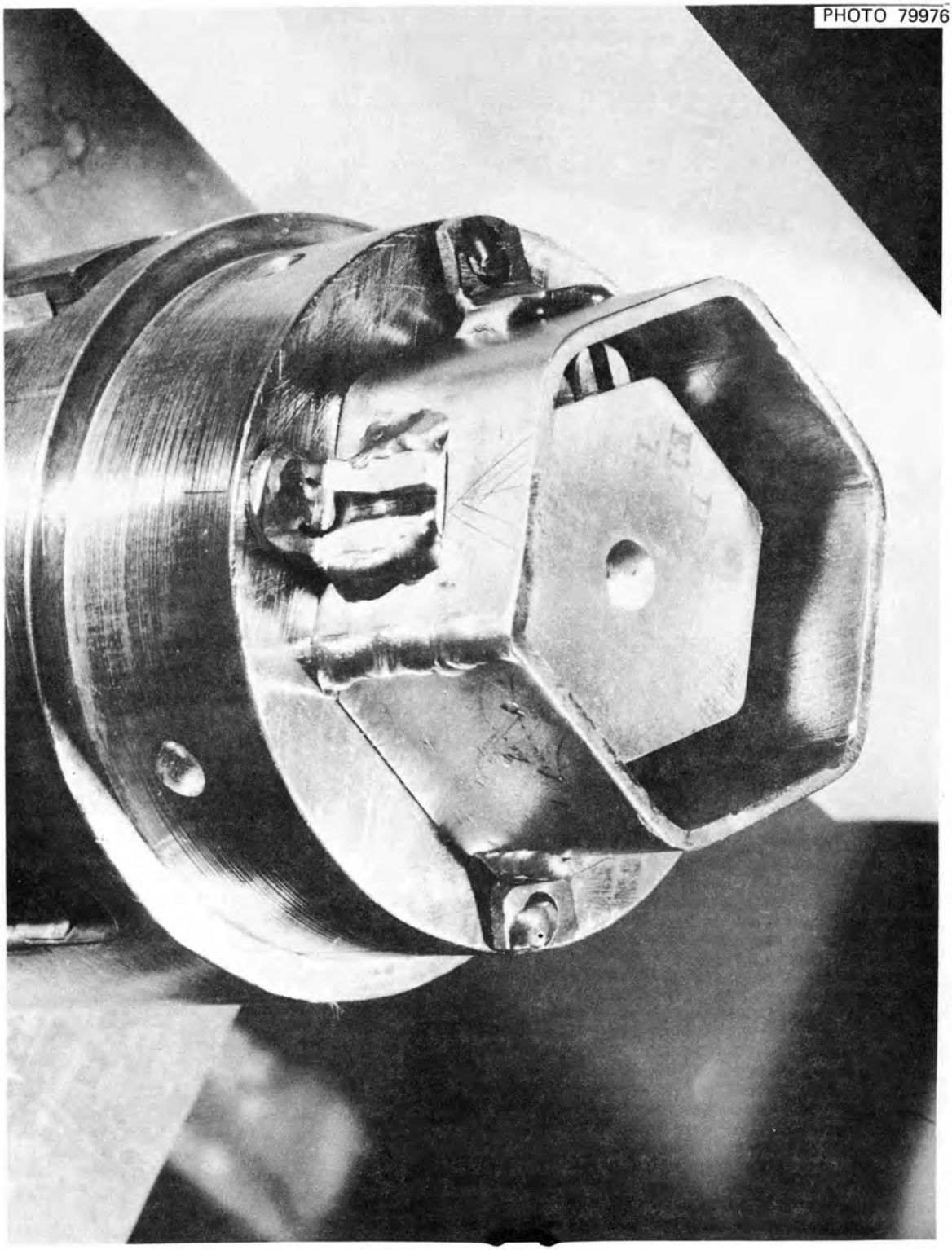

Fig. 6. Inlet end of FFM bundle 2B with the 24-channel inlet blockage plate and the inlet shroud.

Table 1. Temperature rise measurements [$T - T_{in}$ (°F)] of the wire-wrap and heater internal thermocouples for a 24-channel inlet blockage in FFM bundle 2B

Run 741; $T_{out} - T_{in}$ = 76°F; 55 gpm flow; 5 kW/ft per rod, all 19 rods heated; $T_{in} \approx 600$°F

Ungrounded wire-wrap thermocouples				Grounded wire-wrap thermocouples				Heater internal thermocouples			
Rod No.	Axial plane (in.)	Channel No.	$T - T_{in}$ (°F)	Rod No.	Axial plane (in.)	Channel No.	$T - T_{in}$ (°F)	Rod No	Axial plane (in.)	Location[a]	$T - T_{in}$ (°F)
4	0	3	7	1	3	4	35	1	3	AB	89
5	0	19	6	2	3	1	44	1	3	BC	95
10	0	11	7	2	3	6	33	1	3	CD	105
12	0	15	7	3	3	2	40	2	3	CD	90
16	0	39	3	3	3	13	27	2	3	DE	85
15	1	38	9	6	2	(Rod 6)	17	3	3	AB	85
8	2	8	17	6	2	20	9	4	3	AB	84
14	2	36	13	7	2	(Rod 7)	17	4	3	BC	85
9	3	10	29	7	2	22	13	4	3	CD	89
13	3	35	25	17	2	(Rod 17)	15	4	3	AB	122
14	4	35	17	17	2	40	10	5	3	DE	89
18	4	23	29					7	2	AB	72
11	5	32	20					9	3	BC	93
13	5	34	18					10	3	AB	130
18	6	13	37					11	3	AB	83
19	7	8	47					6	2	AB	72
4	12	3	68					16	2	BC	74
5	12	19	58								
10	12	11	73								
12	12	15	37								
16	12	39	34								
15	13	38	36								
8	14	8	97								
9	15	11	92								
11	17	32	56								

[a]See Fig. 4 for identification.

Table 2. Comparison of dimensionless temperature rises [$(T - T_{in})/(T_{out} - T_{in})$] in FFM bundle 2B with all 19 rods heated

Temperature T measured 3 in. from the start of the heated section (6 in. from the inlet blockage)

Run No.	Flow (gpm)	Power (kW/ft)	$T_{out} - T_{in}$ (°F)	Number of blocked channels	$(T - T_{in})/(T_{out} - T_{in})$					
					1 (2)[a]	2 (6)	4 (1)	6 (2)	10 (9)	34 (13)
700	55	4	61	0	0.43	0.34	0.27	0.36	0.34	0.30
701	55	5	76	0	0.43	0.34	0.28	0.37	0.35	0.31
702	55	6	91	0	0.43	0.34	0.28	0.37	0.35	0.31
717	55	2	30	13	0.36	0.32	0.35	0.20	0.34	0.36
718	55	4	61	13	0.38	0.33	0.36	0.22	0.35	0.35
719	55	5	76	13	0.38	0.33	0.35	0.22	0.35	0.36
720	55	5	76	13	0.38	0.33	0.35	0.22	0.35	0.36
731	55	5	76	13	0.38	0.33	0.35	0.22	0.35	0.36
721	55	6	91	13	0.39	0.34	0.35	0.23	0.35	0.35
738	55	2	30	24	0.57	0.46	0.43	0.45	0.40	0.32
739	55	4	61	24	0.56	0.50	0.46	0.43	0.39	0.34
740	55	5	76	24	0.56	0.51	0.44	0.42	0.37	0.32
741	55	5	76	24	0.56	0.51	0.45	0.42	0.37	0.32
742	55	5.5	84	24	0.57	0.51	0.45	0.42	0.37	0.33
747	55	8	122	24	0.56	0.51	0.44	0.42	0.37	0.32
732	44	5	95	13	0.35	0.32	0.34	0.22	0.33	0.34
751	44	5	95	24	0.51	0.47	0.42	0.38	0.33	0.31
733	33	5	127	13	0.31	0.30	0.30	0.20	0.29	0.30
754	33	5	127	24	0.45	0.44	0.39	0.34	0.29	0.28
734	22	5	190	13	0.27	0.28	0.28	0.19	0.25	0.27
753	22	5	190	24	0.37	0.38	0.34	0.30	0.25	0.26
736	14	5	299	13	0.24	0.26	0.25	0.18	0.23	0.26
735	11	5	380	13	0.23	0.25	0.24	0.18	0.18	0.25
752	11	5	380	24	0.31	0.34	0.30	0.27	0.20	0.24

[a]The first number is the channel number, and the number in parentheses is the rod number.

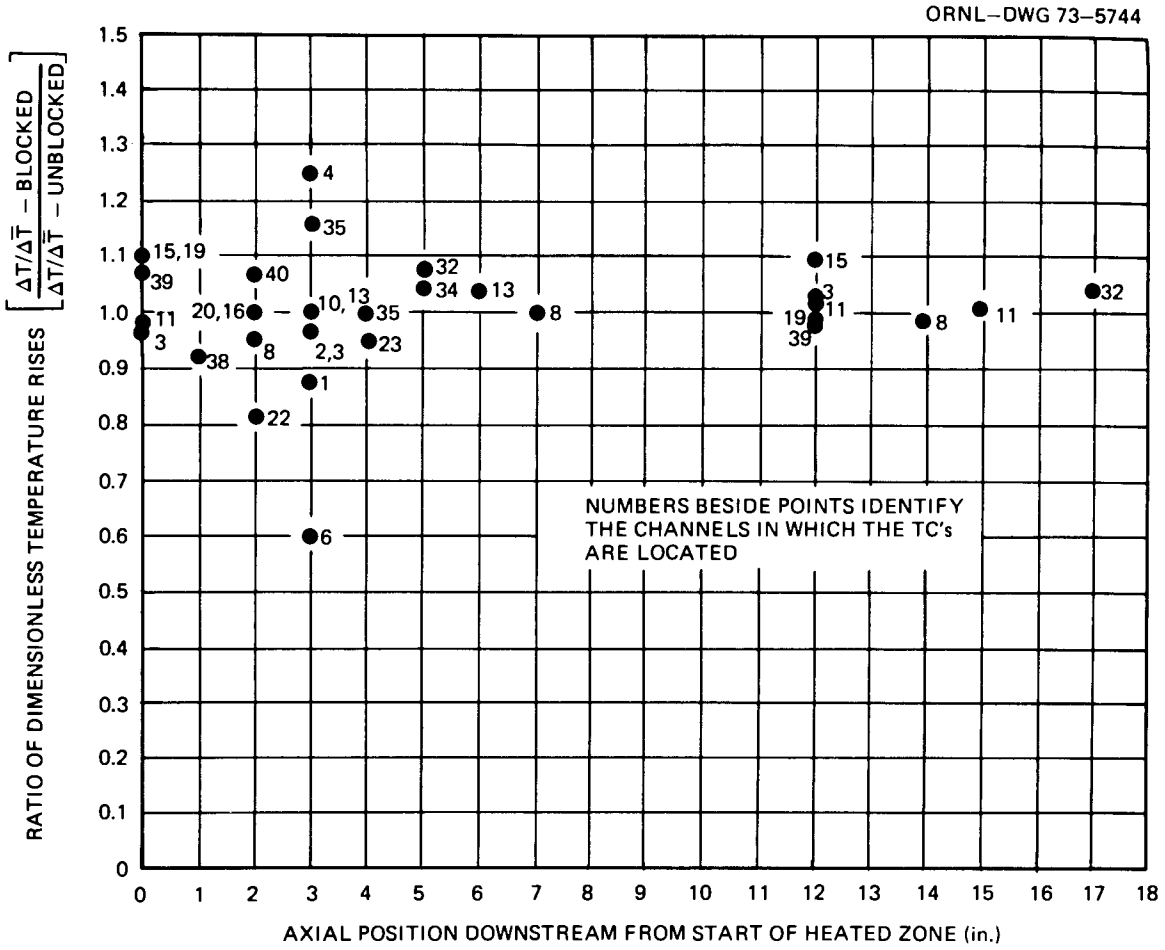

Fig. 7. Ratio of dimensionless temperature rises above inlet vs axial position for FFM bundle 2B with blockage of 13 channels (1–6 and 13–19) at the inlet. 55 gpm flow, ~600°F inlet temperature. Averages of blockage runs 717–721 and 731 compared with averages of unblocked runs 700–702.

monotonically with the flow for a given power level. Since the trends of these blockage results are similar to previously observed trends in unblocked bundles, this phenomenon is not thought to be blockage related but due to the change in thickness of the thermal boundary layer. There have been indications that the thermocouples inside wire-wrap spacers in sodium-cooled bundles are in steep temperature gradients within the thermal boundary layer and do not indicate the bulk-mean channel temperature at that location. The indicated temperature may then be significantly higher than the bulk mean at that location. As the flow is decreased, the transverse spread of the boundary layer should be greater at the fixed thermocouple position and the indicated temperature should be closer to that of the bulk mean.

The dimensionless temperature rises from the wire-wrap thermocouples and from the heater internal thermocouples are given in Tables 3 and 4, respectively, for no blockage, 13-channel inlet blockage, and 24-channel inlet blockage for all 19 rods heated at 4, 5, and 6 kW/ft per rod and a constant flow of 55 gpm. In this range, the effect of power level on the dimensionless temperature rise is small.

The ratios of $[(T - T_{in})/(T_{out} - T_{in})]$ (blocked) to $[(T - T_{in})/(T_{out} - T_{in})]$ (unblocked) for a flow of 55 gpm with all 19 rods heated at 5 kW/ft per rod are given in Fig. 7 for the 13-channel inlet blockage and in Fig. 8 for the 24-channel inlet blockage. It may be seen from these figures that, in general, this ratio

Table 3. Comparison of dimensionless temperature rises $[(T - T_{in})/(T_{out} - T_{in})]$ measured by the wire-wrap thermocouples in FFM bundle 2B with all 19 rods heated, 55 gpm flow, and $T_{in} \approx 600°F$

Rod No.	Axial plane (in.)	Channel No.	4 kW/ft ($T_{out} - T_{in} = 61°F$)			5 kW/ft ($T_{out} - T_{in} = 76°F$)			6 kW/ft ($T_{out} - T_{in} = 91°F$)		
			No blockage	13-channel blockage	24-channel blockage	No blockage	13-channel blockage	24-channel blockage	No blockage	13-channel blockage	24-channel blockage
Ungrounded thermocouples											
15	1	38	0.12	0.11	0.10	0.12	0.11	0.11	0.12	0.12	0.10
8	2	8	0.20	0.20	0.21	0.21	0.20	0.22	0.21	0.20	0.22
14	2	36–37	0.19	0.19	0.19	0.19	0.19	0.17	0.19	0.18	0.18
9	3	10	0.34	0.35	0.39	0.35	0.35	0.37	0.35	0.35	0.37
13	3	35	0.30	0.35	0.34	0.31	0.36	0.33	0.31	0.35	0.32
14	4	35	0.27	0.28	0.24	0.28	0.28	0.22	0.28	0.27	0.23
18	4	23	0.40	0.38	0.37	0.40	0.38	0.38	0.40	0.38	0.38
11	5	32	0.26	0.29	0.27	0.26	0.29	0.26	0.26	0.28	0.26
13	5	34	0.24	0.25	0.24	0.24	0.26	0.24	0.25	0.25	0.24
18	6	13	0.46	0.48	0.49	0.46	0.49	0.48	0.46	0.48	0.50
19	7	8–26	0.65	0.64	0.59	0.65	0.66	0.61	0.66	0.66	0.61
4	12	3	0.79	0.78	0.90	0.74	0.78	0.88	0.74	0.77	0.88
5	12	19	0.80	0.79	0.74	0.80	0.79	0.75	0.80	0.78	0.77
10	12	11	0.83	0.85	0.95	0.84	0.86	0.95	0.84	0.86	0.94
12	12	15	0.48	0.53	0.49	0.48	0.53	0.48	0.48	0.52	0.45
16	12	39	0.53	0.53	0.45	0.53	0.52	0.44	0.53	0.52	0.45
15	13	38	0.60	0.56	0.46	0.60	0.56	0.47	0.60	0.56	0.48
8	14	8	1.06	1.04	1.25	1.08	1.07	1.26	1.08	1.09	1.25
9	15	11	1.07	1.10	1.18	1.09	1.11	1.19	1.10	1.10	1.17
11	17	32	0.77	0.77	0.75	0.75	0.80	0.73	0.75	0.78	0.72
Grounded thermocouples											
1	3	4	0.27	0.36	0.46	0.28	0.35	0.45	0.28	0.35	0.45
2	3	1	0.43	0.38	0.56	0.43	0.38	0.57	0.43	0.39	0.57
2	3	6	0.36	0.22	0.43	0.37	0.22	0.42	0.37	0.23	0.42
3	3	2	0.34	0.32	0.50	0.35	0.33	0.51	0.34	0.34	0.51
3	3	13	0.26	0.25	0.34	0.28	0.26	0.34	0.25	0.26	0.33
6	2	(Rod 6)	0.22	0.23	0.24	0.23	0.23	0.22	0.22	0.23	0.23
6	2	20	0.10	0.11	0.11	0.10	0.11	0.11	0.10	0.10	0.11
7	2	(Rod 7)	0.12	0.10	0.20	0.14	0.10	0.22	0.16	0.13	0.20
7	2	22	0.08	0.07	0.14	0.09	0.08	0.17	0.10	0.09	0.16
17	2	(Rod 17)	0.23	0.23	0.19	0.24	0.23	0.20	0.25	0.23	0.20
17	2	40	0.16	0.15	0.11	0.17	0.15	0.13	0.17	0.15	0.14

Table 4. Comparison of dimensionless temperature rises $[(T - T_{in})/(T_{out} - T_{in})]$ measured by the heater internal thermocouples in FFM bundle 2B with all 19 rods heated, 55 gpm flow, and $T_{in} \approx 600°F$

Rod No.	Axial plane (in.)	Location[a]	4 kW/ft ($T_{out} - T_{in} = 61°F$)			5 kW/ft ($T_{out} - T_{in} = 76°F$)			6 kW/ft ($T_{out} - T_{in} = 91°F$)		
			No blockage	13-channel blockage	24-channel blockage	No blockage	13-channel blockage	24-channel blockage	No blockage	13-channel blockage	24-channel blockage
1	3	AB	1.03	1.01	1.14	1.05	1.01	1.16	1.04	1.03	
1	3	BC	1.13	1.14	1.23	1.14	1.13	1.23	1.13	1.15	1.19
1	3	CD	1.26	1.27	1.37	1.28	1.27	1.37	1.27	1.28	1.31
1	3	DE	1.13	1.14		1.15	1.14		1.15	1.15	
2	3	BC	1.08	1.06		1.09	1.06		1.07	1.09	
2	3	CD	1.07	1.05	1.17	1.07	1.05	1.17	1.06	1.06	1.14
2	3	DE	1.03	0.99	1.10	1.03	1.00	1.10	1.02	1.01	1.08
4	3	AB	1.05	0.99	1.08	1.02	0.99	1.08	1.01	1.00	1.09
4	3	BC	1.05	0.99	1.09	1.02	0.99	1.10	1.02	1.01	1.10
4	3	CD	1.07	1.01	1.14	1.04	1.02	1.15	1.04	1.03	1.15
5	3	AB	1.47	1.50	1.59	1.42	1.50	1.58	1.42	1.50	1.57
5	3	BC	1.14	1.18	*b*	1.11	1.19	*b*	1.11	1.20	*b*
5	3	CD	1.02	1.06	*b*	1.01	1.08	*b*	1.02	1.10	*b*
5	3	DE	1.06	1.03[c]	*b*	1.07	1.11	1.15	1.11	1.15	1.16
6	2	AB	1.12	1.14		1.13	1.13		1.11	1.14	
7	2	AB	0.83	0.86	0.95	0.83	0.83	0.93	0.82	0.82	0.92
9	3	BC	1.15	1.12	1.22	1.15	1.11	1.21	1.15	1.12	1.18
10	3	AB	1.65	1.55[c]	1.55[c]	1.68	1.68	1.68	1.68	1.70	1.67
11	3	AB	*b*	1.00	1.06	1.02	1.00	1.07	1.01	1.00	1.06
6	2	AB	1.07[c]	0.97	0.88[c]	0.96	0.95	0.94	0.97	0.96	0.95
18	3	BC	1.46	1.38		1.46	1.41		1.45	1.41	

[a]See Fig. 4 for identification.
[b]Deleted, standard deviation $\geq \sim 10$.
[c]Suspected of being in error.

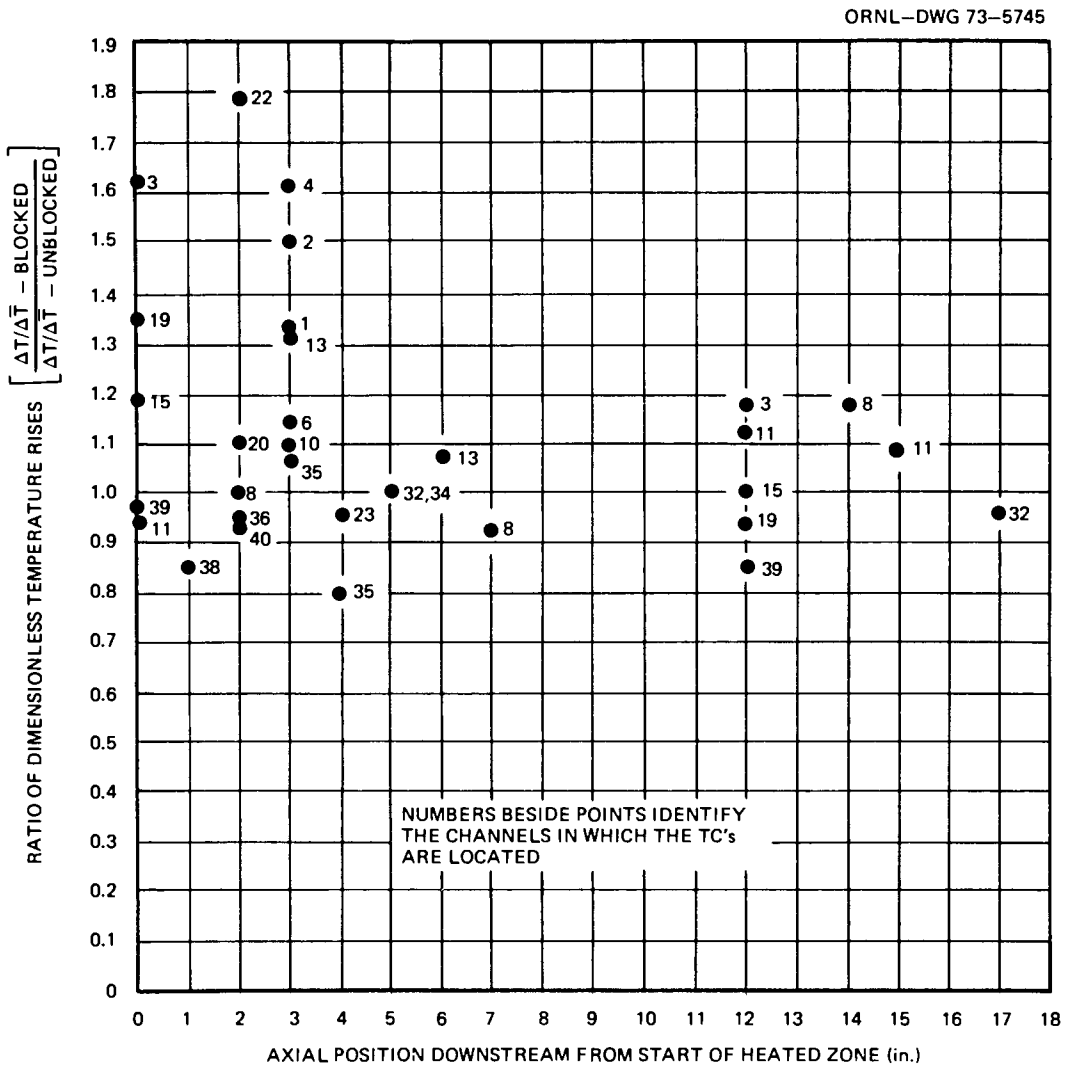

Fig. 8. Ratio of dimensionless temperature rises above inlet vs axial position for FFM bundle 2B with blockage of 24 channels (1–24) at the inlet. 55 gpm flow, ~600°F inlet temperature. Averages of blockage runs 738–742 and 747 compared with averages of unblocked runs 700–702.

is greater than 1 for channels downstream of the inlet blockage and, due to the increased bypass flow, is less than 1 for the unblocked channels (channels 7 to 12 and 20 to 42 for the 13-channel inlet blockage, and channels 24 to 42 for the 24-channel inlet blockage). It may be seen that the effect of blockage, as indicated by substantial departures of the ratio from unity, is limited to about 3 in. downstream of the start of the heated section (6 in. from the inlet blockage plate) or about five to six equivalent blockage diameters downstream. No excessively high temperatures were observed. The highest temperature ratio (see Fig. 8) occurred for a 24-channel blockage (55 gpm flow) in channel 22 (see Fig. 4) at an axial position 2 in. downstream from the start of the heated section (5 in. from the inlet blockage). The ratio at that location was ~1.8, indicating an 80% increase in the temperature rise over that of the unblocked case. Since the temperature rise for the unblocked case at that position was ~7°F and the temperature rise in the blocked case was ~13°F, the blockage caused an increase of only ~6°F. Temperature differences resulting from the wire-wrap perturbations in normal bundles are often greater than this.

3.2.3 Comments on inlet blockage experiment. It is concluded that centrally located inlet blockages of up to one-half of the flow area of a 19-rod bundle with a 3-in. unheated entrance length do not result in excessively high temperatures. The temperature increases attributed to the inlet blockages are of the same order as the temperature variations normally observed in unblocked bundles.

Since the unheated entrance length between a possible inlet blockage and the start of the heat-generating section of the fuel pins in an FFTF 217-pin subassembly is 6 in., twice that of these tests, the flow maldistribution caused by the inlet blockage should be significantly ameliorated in the additional 3 in., and one would expect correspondingly lower temperature increases in the FFTF subassembly than are indicated by these results. However, there are two other differences between the 19-rod experiment and the FFTF whose effects are difficult to extrapolate to the FFTF configuration. In these tests the fractions of the frontal area covered by the inlet blockage plates were quite large, $\sim 1/2$ for the 24-channel inlet blockage. The fluid velocities around the blockage plate were correspondingly higher than nominal. These higher velocities may have aided in correcting the flow maldistributions caused by the blockages. The proximity of the duct wall also may have had some influence in diverting the flow inward behind the blockages as compared with the relative remoteness of the wall in an FFTF subassembly. These two effects (which probably interact) would cause these tests to underpredict local temperature rises caused by similarly sized inlet blockages in larger bundles.

It is not thought that these effects extrapolated to a full-size FFTF bundle will be sufficient to offset the mitigating effect of the longer unheated entrance length and the relatively small temperature increases observed in these tests. It is concluded that inlet blockages of as many as 24 contiguous channels will not result in excessively high temperatures in the FFTF 217-pin subassembly.

3.3 Effect of Internal Blockage in FFM Bundle 3A

Bundle 3A of the FFM program was also of FFTF configuration. It had its central six channels blocked by a non-heat-generating stainless steel device, 1/4 in. long, brazed to the central rod. This section discusses the results of tests using this bundle.

3.3.1 Description of rod bundle 3A. The test section for the bundle 3A experiment is shown in Fig. 9. The bundle was inserted from the bottom of the test section with the free ends of the heaters facing upward. This allowed the use of a thermocouple rake, entering from the opposite end of the test section, for monitoring exit temperatures from selected flow channels.

The bundle instrumentation layout is shown in Fig. 10. The large circles represent the heaters that simulate the fuel rods. These are identified by the central number. The small tangent circles indicate thermocouple junctions at the indicated azimuthal position of the wire-wrap spacers. The junctions are located at an axial level indicated by the numbers in the small circles, which have units of inches from the start of the heated zone. The small circles containing pairs of dots indicate the location of grounded-junction thermocouples. The pair of dots next to the heater surface indicates that a thermocouple junction in the wire wrap is adjacent to the heater, whereas the pair of dots on the opposite side indicates that the other junction, at the same axial level, measures temperatures near the center of the flow subchannel. The flow subchannels, defined by the lines connecting the centers of the heaters, are identified by the numbers in the triangles so defined. The small circles with interior crosses indicate channels that are monitored by exit thermocouples.

The fuel-rod-simulator heaters have thermal elements attached to the inner surface of the cladding as indicated by the dots labeled *A, B, C,* etc., in the large circles. The ends of these thermal elements were grounded to the inner surface of the cladding at 15° azimuthal intervals and at 0.25 in. axial intervals; thus

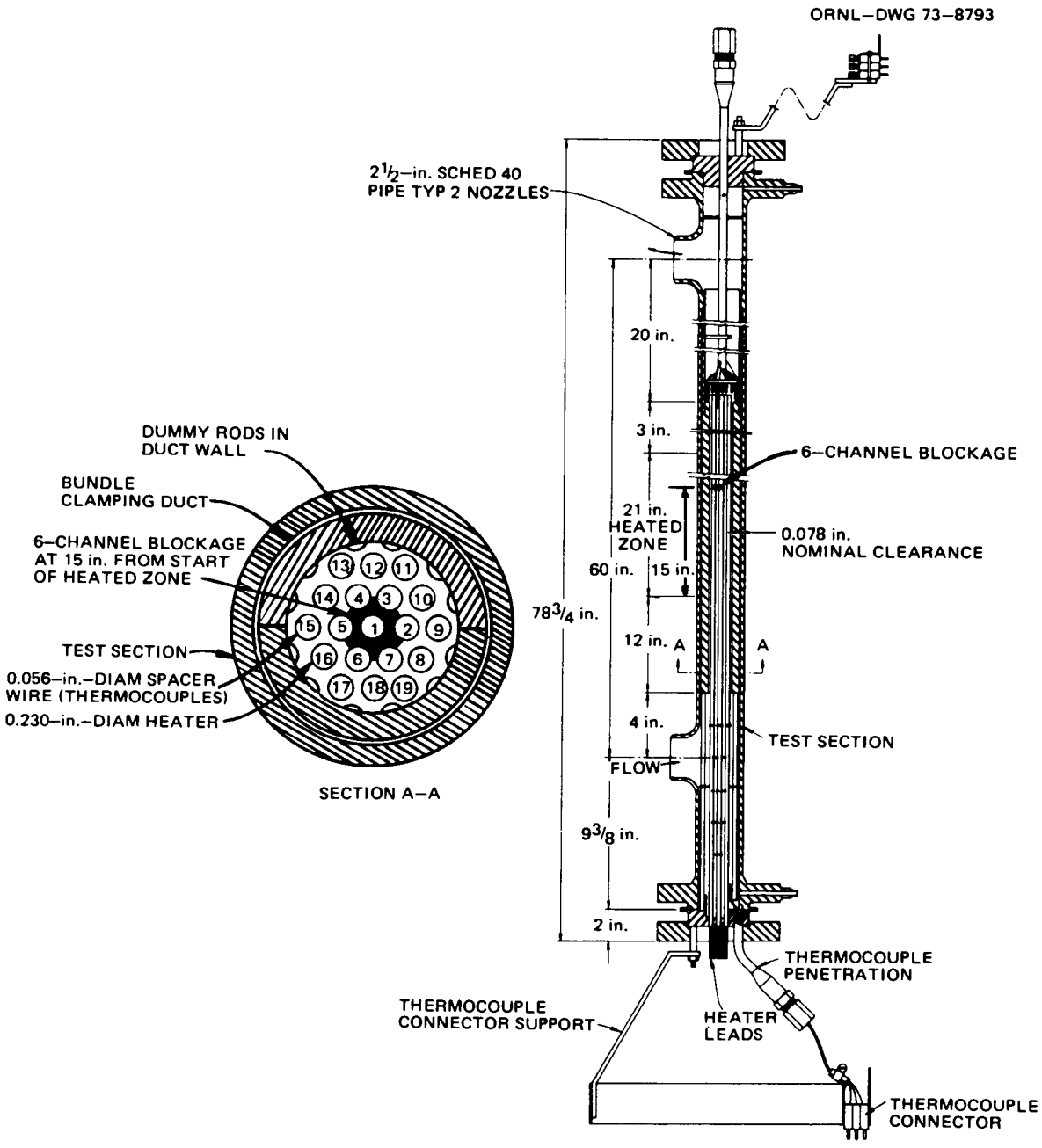

Fig. 9. FFM test section for rod bundle 3A.

the junction formed by two thermal elements measures an average temperature along the spiral path on the inner surface of the cladding between the two junctions. Notice that the thermal elements in heaters 1, 2, and 3 measure temperatures from 15 to 16 in. (from the start of the heated zone) in ¼-in. increments; those in heater 6 measure from 15.22 to 16.22 in.; and those in heaters 4, 5, and 7 measure from 16 to 17 in.

3.3.2 Experiments performed. To date, five sets of experiments have been performed with bundle 3A (out of six planned). These included cases with no power; all rods heated at powers of 5, 7.5, and 10 kW/ft

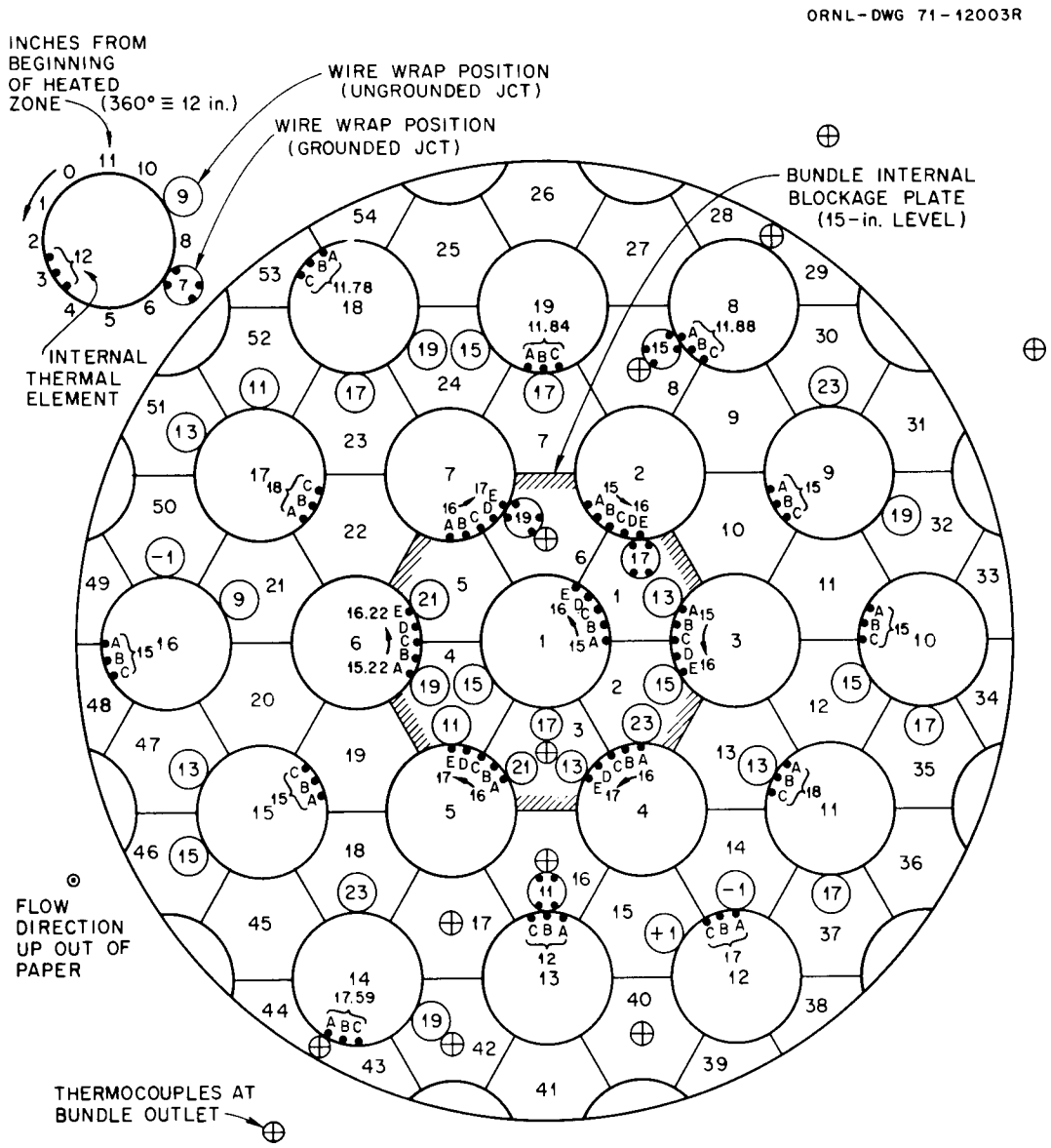

Fig. 10. Spacer wire and internal thermocouple locations for FFM bundle 3A.

with flows of 54, 43.2, and 32.4 gpm (100, 80, and 60% of specific FFTF full flow); rods heated singly at 8 and 10 kW/ft with flows of 54 and 11 gpm (20%); central seven rods heated at 10 kW/ft with a flow of 54 gpm; and three outer rods heated at each "flat" of the hexagon defined by the outer row of rods at a flow of 54 gpm. These latter tests are described in ref. 29.

This discussion is restricted to the experiments performed at 100, 80, and 60% of full flow and 10 kW/ft and at 100% flow and 7.5 kW/ft. These experiments include the base case of full flow at FFTF average power of 7.5 kW/ft, cases with flows considerably smaller than would be allowed to occur in the reactor at full power, and cases with power levels higher than full power. The experimental results were selected from a sequence of tests shown in Table 5. The experiments were first performed in order of

Table 5. Experiments performed with FFM bundle 3A with power on all 19 heaters (series IV, test 2)

Purpose: To measure the effect of flow and power on bundle performance

Control

Run	Test section			Heaters
	Flow (gpm)	Power		
		kW/ft	kW/rod	
101	54	10	17.5	All
109	32.4	5	8.75	All
106	43.2	5	8.75	All
102	54	7.5	13.13	All
108	32.4	7.5	13.13	All
105	43.2	7.5	13.13	All
107	32.4	10	17.5	All
103	54	5	8.75	All
104	43.2	10	17.5	All

Measure: Test section outlet temperature, °F
Spacer wire temperatures, °F
Heater internal temperatures, °F
Test section inlet pressure, psig
Test section outlet pressure, psig

Special instructions:

Runs to be performed in the order listed

Project management to evaluate results from tests 101 through 109 before proceeding to duplicate tests

Duplicate tests

Rod	Test section			Heaters
	Flow (gpm)	Power		
		kW/ft	kW/rod	
118	32.4	5	8.75	All
112	54	5	8.75	All
115	43.2	5	8.75	All
117	32.4	7.5	13.13	All
113	43.2	10	17.5	All
116	32.4	10	17.5	All
114	43.2	7.5	13.13	All
110	54	10	17.5	All
111	54	7.5	13.13	All

ascending stress on the heaters (increasing power and decreasing flow) and then replicated in random sequence to minimize any effect of operating sequences in the results. Multiple readings taken for each point were averaged, and standard deviations were computed by data-handling programs.

Radial heat loss from the test section was reduced by the use of insulation and guard heaters which were controlled to give zero temperature gradient in the insulation next to the test section wall as measured by two thermocouples in the insulation between the test section wall and the external guard heaters. Previous experiments[27] with bundle 2A indicated that extreme variations in guard heat settings did not

affect experimental results significantly. However, since the guard heaters were already installed, they were operated for the small benefit they would provide.

3.3.3 Summary of results from bundle 3A. The results are presented in four ways: (1) $T - T_{in}$ of thermal elements inside the heater sheath and in wire-wrap spacers within the central six channels, (2) exit temperature distributions, (3) normalized temperatures of heater internal thermocouples, and (4) normalized temperatures of selected wire-wrap spacer and exit thermocouples.

Temperatures in the central subchannels. The experimental runs described in this section are identified as run 101 (10 kW/ft, 100% flow), run 104 (10 kW/ft, 80% flow), run 107 (10 kW/ft, 60% flow), and run 102 (7.5 kW/ft, 100% flow).

Figure 11 shows the central subchannel temperatures (above inlet temperature) vs distance from the start of the heated zone for run 101 (10 kW/ft, 100% flow). This run is of particular interest because it represents the case of 100% of FFTF specific flow (54 gpm for 19 rods) and a power of 10 kW/ft, which is significantly above the average FFTF linear power density. In these experiments, temperatures were measured by thermocouples inside the central seven heaters and by the wire-wrap thermocouples in the central six subchannels.

The temperatures measured by the thermocouples inside the heaters are shown in Fig. 11 as horizontal lines extending the axial distance between the two thermal elements that make up the particular thermocouple being plotted. This distance is usually $\frac{1}{4}$ in., and the indicated temperature can be considered as an average along that length. The number near each line indicates the rod within which that particular thermocouple resides. The outer cladding surface temperature was computed by subtracting a temperature drop across the cladding calculated for the given heat flux assuming radial heat flow (the latter assumption should be valid everywhere except directly underneath the blockage device). These computed outer cladding surface temperatures are indicated in the figures by the letter *c*.

Temperatures measured by thermocouples in the wire-wrap spacers are plotted and labeled so that the first two digits indicate the heater to which the wire-wrap spacer is attached. The second two digits indicate the axial distance downstream from the start of the heated zone, and the last digit indicates the channel in which the spacer resides at that particular axial elevation. For example, 04 13 CH 3 indicates heater 4, 13 in. from start of heated zone, channel 3. Grounded-junction thermocouples in the wire-wrap spacers indicate two temperatures at the same elevation, one near the heater surface and the other near the center of the flow subchannel. These are also plotted.

The 90% confidence limit bands (2σ) are not shown because of their small and relatively constant values. Except for internal thermocouples 0115AB, which had a standard deviation σ of 3.1°F for the worst case, and 0115DE, for which σ was 3.7°F, all other internal thermocouples had standard deviations of about 0.3 to 1°F. Those of the wire-wrap thermocouples were about 0.5°F.

The abscissa in Fig. 11 starts at 13 in. from the start of the heated zone because all information of interest is downstream of this point. The blockage plate was at the 15-in. level. The estimated length of the recirculation zone is shown as 2 in., which is about seven times the radius of the blockage disk, or 12 times the step height of the blockage device above the surface of the central rod. Several investigators have indicated that the recirculation zone for flow over a step is 5.2 to 17 times the height of the step.[17,30] The first value is for flow over a sharp edge disk in a free stream, and the second is for flow over a sharp edge wall on a flat plate. Other configurations have intermediate values.

Figure 11 also shows bulk mixed-mean temperature rises calculated by heat balances. At the plane of the blockage the highest measured temperature (rod 7 at 16 to 16.25 in.), adjusted to give the external cladding temperature, is approximately 220°F higher than the mixed-mean temperature at that point.

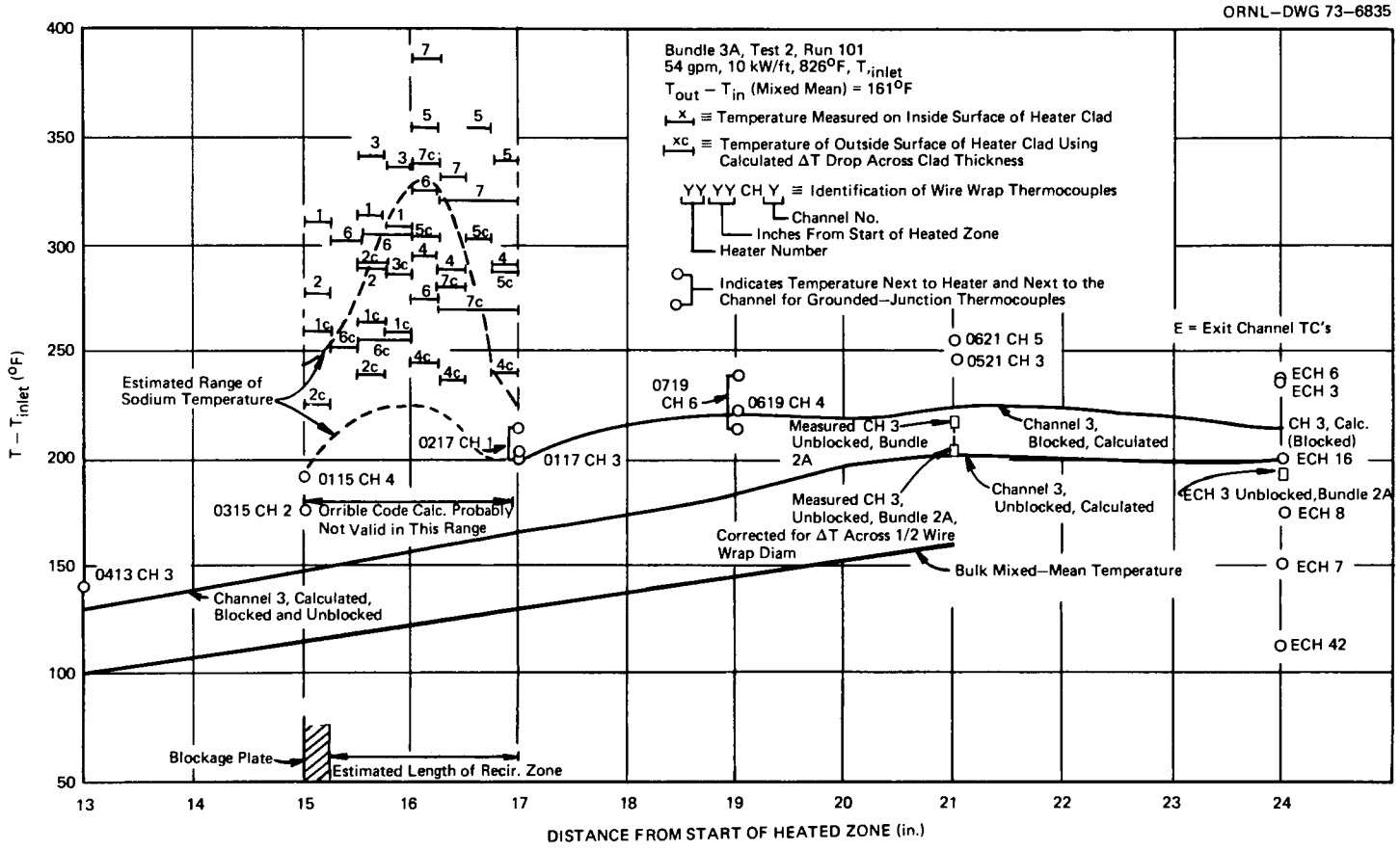

Fig. 11. Temperatures along the central six channels, bundle 3A, run 101. 100% flow, 10 kW/ft.

However, it is not appropriate to use the mixed-mean temperature as a base for comparison because temperature peaking would also exist in the center of unblocked rod bundles.

For comparison with a more realistic temperature for the unblocked case, the calculated temperature for channel 3 of unblocked bundle 2A, run 1109 (54 gpm, 10 kW/ft), is shown in Fig. 12 along with some pertinent experimental data points.[28] The channel 3 profile was calculated using the ORRIBLE code[1] with parameters C_T = 0.005, C_D = 0.6, and C_S = 1.0, where C_T is a parameter related to the turbulent mixing between subchannels, C_D is related to the pressure diversion cross flow, and C_S is related to the sweeping of fluid by the spiral wire-wrap spacers. (See ref. 1 for a definition of these parameters.) Calculated temperatures are most sensitive to C_S and are relatively insensitive to the other two coefficients. It may be inferred from Fig. 12 that the temperature of channel 3 for the unblocked case as calculated by ORRIBLE should be a reasonably good reference for comparison of the results of blocked bundle 3A.

The calculated axial temperature distribution of channel 3 (if it were unblocked) is shown on the second line from the top in Fig. 11. The cladding outer surface temperatures appear to be about 80 to ~180°F above the average temperature of the unblocked channel at the 15- to 17-in. level. The hottest temperature measured on the inner surface of the cladding was about 380°F above the 826°F inlet temperature and about 220°F higher than the predicted bulk mixed-mean sodium temperature at the elevation of the thermocouple (16 in.) for the unblocked case. Figure 11 also shows the temperatures measured by the ungrounded thermocouples in the wire-wrap spacers in the central six subchannels: 04 13 CH 3, 01 15 CH 4, 03 15 CH 2, 01 17 CH 3, 06 19 CH 4, 06 21 CH 5, and 05 21 CH 3. Also plotted are the grounded-junction thermocouple readings that show the radial temperature difference across the wire-wrap spacers: 02 17 CH 1 and 07 19 CH 6. These indicate that the ΔTs across the wire wraps are about 15°F (02 17 CH 1) to 25°F (07 19 CH 6). Since the ungrounded thermocouple junctions are approximately in the center of the wire-wrap spacers, a rough estimate can be made of the sodium channel temperatures by subtracting half the ΔT obtained from the grounded-junction thermocouples (7 to 12°F) from the readings obtained with the ungrounded-junction thermocouples. Adjusted readings (plotted in Fig. 11) are compared with ORRIBLE predictions for temperatures in channel 3 (which serves as an indicator of the behavior of all six central channels) in the blocked configuration. Apparently, the prediction of temperatures downstream from the blockage is reasonably good for our purposes. Exit temperatures are also plotted and discussed more fully later.

Since ORRIBLE has no provisions for calculating recirculating flow, predictions obtained with it should not be valid in the recirculating zone. If it is assumed that a 10 to 20°F "film drop ΔT" exists between the cladding outer surface and the average channel sodium temperature, the temperatures of the sodium in the recirculating zone could be estimated as being in the range enclosed by the two dashed lines in Fig. 11.

It is interesting to note the factors that could affect some of the measurements plotted in Fig. 11. Referring to Fig. 10, the thermal elements in rod 7 are located from 1 in. upstream from the six o'clock (17 in.) position of the associated wire wrap to 2 in. upstream of the four o'clock position of the wire wrap. At the 16-in. level, the wire wrap on rod 7 creates a dam between rods 6 and 7 and could "trap" hot fluid below this zone, thus possibly accounting for the higher temperatures indicated by rod 7 in Fig. 11.

The spiral formed by the wire-wrap spacer on rod 1 touches rod 5 0.5 in. below the spiral defined by the rod 5 thermal elements. The closeness of the rod 1 spacer might be affecting the temperatures in rod 5.

The thermal elements in rods 1, 3, 4, and 6 appear to be relatively free of the influence of wire wraps. Those on heater 1 face channel 1, whereas the others face adjacent rods.

The low temperatures in heater 2 are somewhat puzzling. One possible explanation is that the wire wrap, which penetrates the blockage plate at the eight o'clock position, might be leaking sufficient fluid to depress the local temperatures.

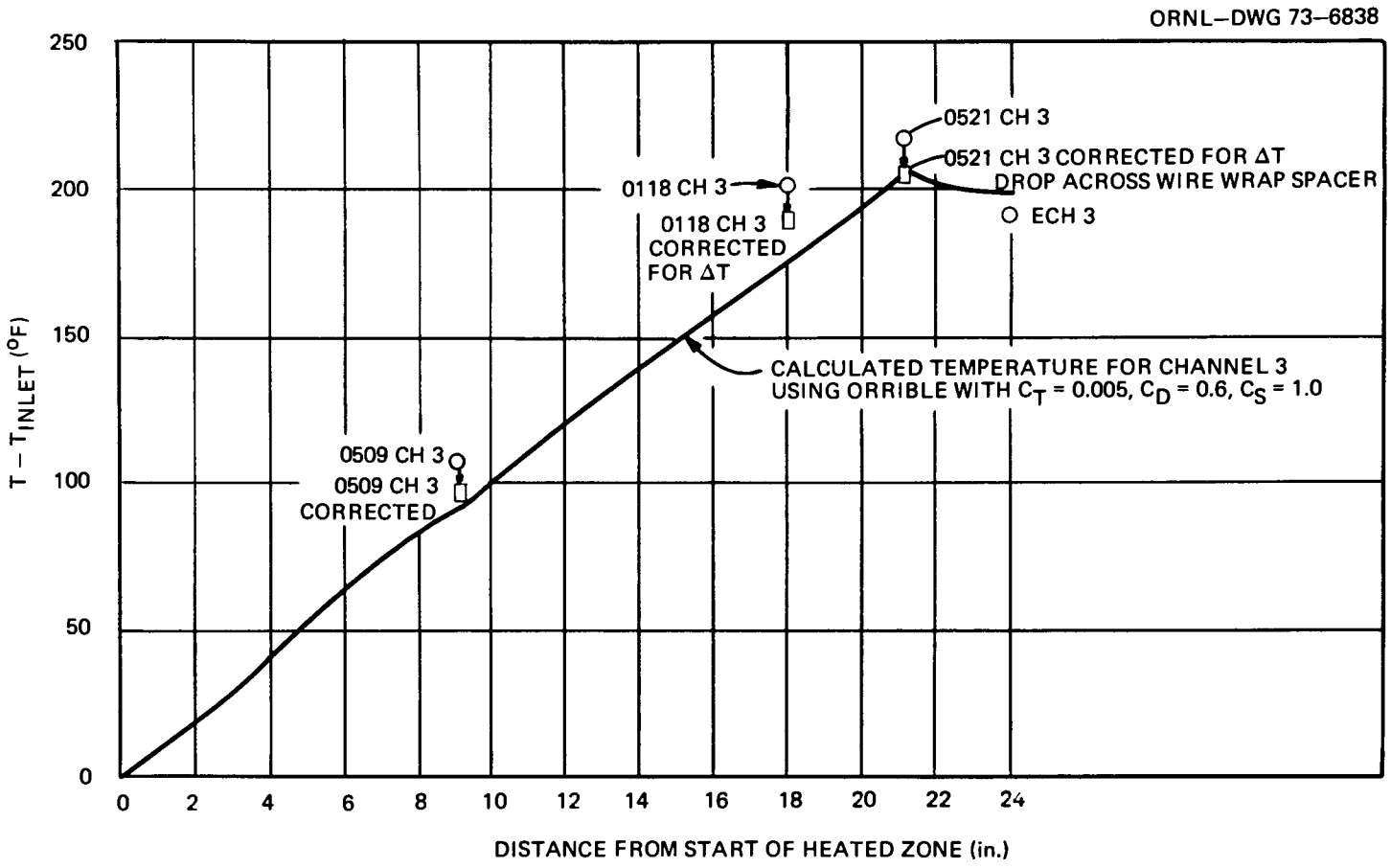

Fig. 12. Measured and calculated temperatures in channel 3 in unblocked bundle 2A, run 1109. 100% flow, 10 kW/ft.

All these second-order effects do not significantly affect the main conclusion that can be drawn from these results: a blockage of the shape tested is tolerable at full flow and power.

Figure 13 shows the central subchannel temperatures for run 104 (10 kW/ft, 80% flow). The comments made for Fig. 11 also apply here except that the temperatures measured were higher because of the lower flow. The blockage tested can be tolerated at this flow.

Figure 14 shows the central subchannel temperatures for run 107 (10 kW/ft, 60% flow), which is of particular interest because it represents the most severe condition imposed on the test bundle up to this time. (Approach-to-boiling tests have not been done as of this writing.) Results are plotted in Fig. 14 in the same manner as in Figs. 11 and 13.

For this case the cladding outer surface temperatures in the vicinity of the blockage ranged from 80 to 220°F higher than the sodium temperature in the central channels (represented by channel 3) expected for the unblocked case. The hottest cladding internal surface temperature was 1327°F, which is about 540°F higher than the inlet temperature of 785°F. It should be noted that the temperature increase caused by the blockage is only slightly affected by flow.

These results indicate that a non-heat-generating blockage of the size tested is still acceptable even at 60% flow conditions.

Figure 15 shows the results for run 102 (7.5 kW/ft, 100% flow), which represents the full flow and average power conditions for the FFTF. Note that cladding temperatures are only 280°F higher than inlet temperature and 150°F higher than the anticipated sodium temperature in channel 3 if it were unblocked.

Exit temperatures. The temperatures at the exits of selected subchannels (see Fig. 10) were measured using the exit thermocouple rake. These indicated temperatures should represent the particular subchannel exit mixed-mean temperature because of the mixing that occurs in the 3 in. of unheated length between the end of the heated zone and the channel exit. Thus these measurements provide results that can be directly compared with analytical predictions of subchannel temperatures. In addition, they indicate the magnitude of the influence of an in-core blockage on the exit temperature profile and should help indicate the feasibility of detecting the blockage by thermal devices located in the exit region.

To provide an exit temperature profile from an unblocked case for comparison, a diametral traverse of the normalized temperature distribution $[(T - T_{in})/(T_{out} - T_{in})]$ measured in unblocked bundle 2A (10 kW/ft; 53 gpm) along with ORRIBLE predictions for that case are plotted in Fig. 16 (see Fig. 10 for identification of channel numbers). Bundle 2A was identical to bundle 3A except that it was unblocked and had a hexagonal duct instead of a duct containing wire-wrap dummy rods. The agreement between experimental results and analysis (within ~6°F) indicates that ORRIBLE is a good predictor for that case.

Also plotted in Fig. 16 is the calculated normalized exit temperature distribution for bundle 3A if it were unblocked. The agreement between the calculated and the measured bundle 2A temperature distribution indicates that the calculation for the unblocked bundle 3A may serve as a reference for comparison with the results of the blocked bundle experiments.

Figure 17 shows the exit temperature distribution expressed as $T - T_{in}$ for the experimental case of 10 kW/ft, 100% flow (54 gpm), and for the pertinent calculated blocked and unblocked case. The pertinent experimental results for bundle 3A plotted in Fig. 17 show a temperature increase in the blocked region over the unblocked case of ~30°F. The ORRIBLE predictions for the blocked case show a better agreement at channel 6 (~6°F) than at channel 3 (~16°F) and poorer agreement in the exterior channels. The poorer agreement in the exterior channels may be due to steeper temperature gradients in that region. The ORRIBLE code calculates average subchannel temperatures, whereas the thermocouples might be in a subchannel temperature gradient. Investigations of this effect are continuing. However, these variations do not have a major effect.

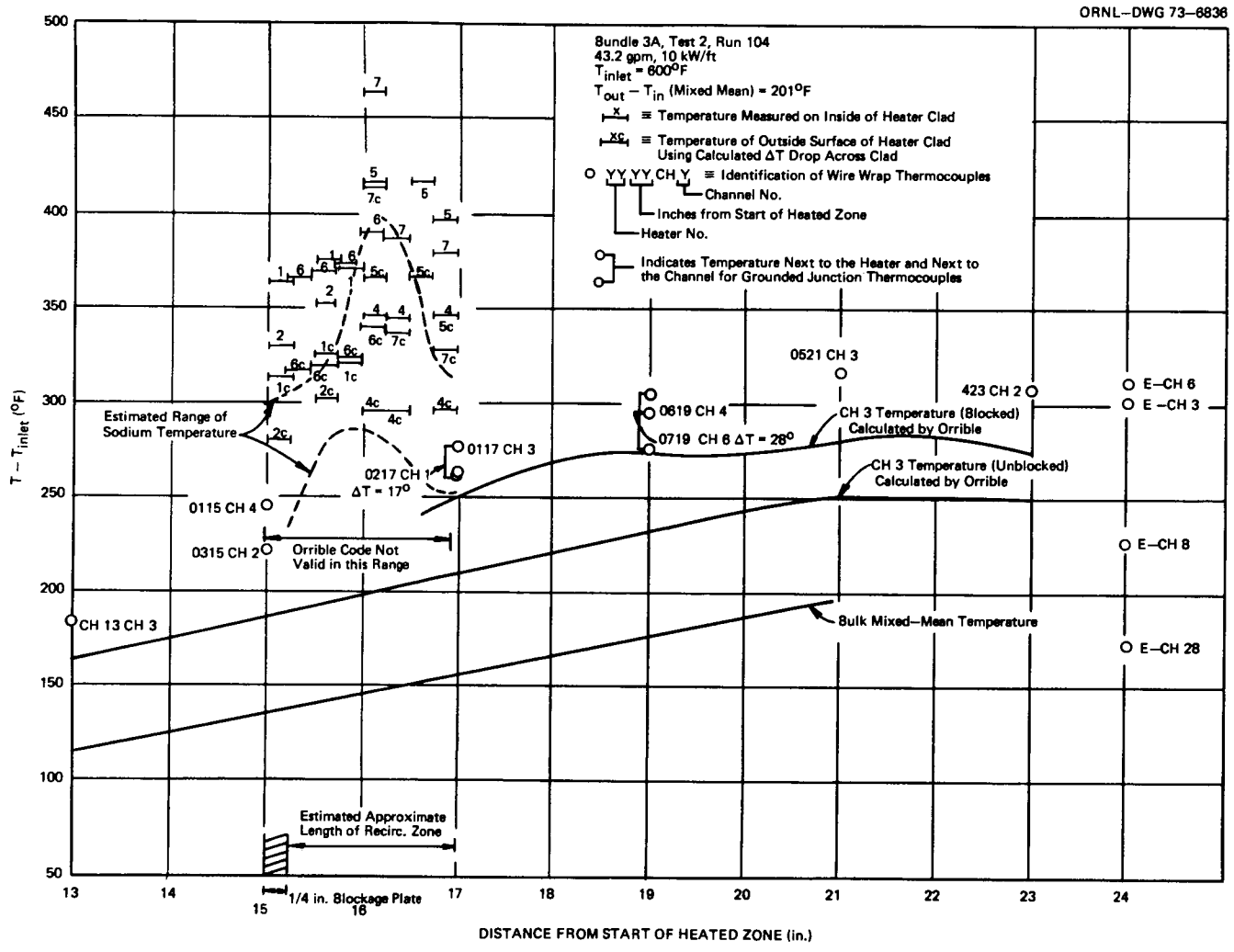

Fig. 13. Temperatures along the central six channels, bundle 3A, run 104. 80% flow, 10 kW/ft.

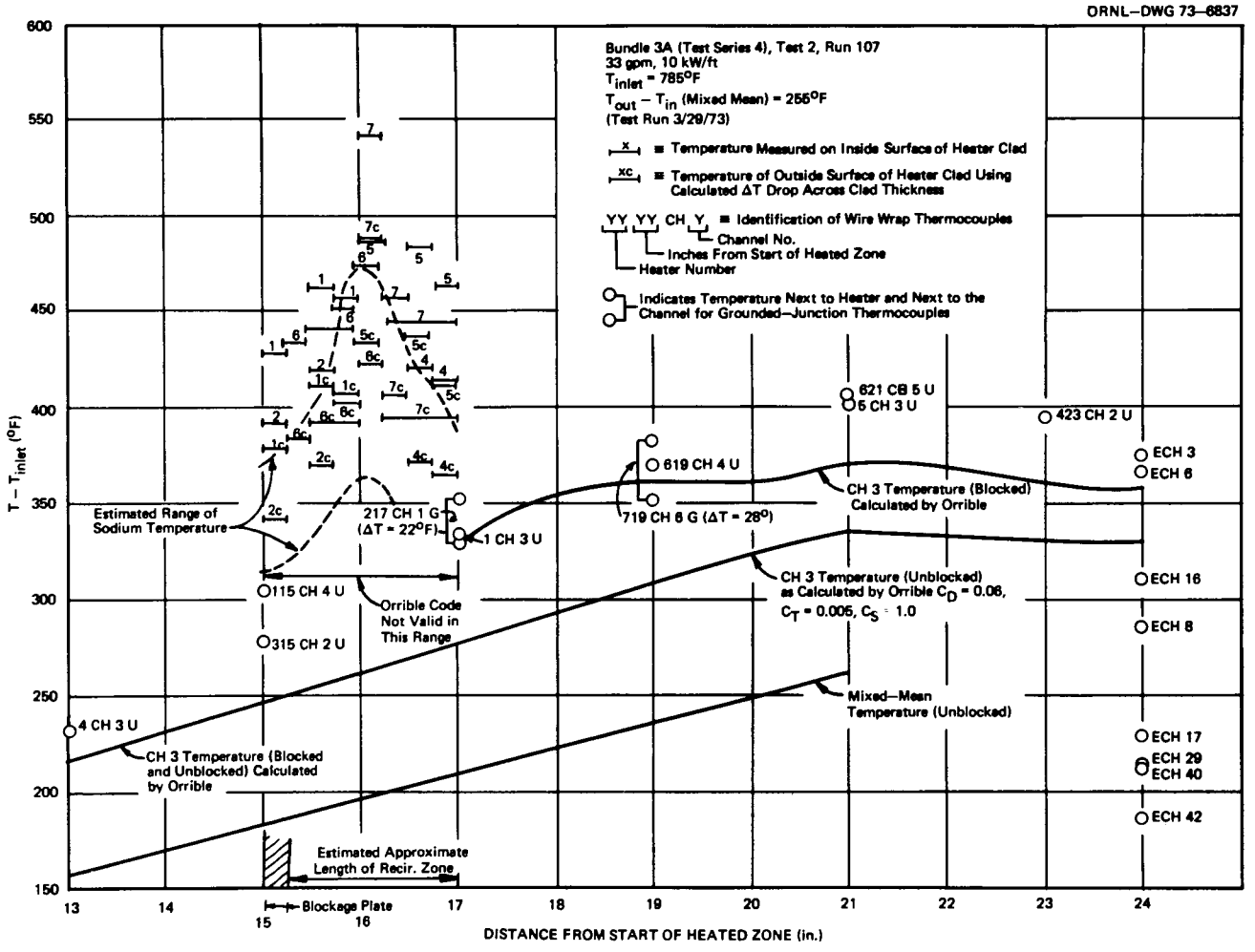

Fig. 14. Temperatures along the central channels, bundle 3A, run 107. 60% flow, 10 kW/ft.

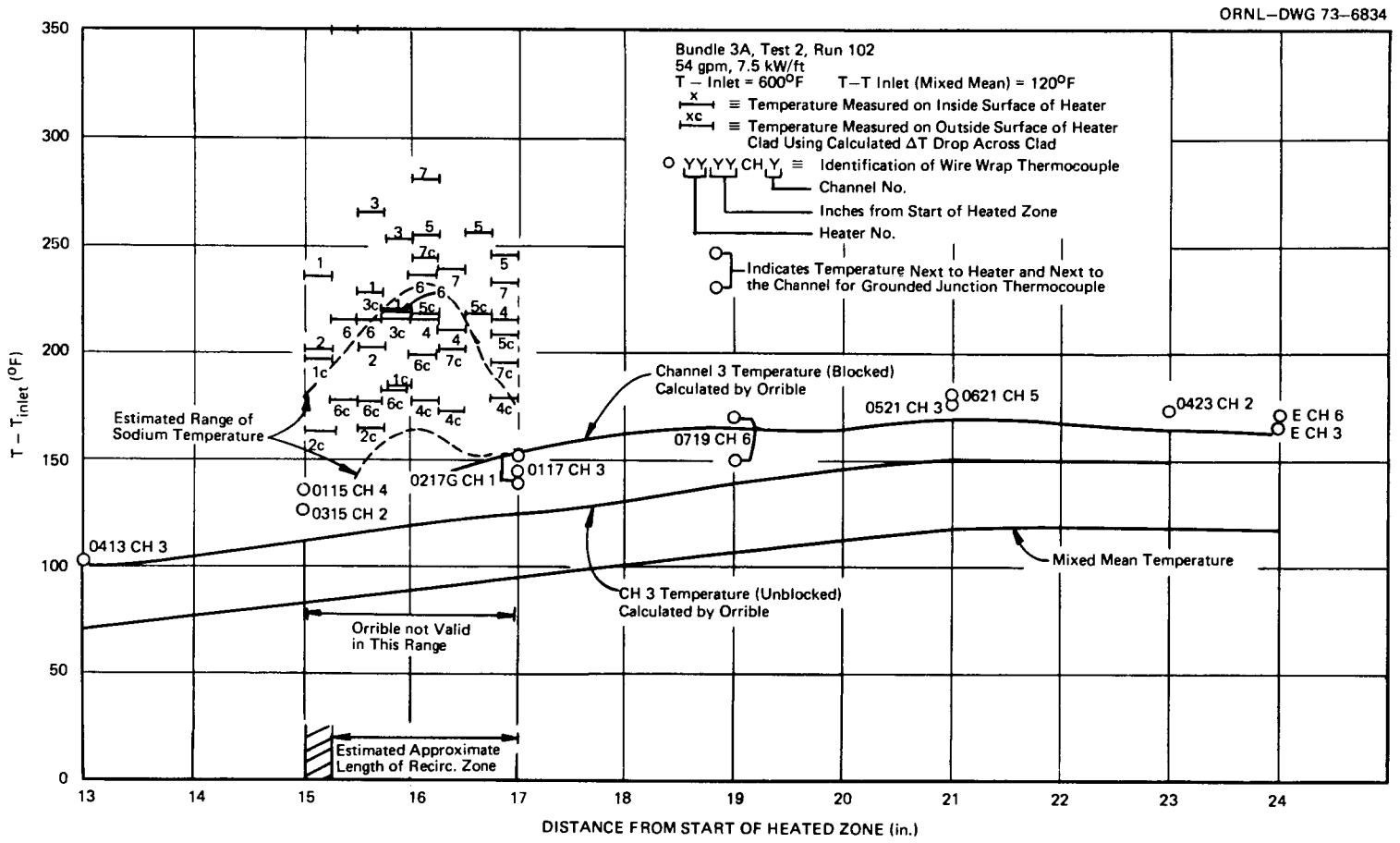

Fig. 15. Temperatures along the central channels, bundle 3A, run 102. 100% flow, 7.5 kW/ft.

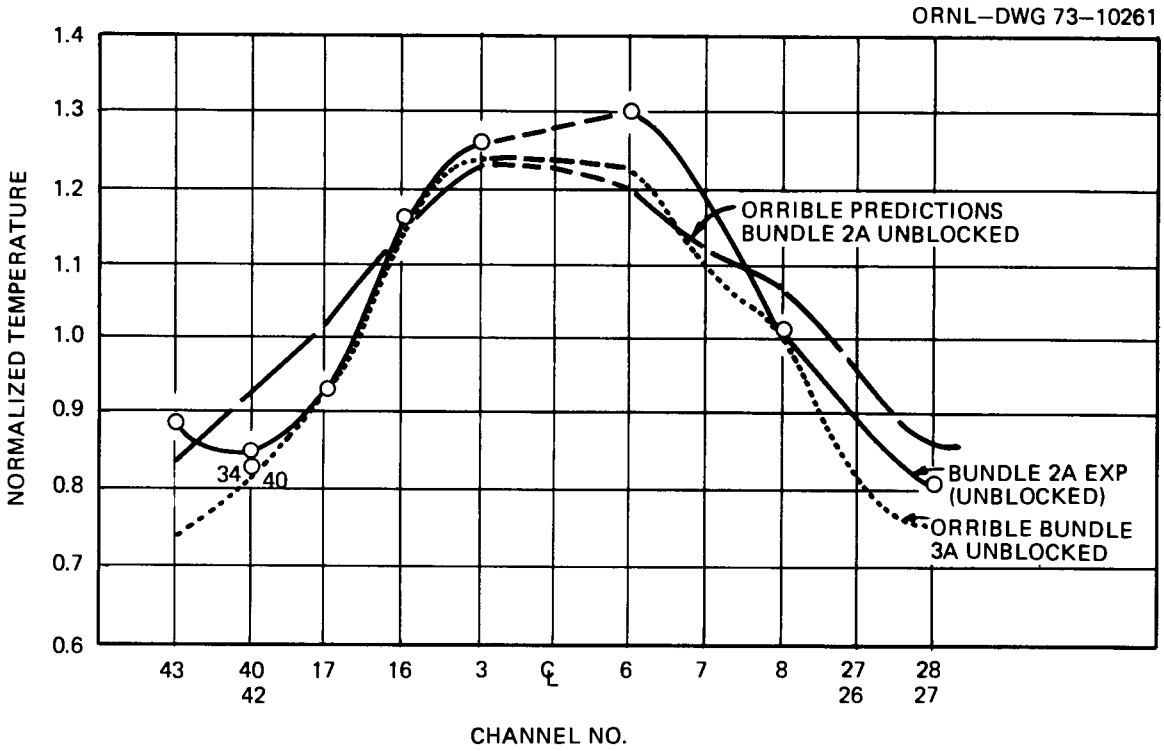

Fig. 16. Measured and calculated normalized exit temperatures, unblocked bundle 2A and blocked bundle 3A.

Figure 18 shows similar results for the most severe case of 10 kW/ft, 60% flow (33 gpm). Both imply 30 to 40°F differences between blocked and unblocked cases.

The FFTF fuel has exit gas plenums of 42 in. If the FFM bundle 3A had an exit unheated length of 42 in., the temperature distribution as calculated by ORRIBLE would be as shown in Fig. 19. The variation in profile between blocked and unblocked cases at full flow shows that, in this case, correlation techniques on a small number of exit thermocouples per channel might detect a blockage of as few as six channels with as little as 6 in. of heated zone adding heat to the perturbed flow downstream from the blockage. This observation is not directly relevant to the present FFTF design but might be considered for future use.

Figure 20 shows the exit temperature distribution for the 3- and the 42-in. unheated zones for the average operating case of 7.5 kW/ft and 100% (54 gpm) flow.

Normalized temperatures of heater internal thermocouples. The normalized temperatures $[(T - T_{in})/(T_{out} - T_{in})]$ for all operative heater internal thermocouples are shown in Table 6. The highest normalized temperature of 2.76 was obtained from thermocouple 07 16AB (see Fig. 10) for the case of 54 gpm and 5 kW/ft, where $T_{out} - T_{in}$ was 80°F. Because of the nonlinear relationships between the various ΔTs from the point of temperature measurement to the inlet and outlet temperatures that serve as normalization base points, the normalized temperatures are not uniform over variations of power and flow. Preliminary analysis indicates that the normalized temperatures should be less sensitive to power difference than to flow. These evaluations are continuing.

Normalized temperatures of wire-wrap and exit thermocouples. The normalized temperatures for selected exit, ungrounded wire-wrap, and grounded wire-wrap thermocouples are given in Table 7. These

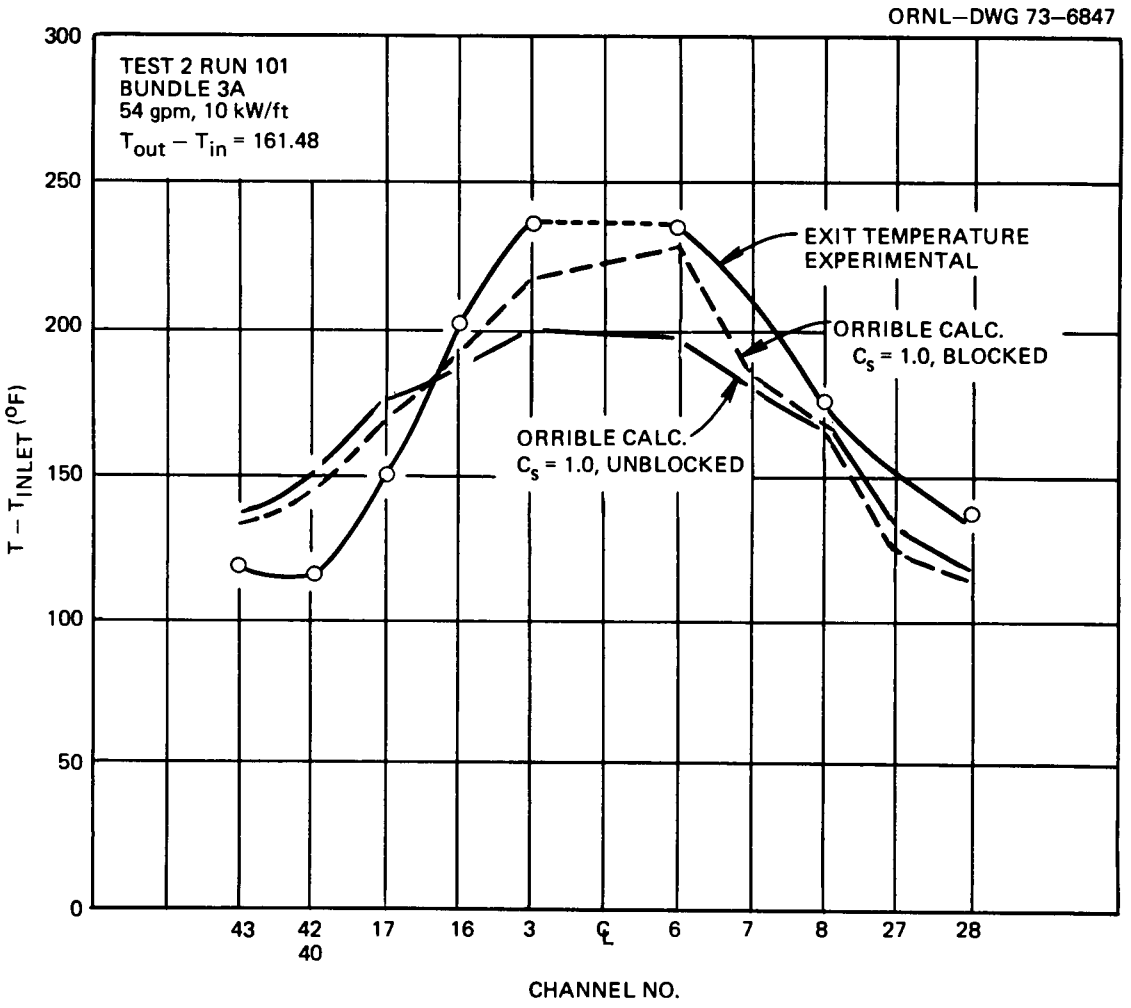

Fig. 17. Measured and calculated exit temperatures, bundle 3A. 100% flow, 10 kW/ft.

indicate that the highest temperature near the heaters (e.g., see TC 0719A heater 7) is of the same magnitude as the highest exit temperature (see exit channels 3 and 6). For each thermocouple the normalized results are more constant than was the case for the heater internal thermocouples because the ΔT across the cladding was not involved in the normalization.

3.3.4. Comments on internal blockage experiments. Excessive temperatures are not generated in the heater rods as a consequence of a 0.25-in.-long, non-heat-generating blockage over an area of six subchannels in the 19-pin FFM bundle 3A even at 10 kW/ft and 60% flow. The blockage covers a flow area of only about 10% of the total area. Therefore, one would expect the wall effects on the flow in the vicinity of the blockage to be small. A similar non-heat-generating blockage would be expected to behave essentially the same way in a full-size 217-pin FFTF fuel subassembly and therefore would not cause excessive temperatures. It also appears that relatively small blockages affect the exit temperature distribution to an extent that correlation techniques between various thermocouples might eventually be used to detect such anomalies.

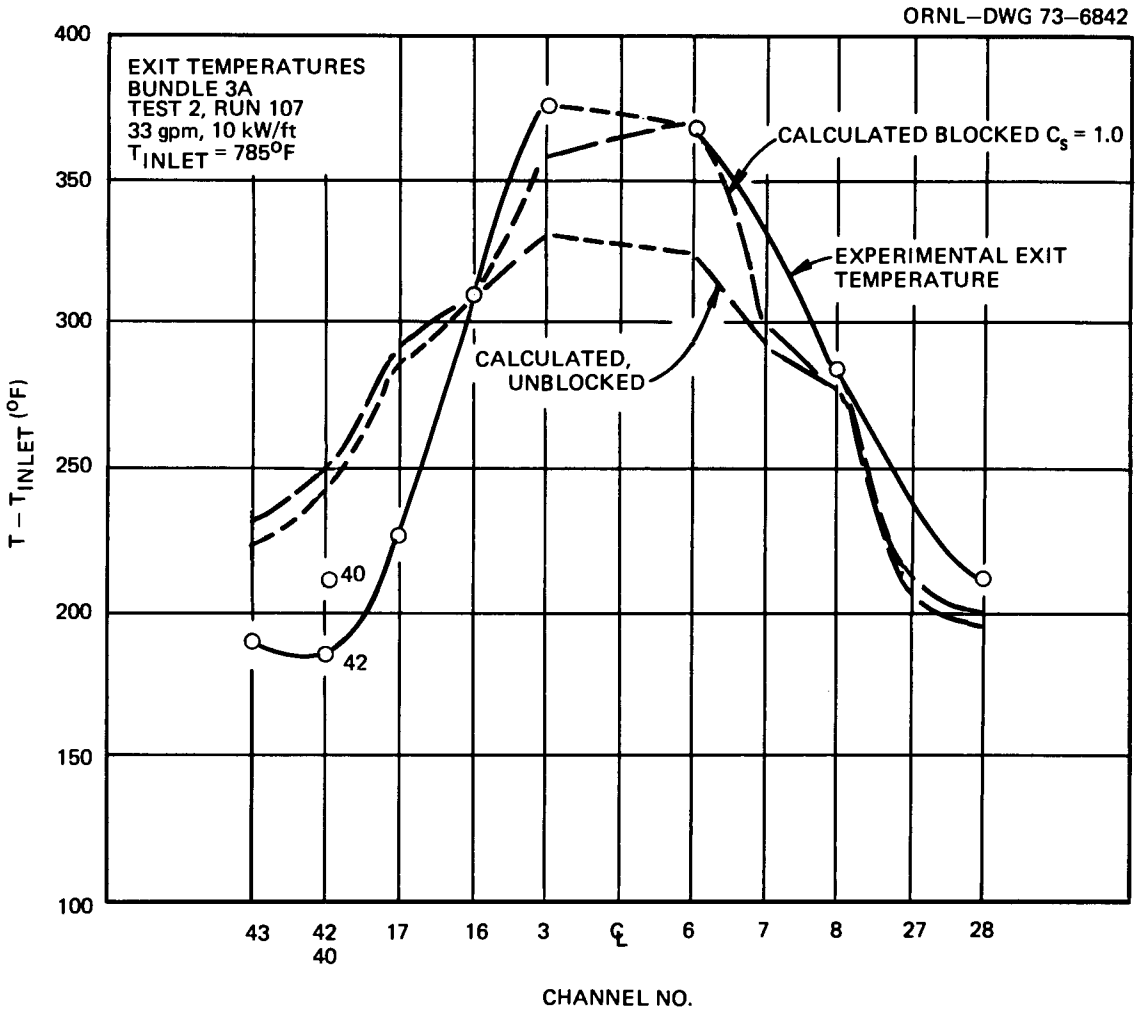

Fig. 18. Measured and calculated exit temperatures, bundle 3A. 60% flow, 10 kW/ft.

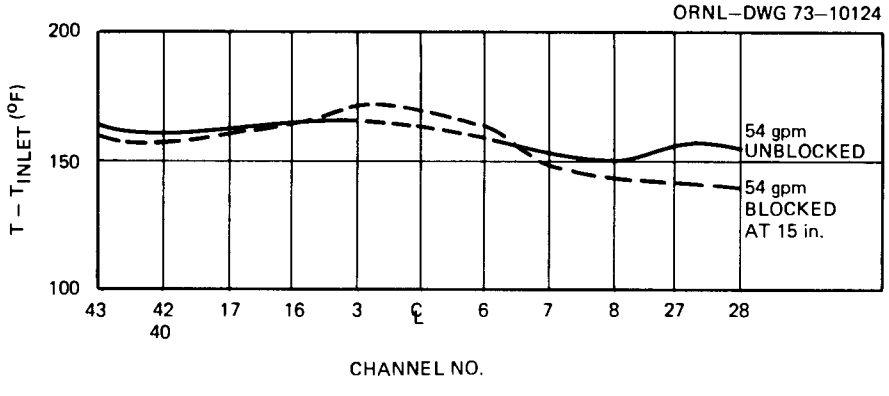

Fig. 19. Calculated exit temperature distribution, bundle 3A type with 42-in. exit plenum.

Table 6. Normalized temperatures of heater internal thermal elements – FFM bundle 3A, series IV

Run No.	101	109	106	102	108	105	107	103	104
Flow, gpm	54	32.4	43.2	54	32.4	43.2	32.4	54	43.2
Power, kW/ft	10	5	5	7.5	7.5	7.5	10	5	10
Mixed-mean temp. ($T_{out} - T_{in}$), °F	161	134	101	121	201	151	268	80	201
Normalized temperature									
TC R1312BC Htr. 13	[a]	0.477	0.659	[a]	0.190	0.168	[a]	0.423	[a]
TC R1812AB Htr. 18	1.044	0.844	0.988	1.095	0.854	0.990	0.846	1.137	0.960
TC R1912AB Htr. 19	1.377	1.168	1.318	1.428	1.190	1.327	1.185	1.482	1.304
TC R1912BC Htr. 19	1.389	1.188	1.334	1.448	1.209	1.351	1.199	1.498	1.324
TC F0115AB Htr. 1	1.931	1.689	1.896	2.054	1.719	1.910	1.681	2.147	1.833
TC R0116CD Htr. 1	1.945	1.845	1.952	2.106	1.869	1.984	1.816	2.151	1.895
TC R0116DE Htr. 1	1.916	1.731	1.860	1.955	1.782	1.902	1.793	2.015	1.876
TC R0215AB Htr. 2	1.732	1.486	1.647	1.797	1.522	1.676	1.533	1.851	1.664
TC R0215CD Htr. 2	1.806	1.589	1.711	1.895	1.617	1.743	1.647	1.883	1.774
TC R0316CD Htr. 3	2.147	1.879	2.145	2.282	[a]	[a]	[a]	[a]	[a]
TC R0316DE Htr. 3	2.139	1.834	2.023	2.167	[a]	[a]	[a]	[a]	[a]
TC R0615AB Htr. 6	1.879	1.680	1.819	1.951	1.716	1.849	1.718	1.993	1.846
TC R0615BD Htr. 6	1.863	1.668	1.793	1.906	1.708	1.837	1.737	2.006	1.861
TC R0616CD Htr. 6	1.902	1.700	1.823	1.949	1.738	1.852	1.770	2.017	1.878
TC R0616DE Htr. 6	2.019	1.809	1.952	2.080	1.840	1.987	1.858	2.086	1.967
TC R0915AB Htr. 9	1.859	1.530	1.745	1.932	1.571	1.780	1.574	1.965	1.763
TC R0915BC Htr. 9	1.937	1.623	1.855	2.030	1.632	1.860	1.612	2.088	1.809
TC R0416AB Htr. 4	1.836	1.637	1.768	1.874	1.673	1.794	1.653	1.935	1.742
TC R0416BC Htr. 4	1.802	1.596	1.746	1.851	1.645	1.780	1.628	1.915	1.737
TC R0417DE Htr. 4	1.815	1.611	1.769	1.884	1.646	1.798	1.626	1.952	1.746
TC R0516AB Htr. 5	2.209	1.924	2.142	2.310	1.934	2.147	1.917	2.408	2.104
TC R0517CD Htr. 5	2.207	1.921	2.148	2.312	1.940	2.157	1.914	2.397	2.102
TC R0517DE Htr. 5	2.112	1.828	2.032	2.220	1.840	2.048	1.819	2.292	2.000
TC R0716AB Htr. 7	2.400	2.177	2.460	2.639	2.146	2.414	2.127	2.760	2.341
TC R0716BC Htr. 7	2.060	1.806	2.025	2.187	1.817	2.024	1.792	2.258	1.950
TC R0717BE Htr. 7	1.993	1.737	1.953	2.122	1.768	1.980	1.744	2.190	1.903
TC R1217AB Htr. 12	1.511	[a]	[a]	1.570	1.327	1.468	1.320	1.598	1.445
TC R1217BC Htr. 12	1.543	[a]	[a]	1.605	1.353	1.497	1.352	1.642	1.473
TC R1418AB Htr. 14	1.307	1.110	1.271	1.389	1.097	1.246	1.081	1.429	1.208
TC T1418BC Htr. 14	1.396	1.120	1.277	1.447	1.147	1.320	1.143	1.422	1.288

[a]Thermocouple failed.

Table 7. Selected normalized temperatures[a] from FFM bundle 3A, test 2

Run No.	101	102	103	104	105	106	107	108	109
Power, kW/ft	10	8	5	10	8	5	10	8	5
Flow, gpm	54	54	55	43	44	44	33	32	32
Mixed-mean temp. rise, °F	162	129	79.5	203	159	99.4	265	219	137
Normalized temperature									
Exit ch. 3	1.455	1.473	1.488	1.512	1.500	1.448	1.466	1.471	1.438
Exit ch. 16	1.246	1.266	1.288	1.262	1.260	1.243	1.215	1.211	1.218
Exit ch. 17	0.938	0.972	0.966	0.930	0.940	0.950	0.891	0.910	0.938
Exit ch. 40	0.826	0.847	0.858	0.843	0.841	0.853	0.831	0.837	0.850
Exit ch. 42	0.711	0.706	0.714	0.729	0.722	0.720	0.725	0.724	0.719
Exit ch. 43	0.738	0.660	0.661	0.757	0.759	0.682	0.743	0.760	0.701
Exit ch. 6	1.473	1.481	1.496	1.562	1.517	1.460	1.534	1.504	1.435
Exit ch. 8	1.088	1.109	1.154	1.138	1.150	1.112	1.106	1.113	1.097
Exit ch. 28	0.846	0.837	0.856	0.863	0.853	0.838	0.838	0.851	0.835
TC 0117U ch. 3	1.274	1.285	1.309	1.329	1.313	1.271	1.310	1.297	1.254
TC 1017U ch. 35	1.033	1.035	1.050	1.045	1.037	1.002	1.007	0.997	0.962
TC 0619U ch. 4	1.423	1.429	1.463	1.486	1.452	1.397	1.451	1.430	1.386
TC 0919U ch. 32	0.939	0.959	0.968	0.960	0.954	0.931	0.931	0.921	0.894
TC 0521U ch. 3	1.527	1.541	1.577	1.594	1.568	1.516	1.567	1.541	1.494
TC 0423U ch. 2	1.509	1.521	1.555	1.576	1.554	1.504	1.550	1.544	1.494
TC 0815A htr. 8	1.052	1.061	1.071	1.061	1.045	1.021	1.023	1.005	0.979
TC 0815B ch. 8	0.927	0.933	0.953	0.967	0.948	0.924	0.957	0.944	0.920
TC 0217A htr. 2	1.326	1.339	1.348	1.396	1.373	1.320	1.381	1.363	1.307
TC 0217B ch. 1	1.244	1.245	1.288	1.309	1.278	1.229	1.292	1.276	1.229
TC 0719A htr. 7	1.482	1.487	1.513	1.533	1.506	1.447	1.503	1.475	1.413
TC 0719B ch. 6	1.325	1.334	1.355	1.391	1.364	1.311	1.375	1.350	1.300

[a]Normalized temperature $\equiv (T - T_{in})/(T_{out} - T_{in})$.

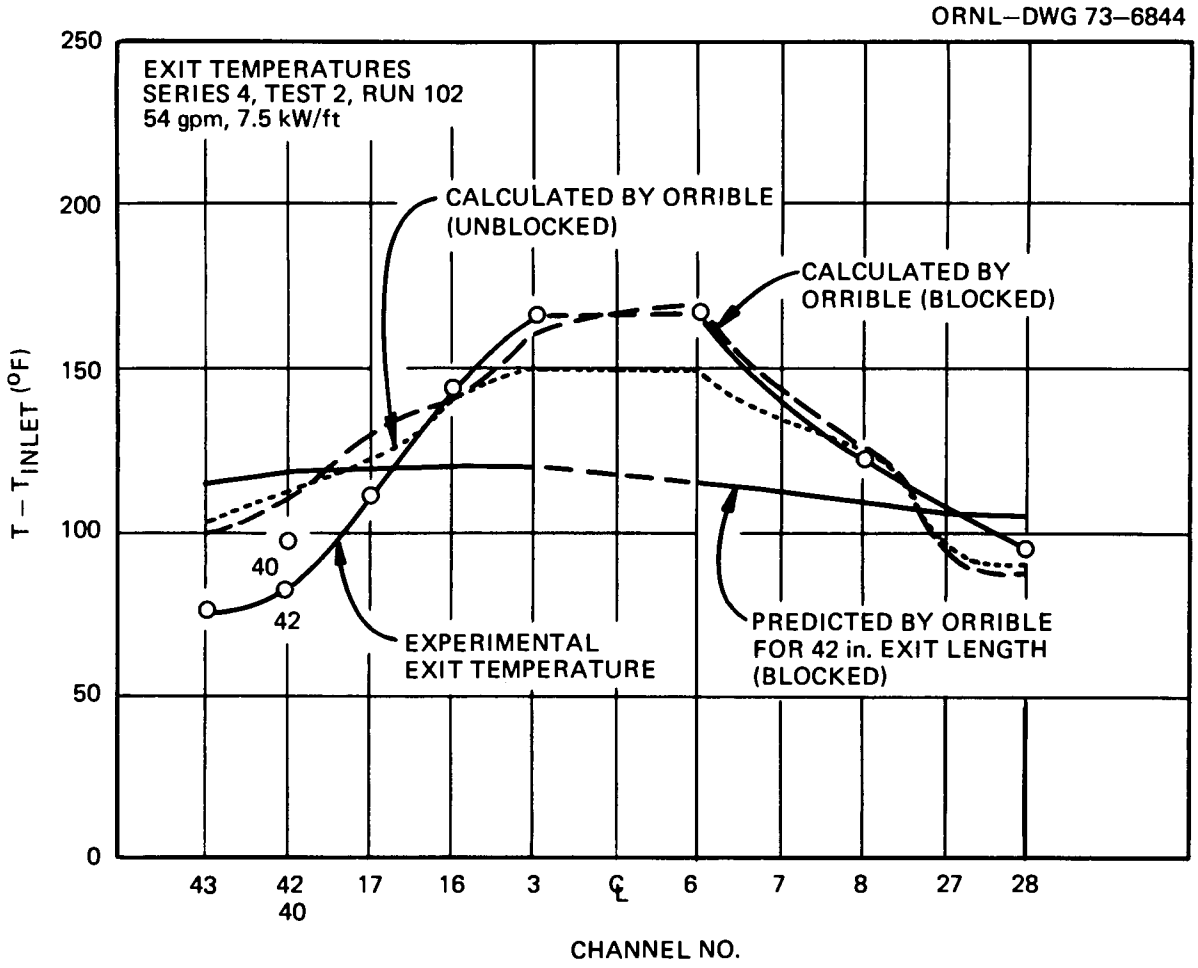

Fig. 20. Exit temperature distribution for bundle 3A type with 3- and 42-in. exit plenums.

4. ANALYSES AND EXTRAPOLATION OF BLOCKAGE EFFECTS

4.1 Calculated Effect of a Six-Channel Internal Blockage in a Full-Size Fuel Subassembly

The six-channel blockage tested in FFM bundle 3A covers a small fraction of the total flow area of the 19-pin experimental bundle. Therefore, the local temperatures measured in the vicinity of the blockage can be expected to be typical of local temperatures of identical blockages in a larger bundle. Because of the effect of the walls on the rod bundle, however, one might expect that the temperature distribution some distance from the blockage might be different in the full-size bundle.

The 217-pin version of ORRIBLE was used to compute the temperature distributions for 42 in. along one of the central heated channels (channel 3) at the exit of the heated zone and at the exit of the 42-in. unheated length.

Figure 21 shows the predicted axial temperature distribution for channel 3 for the unblocked case and the case where the blockage exists 6 in. from the exit end of the heated zone. This position was chosen so that comparison could be made with bundle 3A, which had the same length over which heat could be added

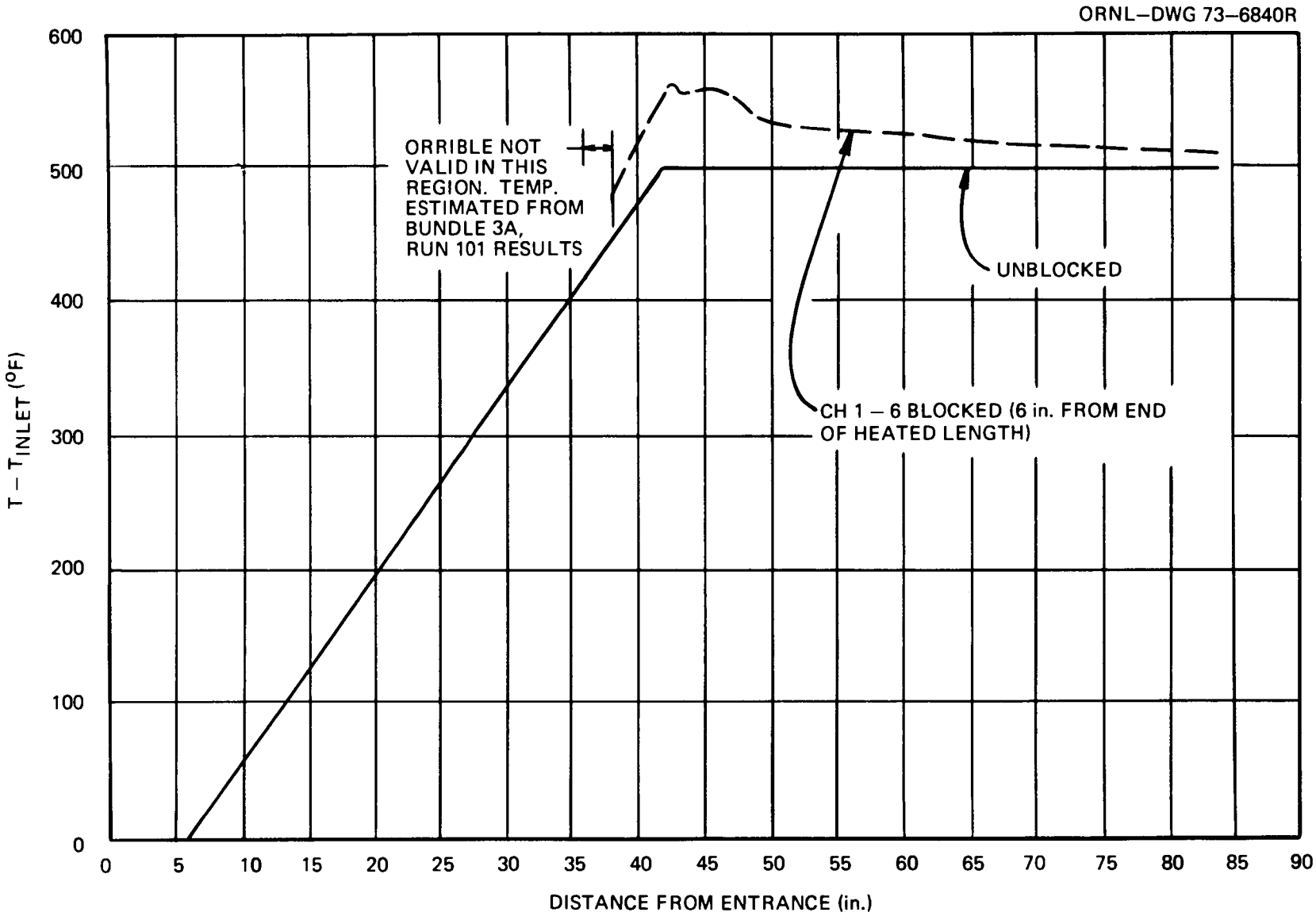

Fig. 21. Calculated temperature distribution in channel 3 for 217-rod bundles. 60% flow, 10 kW/ft.

to the perturbed flow (thereby acting as a tracer) prior to leaving the bundles. The temperature in the zone 2 in. downstream of the blockage was inferred from bundle 3A experimental results.

Figure 22 shows the calculated temperature distribution plotted across the exit of the 217-pin bundle heated zone. The numbers on the abscissa identify the channels from the eleven o'clock corner of the rod bundle to the five o'clock corner. This figure shows a temperature spike of about 90°F for channel 6, which is considerably hotter than the 20°F measured in bundle 3A at the plane 3 in. downstream from the end of the heated zone. Inspection of Fig. 22 indicates that the computed temperature of the central channel of the 217-rod bundle does not drop to within 20°F of the unblocked case until the flow reaches a level around 13 in. downstream from the end of the heated zone. The reasons for the difference between the 19-pin case and the 217-pin case are not known at this time. Perhaps mixing with cooler wall sodium from peripheral channels might be responsible for lower temperatures in the 19-pin bundle.

Figure 23 shows the temperature distribution at the exit of the rod bundle after the flow had traversed 42 in. of unheated zone representing the exit reflector and fission gas plenums. This figure shows that the blockage would perturb the exit temperature distribution by about 10°F, although the exit mixed-mean temperature would remain the same. This indicates that FFTF exit instrumentation, since it measures mixed-mean temperature, could not detect the six-channel blockage. However, a future system using several thermocouple and cross-correlation techniques might detect changes in temperature distribution caused by blockages of the size considered here (and larger).

4.2 Analytical Representation of Flow Downstream from Planar Blockages

If the flow patterns resulting from blockages within an LMFBR core could be described in detail, the calculation of local cladding and coolant temperatures, in principle, would be straightforward. However, at present there have been no demonstrated reliable calculations of recirculating flows downstream of planar blockages. Consequently, to gain insight into the problem and to guide in interpreting experimental data, we have calculated internal temperatures within artificial cylindrically shaped "recirculation cells." These cells are essentially simple arbitrary models of recirculation zones. They contain no surfaces or subchannels that correspond to fuel rods, although such surfaces surely cause significant local perturbations. This difference can be rationalized by the evidence that recirculation zones in blocked bundles *may resemble* wakes in free stream flow.[24]

4.2.1 Description of the model. Figure 24 shows a half cross-sectional view of a typical hypothetical cell in which the recirculating fluid is invested with sodium properties and internal heat generation. The flow is specified to recirculate within an arbitrary number of equal-area internal flow "channels" (five are shown in Fig. 24) corresponding perhaps to stream tubes in real wakes. The flow in each channel is assumed to be constant at values that change stepwise linearly from zero at the stagnation center of the cell to an arbitrary maximum with velocity V_0 in the outermost channel. The flow essentially makes right-angle turns at the top and bottom of each channel and moves radially within varying area channels that divide the length of the cell into equal axial increments. We do not imply that such a flow pattern, satisfying only continuity, is realistic. However, the resulting calculated temperatures may behave similarly to those in real wake zones.

Heat is assumed to be uniformly generated internally within the cell volume at a rate equivalent to 8 kW/ft per rod in a fuel bundle of the size and spacing of the FFTF. This heat is transferred internally by forced convection, molecular conduction, and turbulent mass exchange between adjacent channels. At the outer and top side boundaries of the cells, the heat is transferred to a main stream flow by forced convection using an assigned heat transfer film coefficient. The main stream temperature is assumed to be

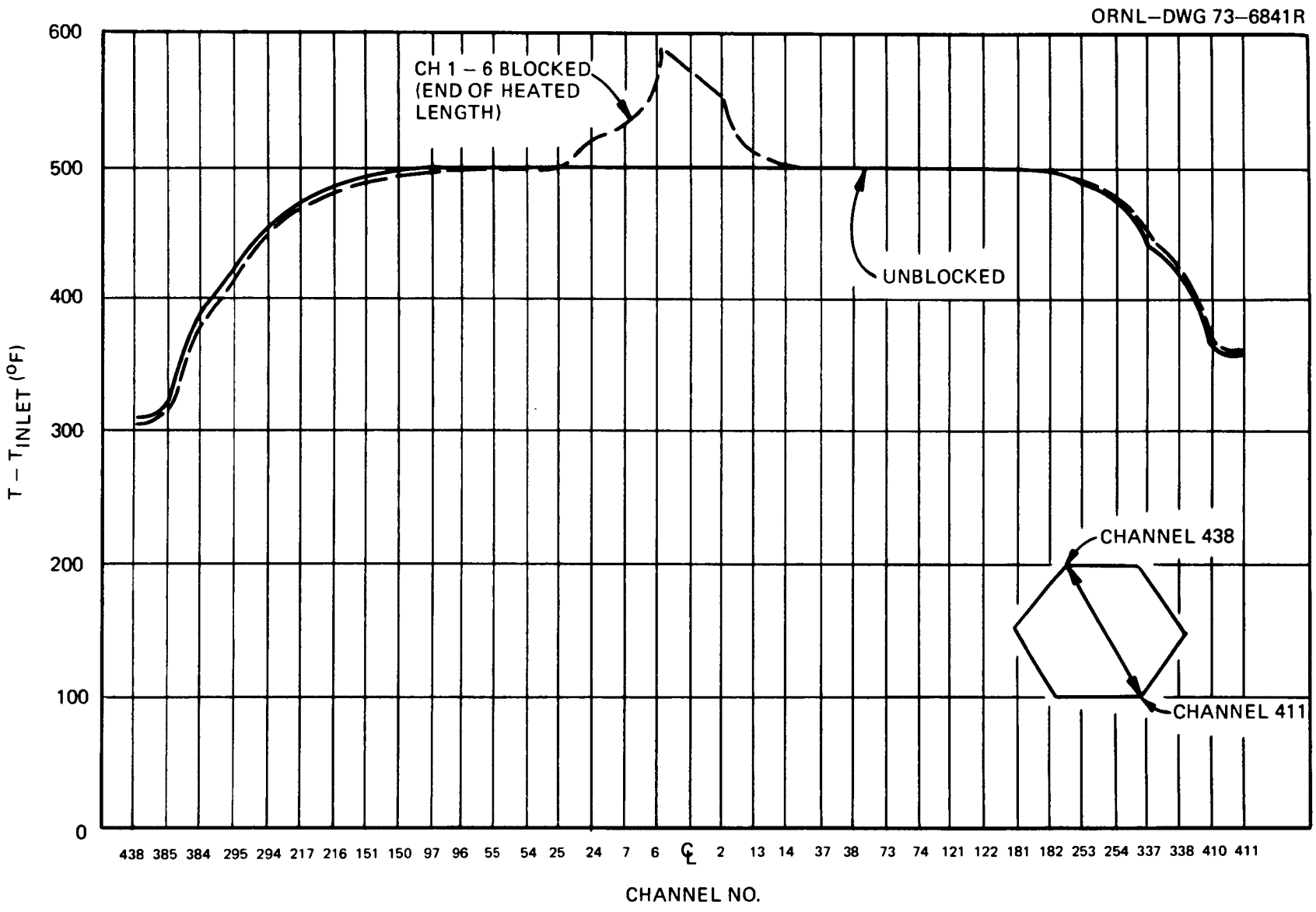

Fig. 22. Calculated temperature for 217-rod bundle, end of heated zone.

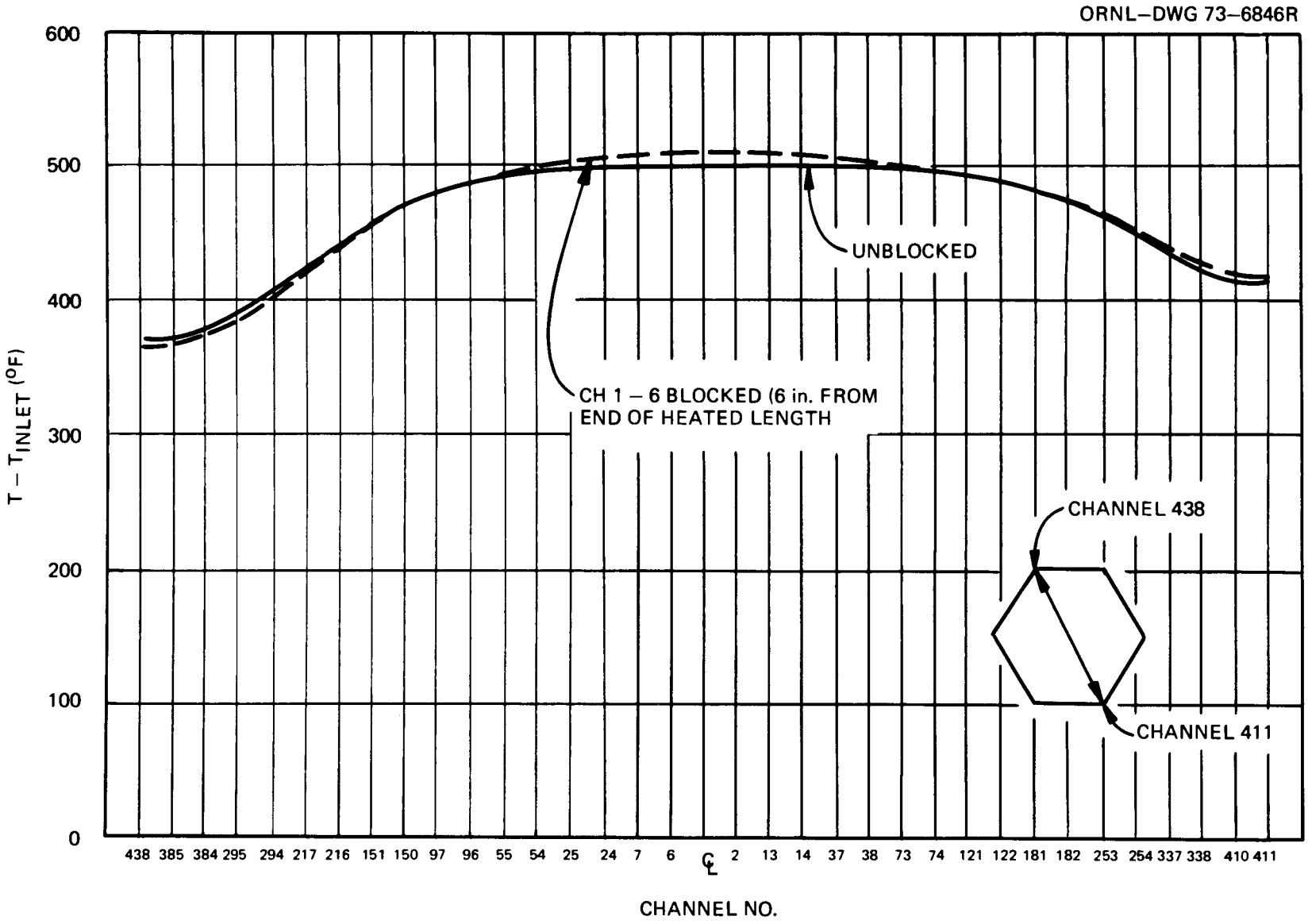

Fig. 23. Calculated temperature for 217-rod bundle, end of 42-in. exit plenum.

ORNL–DWG 73–7056

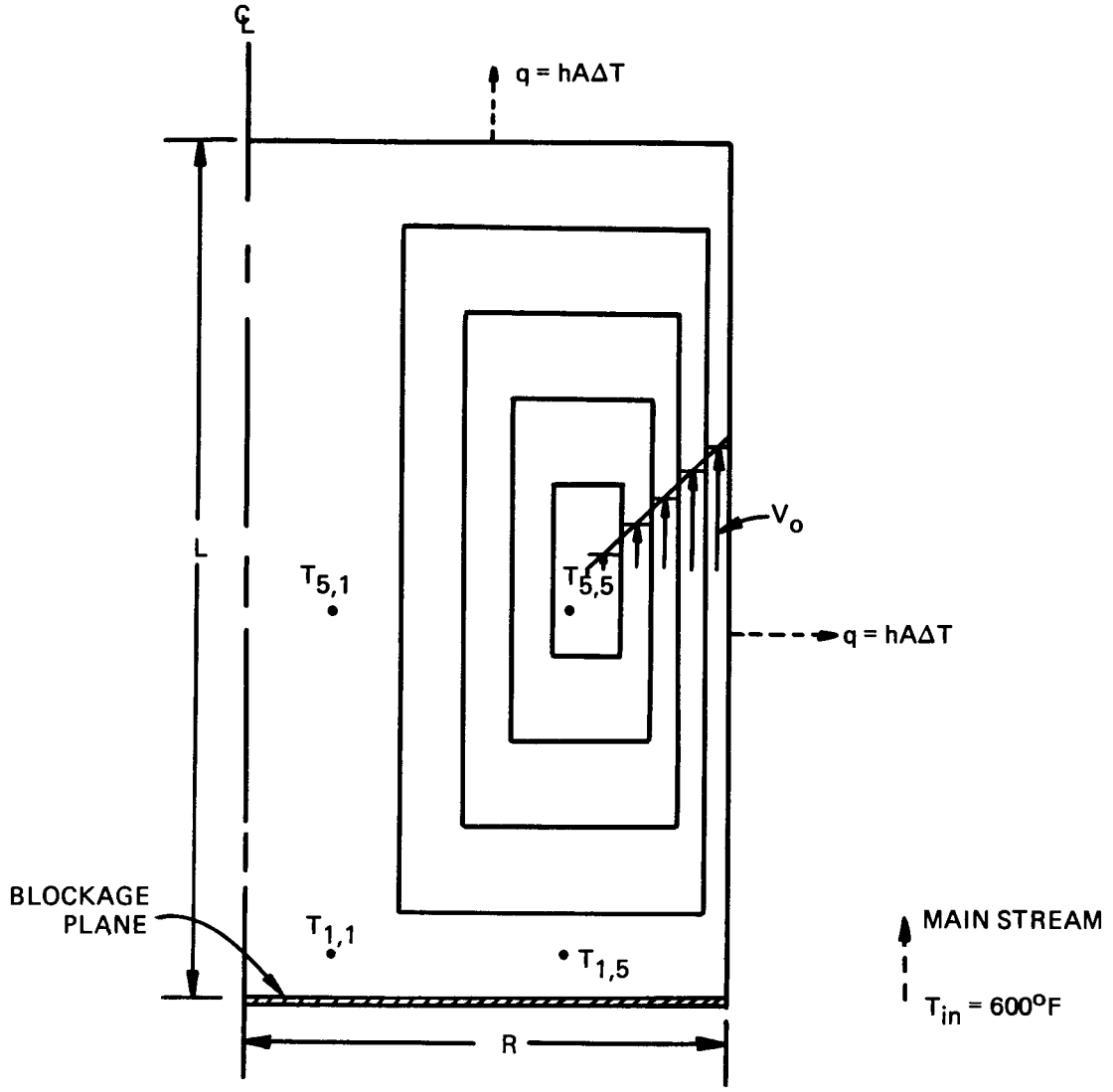

Fig. 24. Illustration of an artificial recirculation cell.

600°F at the blockage plane and is allowed to increase linearly along the length of the cell at a rate of 72.2°F/ft (equivalent to ~2.8 gpm flow for each fuel pin with a heat output of 8 kW/ft per rod).

Internal temperatures were determined by dividing the cells into a finite number of nodes, applying a heat balance to each node, and solving the resulting set of simultaneous equations on a digital computer. The equations and their derivation are presented in the Appendix. The ratio of length of the recirculation zone to radius of the blockage (L/R), the blockage size (R), the recirculation rate (V_0), and the boundary heat transfer coefficient (h) were treated as independent parameters and were varied in the calculations. Cell sizes considered were 0.247 in. (corresponding to a blockage of approximately 6 channels), 0.57 in. (corresponding to a blockage of approximately 24 channels), and 2.18 in. (corresponding to an area blockage of approximately 50% of a full-sized FFTF 217-pin subassembly).

4.2.2 Results of computations. Figure 25 is a plot of typical calculated isotherms for a 0.57-in. blockage, $L/R = 6$, $V_0 = 30{,}000$ ft/hr, and $h = 5 \times 10^4$ Btu hr^{-1} ft^{-2} $(°F)^{-1}$. For this case with a moderate rate of recirculation, the maximum temperature occurred at the cell stagnation point, which was located a considerable distance away from the actual blockage plane. In general, however, the location of the maximum calculated temperature depends on the recirculation rate. For example, Figs. 26–28 show

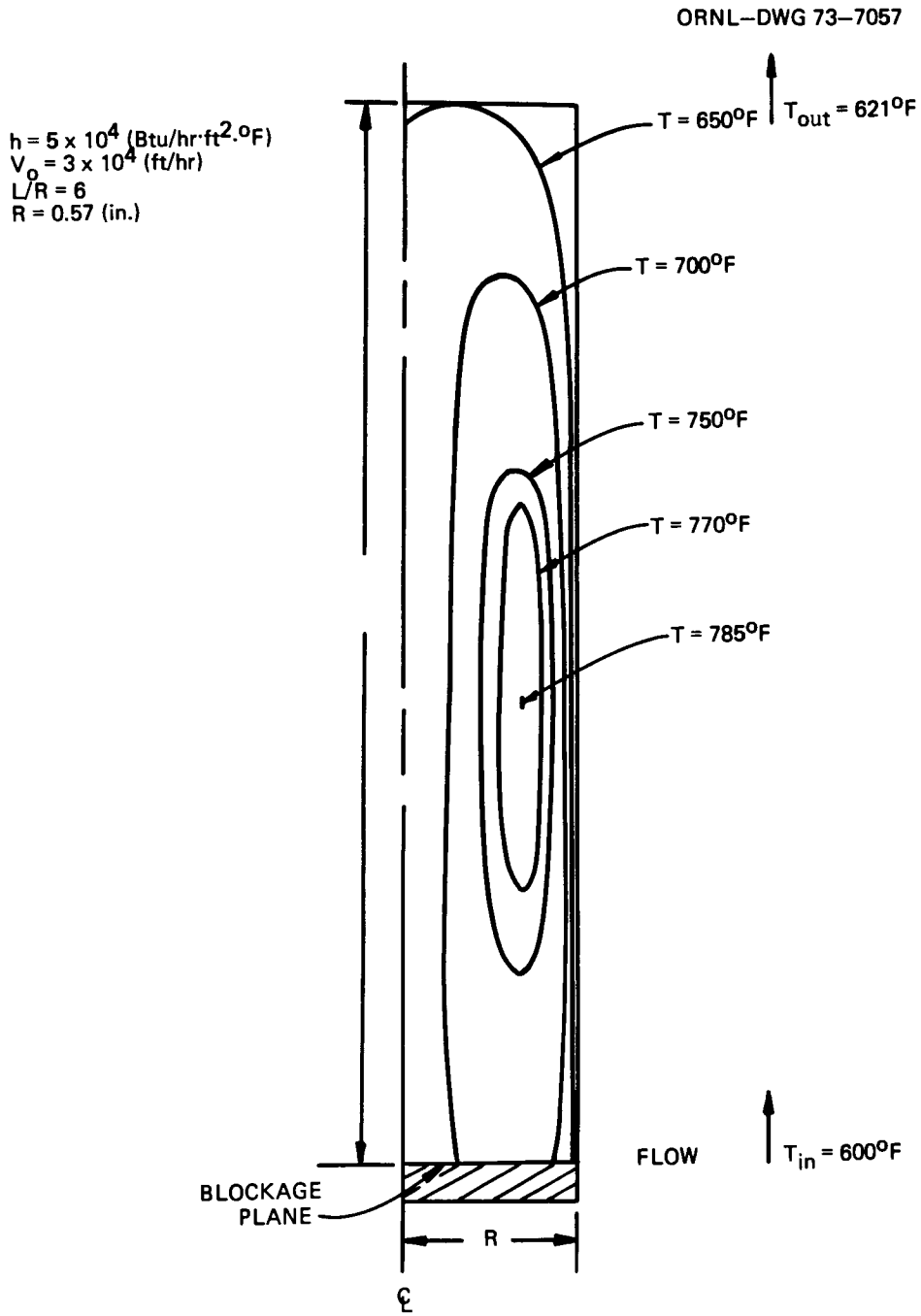

Fig. 25. Typical calculated isotherms in a recirculation cell.

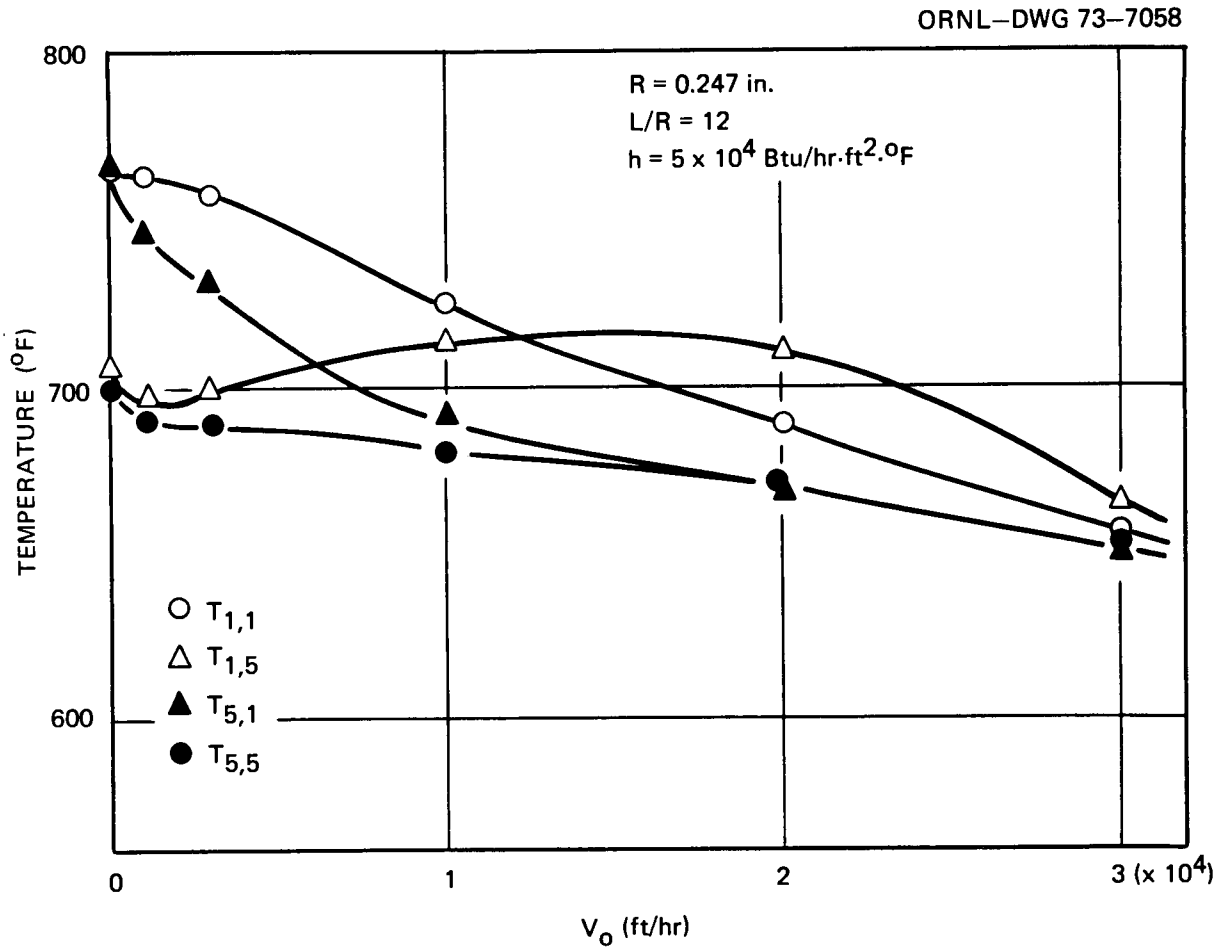

Fig. 26. Recirculation cell internal temperature vs recirculation rate.

calculated temperatures at selected locations (identified in Fig. 24 as $T_{1,1}$, $T_{1,5}$, $T_{5,1}$, and $T_{5,5}$). In these calculations, the heat transfer film coefficient was held constant at 5×10^4 Btu hr^{-1} ft^{-2} $(°F)^{-1}$, while the recirculation rate was varied from 30,000 ft/hr to zero, where only pure molecular conduction acts to remove the heat. The L/R was 12 and the blockage radii (R) were 0.247 and 0.57 in., respectively, for Figs. 26 and 27. Figure 28 was for $R = 0.57$ and $L/R = 6$.

Figure 26 demonstrates that for small blockages (equivalent to 6 channels), molecular conduction alone, without recirculation in the wake zone, is sufficient to prevent excessively high temperatures. However, for larger blockages (equivalent to 24 channels), moderate rates of recirculation are necessary (Figs. 27 and 28). Values greater than ~8000 ft/hr (2.22 ft/sec) for the maximum velocity in the recirculation zone are needed to result in calculated maximum temperatures lower than 1000°F.

Comparison of Figs. 26 and 27 indicates that the value of the maximum temperature depends strongly on blockage size. This is seen more clearly in Fig. 29, which presents the temperature of the location $T_{1,1}$ (see Fig. 24) as a function of blockage radius for different recirculation rates. Values held constant were $L/R = 6$ and $h = 5 \times 10^4$ Btu hr^{-1} ft^{-2} $(°F)^{-1}$. The temperature is seen to depend strongly on the blockage size and the recirculation rate. The effects of independently varying L/R and h at a constant recirculation rate of 30,000 ft/hr are indicated in Fig. 30.

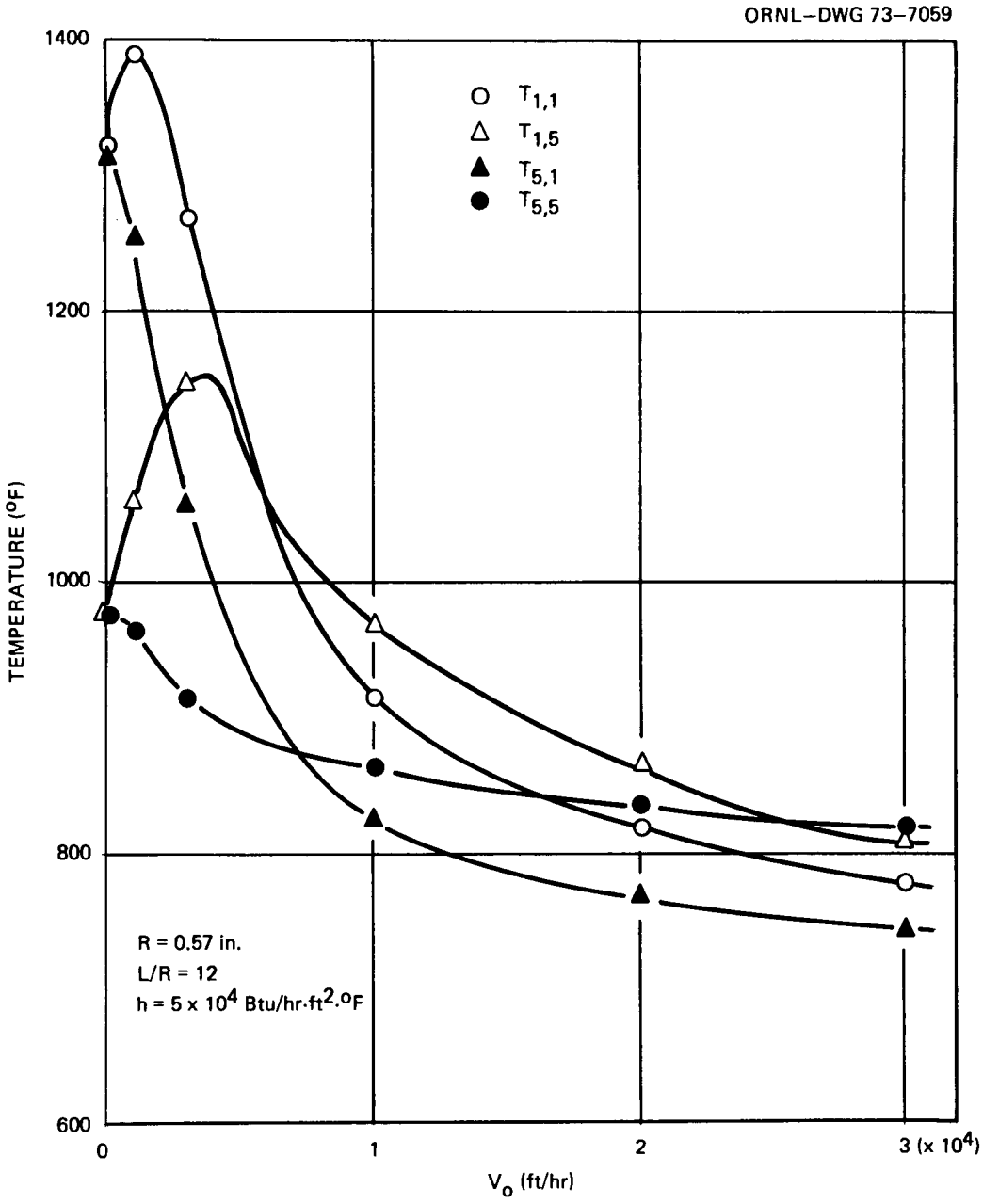

Fig. 27. Recirculation cell internal temperature vs recirculation rate.

4.2.3 Comments on the recirculation model. These results for artificial recirculation cells indicate that, for small blockages (equivalent to ~6 channels), conduction alone is sufficient to prevent excessively high temperatures. There may even be small rates of recirculation that would result in maximum temperatures greater than for pure conduction alone (see Figs. 27 and 28). The location of the maximum temperature depends on the recirculation rate and the blockage size and may be a considerable distance away from the blockage plane. The internal temperatures are seen to depend strongly on the blockage size and its *L/R*

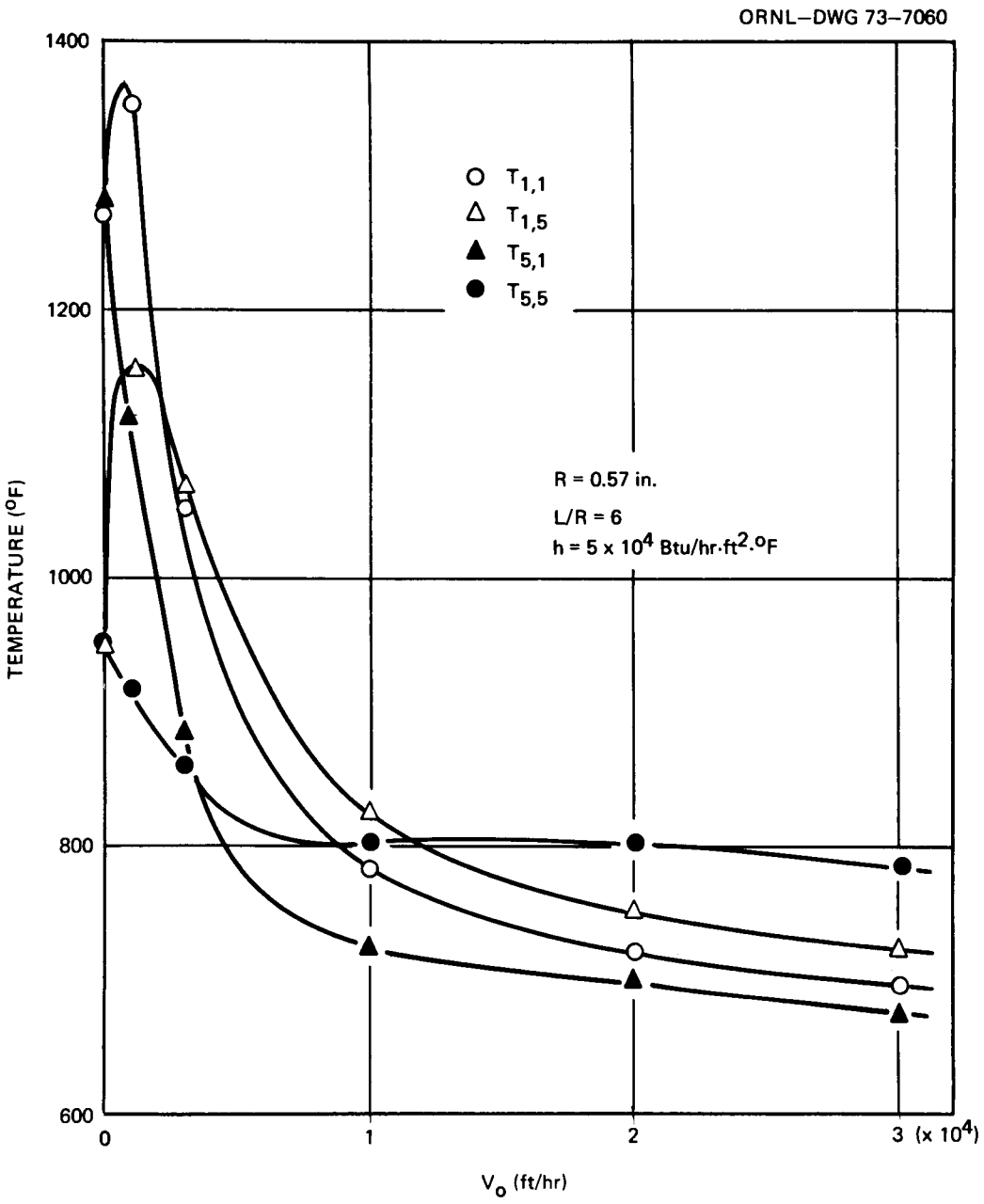

Fig. 28. Recirculation cell internal temperatures vs recirculation rate.

proportion, on the recirculation rate, and on the rate of heat exchange with the main stream flow. Consequently, additional firm conclusions concerning the effects of real blockages cannot be drawn from calculations of this nature until more explicit knowledge of the actual values of these parameters is available. In addition, more realistic modeling of the wake zone is desirable.

The study of artificial recirculation cells appears to be a convenient means for gaining insight into the blockage problem and may serve as an intermediate step toward analyzing blockages until more realistic models become available.

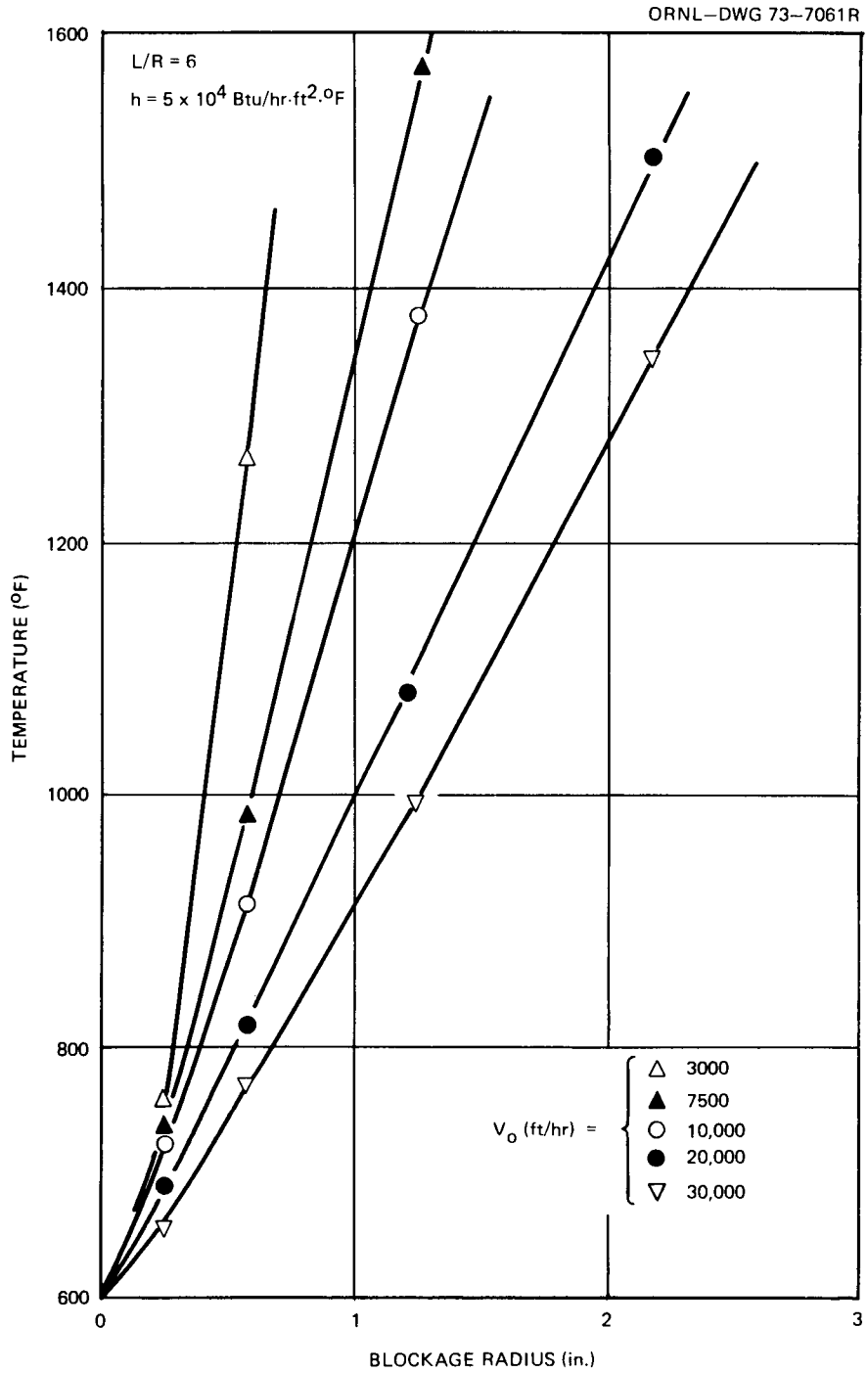

Fig. 29. Recirculation cell internal temperature vs blockage radius as a function of recirculation rate.

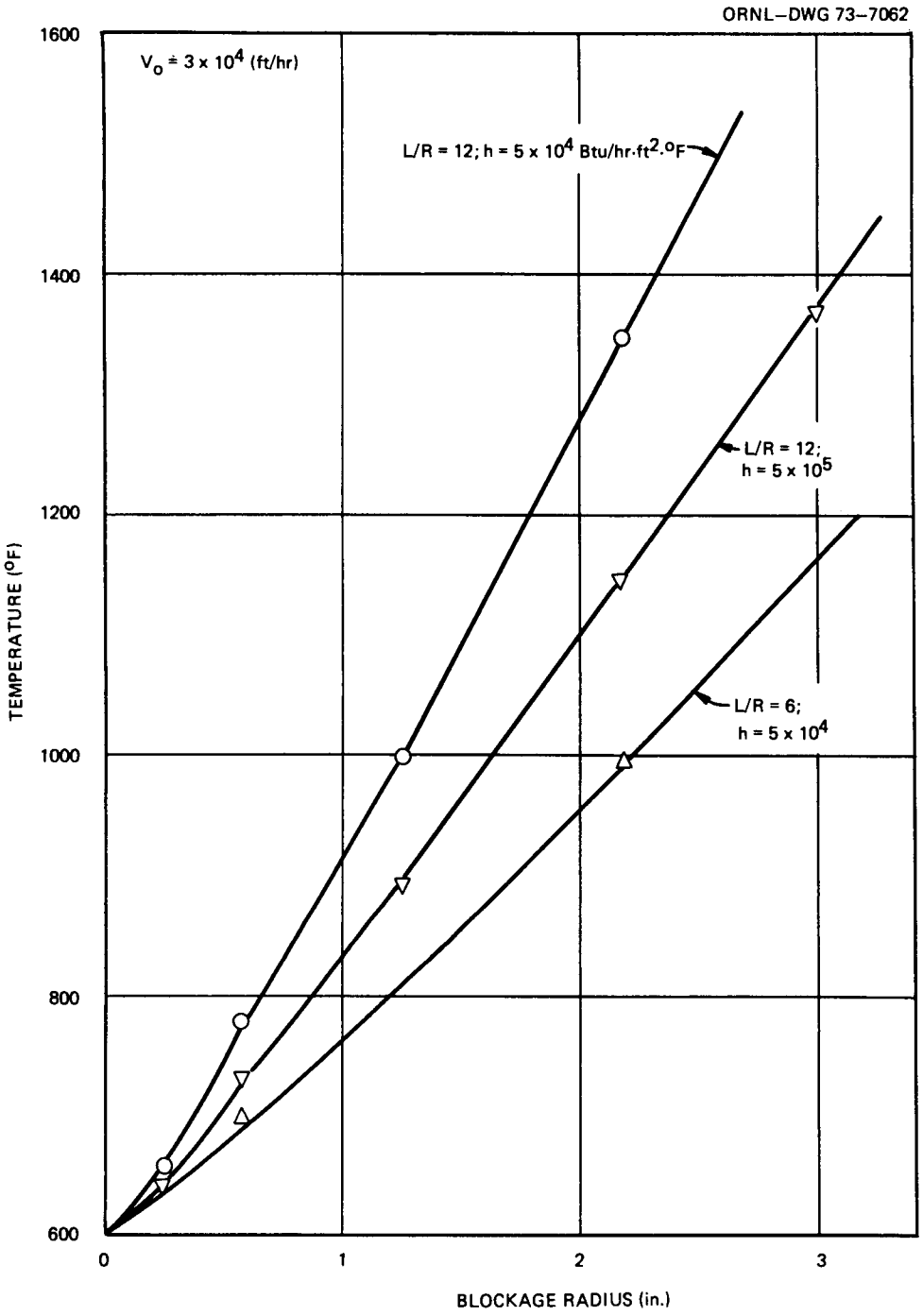

Fig. 30. Recirculation cell internal temperature vs blockage radius for two different values of h and L/R.

4.3 Temperature Distributions within Blockages

In order to obtain estimates of the temperature distribution in in-core blockages, some simple cases have been analyzed using the HEATING[2,3] computer code. The cases examined were (1) infinitely long blockages of one, two, and three adjacent subchannels adjoining a single rod; (2) thin planar blockages of infinite radius (0.1 and 0.25 in. thick); and (3) thin planar blockage of a radius equivalent to a six-channel blockage. Blockages composed of both heat-generating material (UO_2) and non-heat-generating material (stainless steel) have been investigated.

4.3.1 Results of heat conduction computations. Figure 31 shows calculated results for a single channel blocked by a heat-generating material of infinite length. (Lengths greater than ~0.5 in. are essentially infinite with respect to heat flow paths.) The temperatures are predicted to reach a maximum value of less than 2500°F at the center of the fuel and 1850°F in the center of the blocked channel and therefore are acceptable.

The results calculated for the case of blockage of two adjoining channels (Fig. 32) show that temperatures at the center of the blockage region will approach the melting point of UO_2. It appears that the direction of heat flow is into the fuel pins and then out into the unblocked region. This configuration is not acceptable.

Figure 33 shows temperatures at the center planes of non-heat-generating planar blockages 0.10 and 0.25 in. thick having infinite radius. This figure indicates that 0.25 in. is near the maximum allowable thickness of a stainless steel blockage which is too wide for significant radial heat conduction.

Figure 34 shows the temperatures in the center plane of a 0.25-in.-thick heat-generating blockage of infinite radius. This indicates that without radial conduction, temperatures of the cladding will be excessive.

Figure 35 shows the temperature distribution in a heat-generating planar blockage ring, 0.25 in. long and 0.20 in. in radius, where the outer surface of the blockage transfers heat to the sodium at 1200°F. For this case the cladding temperature is about 2500°F. Even if this type of blockage should accumulate in a zone where the temperature is 800°F, the cladding temperature would be above 2100°F and likely would fail. Figure 36 shows that if the heat-generating ring blockage similar to that of Fig. 35 is reduced to 0.125 in. thickness instead of 0.250, its presence would be acceptable.

5. FLOW BLOCKAGE TESTS WITH THE FFM WATER MOCKUP

The objective of studies with the FFM water mockup is to obtain information on the effect of various flow-blockage geometries on (1) temperature distribution in heated rods; (2) flow patterns in the vicinity of a blockage (i.e., the extent of regions of recirculation, cross flow, countercurrent flow, etc.); (3) the exchange rate between the "bubble" behind the blockage and the main flow; and (4) the hydrodynamic characteristics of the tube bundle. Advantages of using water for such tests are: (1) the shroud can be fabricated from clear plastic to permit flow visualization studies, (2) exchange coefficients may be determined using either hot water or salt solution as tracers, and (3) water is much easier to work with than liquid sodium. The principal disadvantage is that some care must be used in interpreting the results in terms of possible consequences of a flow blockage in a liquid-metal-cooled system.

5.1 Description of the Facility

The facility is a triple-scale water-cooled mockup of the Fuel Failure Mockup (FFM) facility. Reynolds number similarity with the FFM is achieved when fluid velocities in each facility are equal.

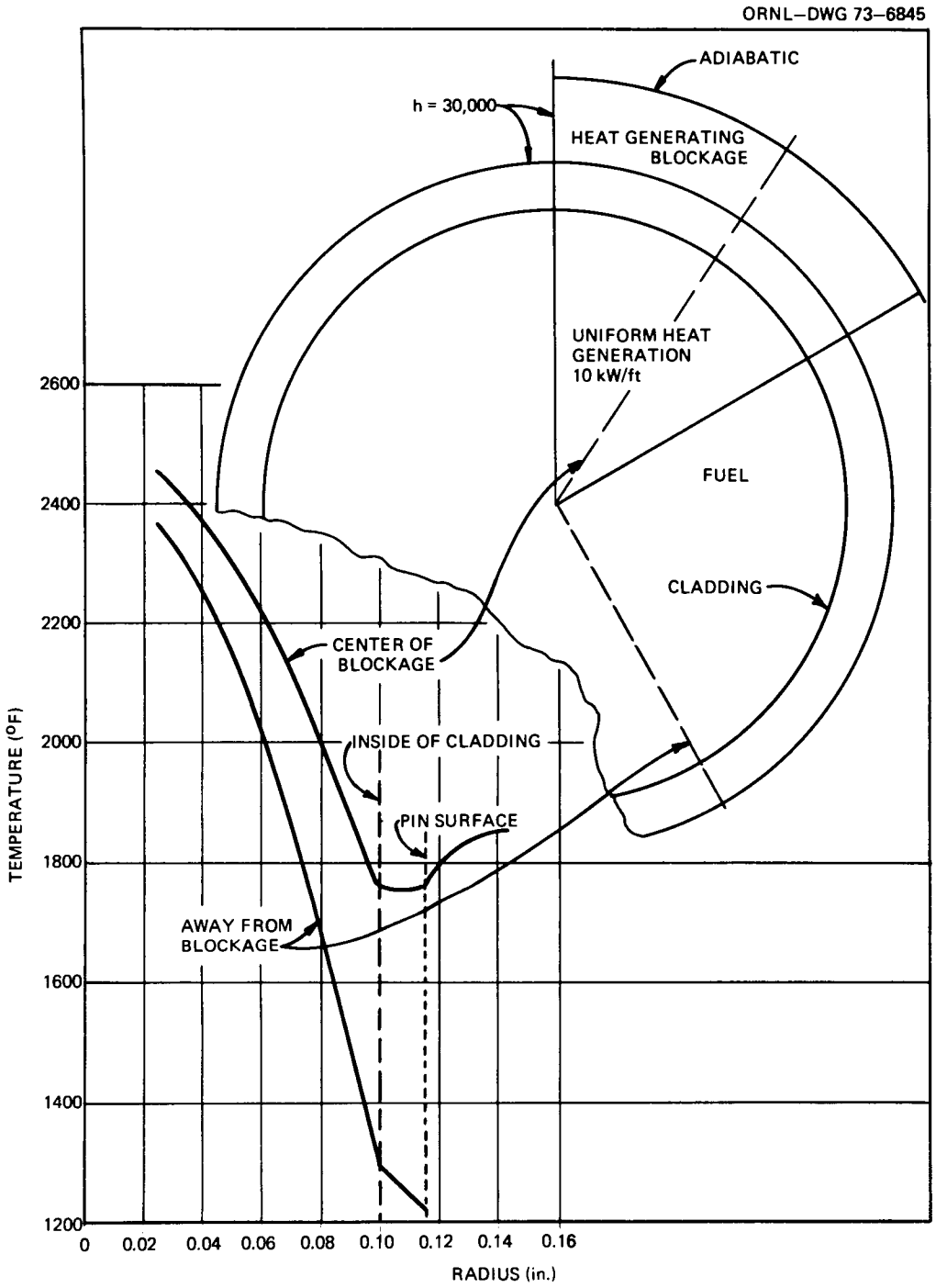

Fig. 31. Radial temperature profile in fuel rod and blockage with single-channel heat-generating blockage.

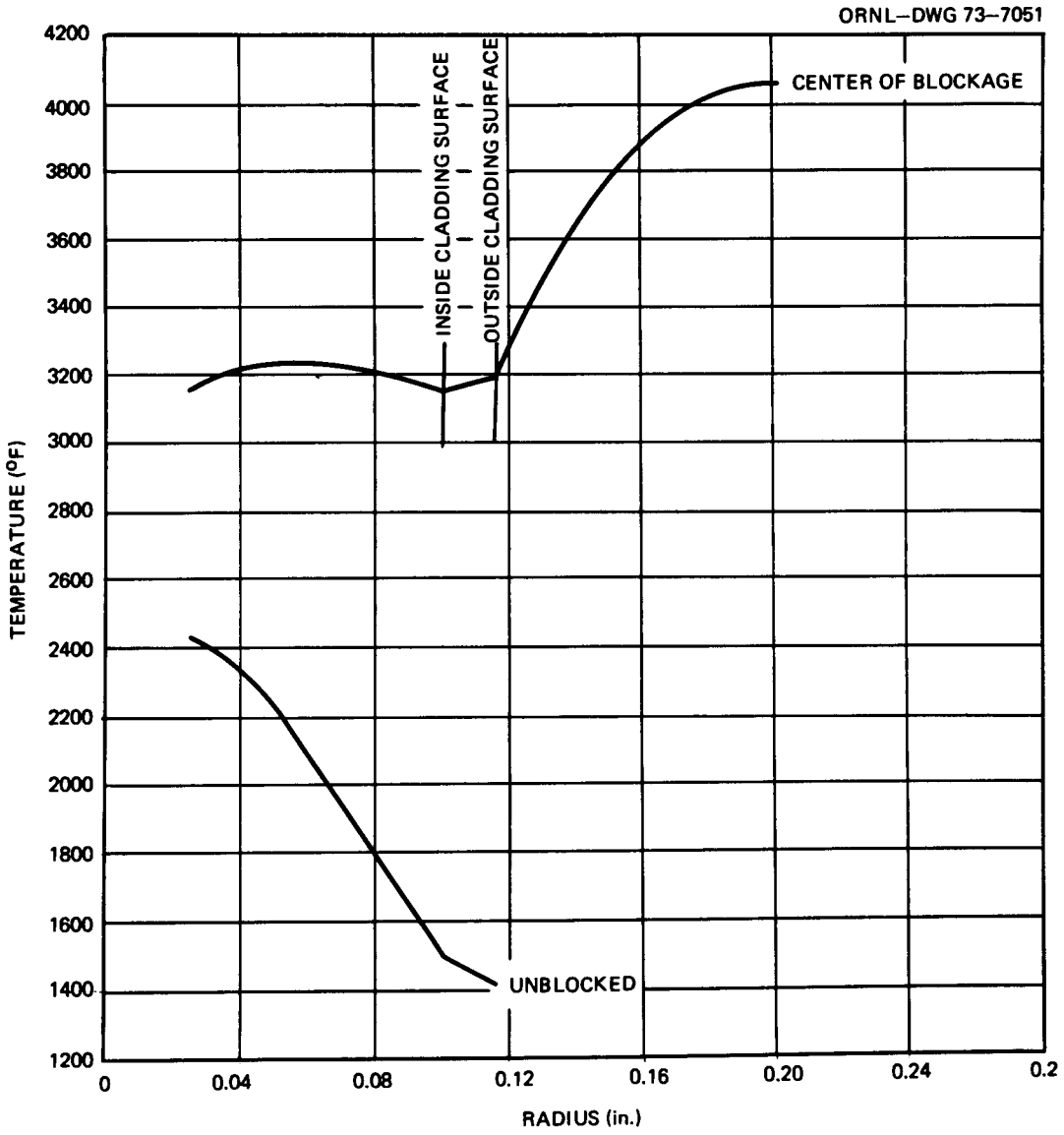

Fig. 32. Radial temperature profile in fuel rod and blockage with heat-generating blockage of two adjacent subchannels.

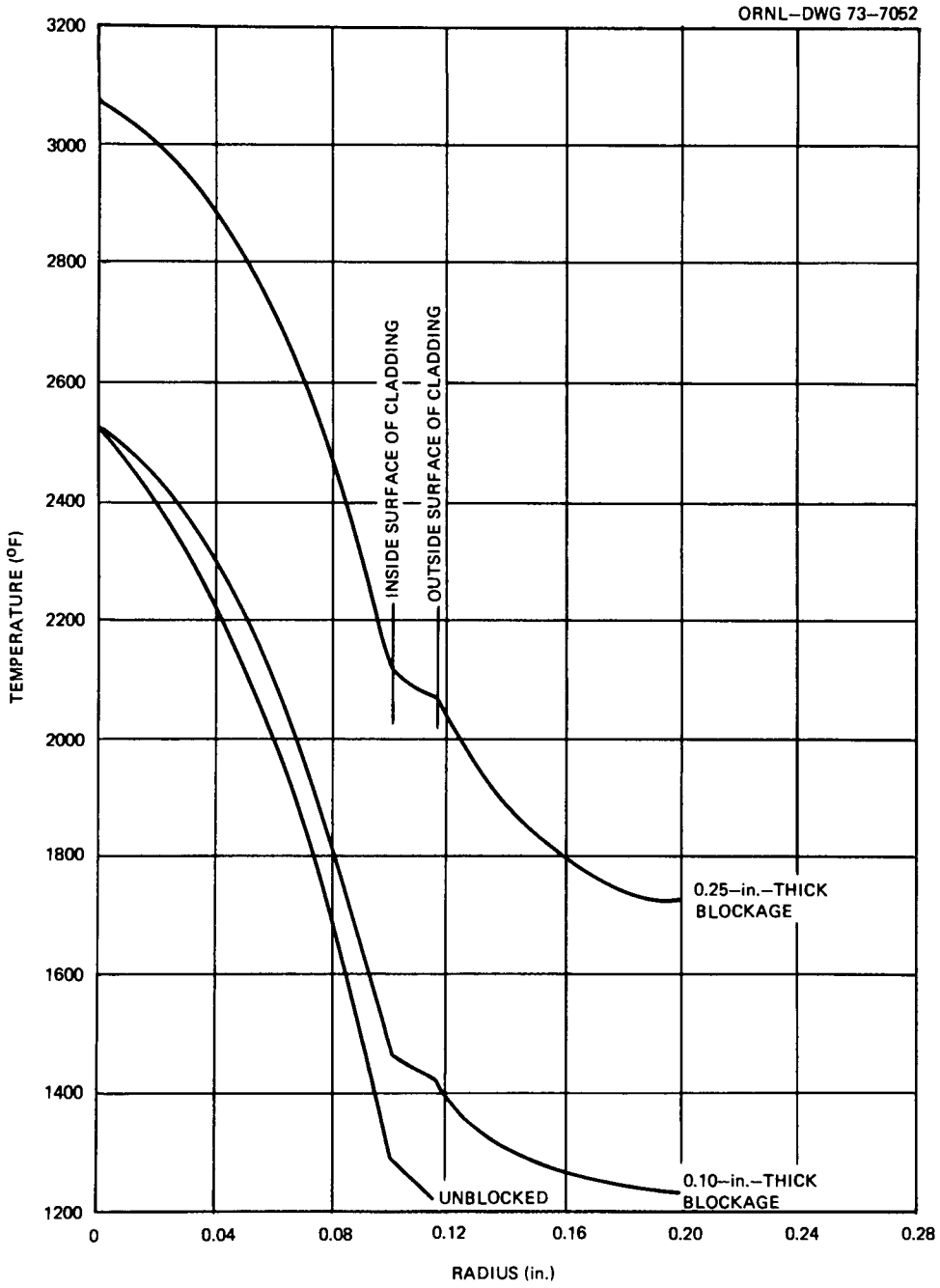

Fig. 33. Radial temperature distribution in fuel and blockage for non-heat-generating planar blockage of infinite radius.

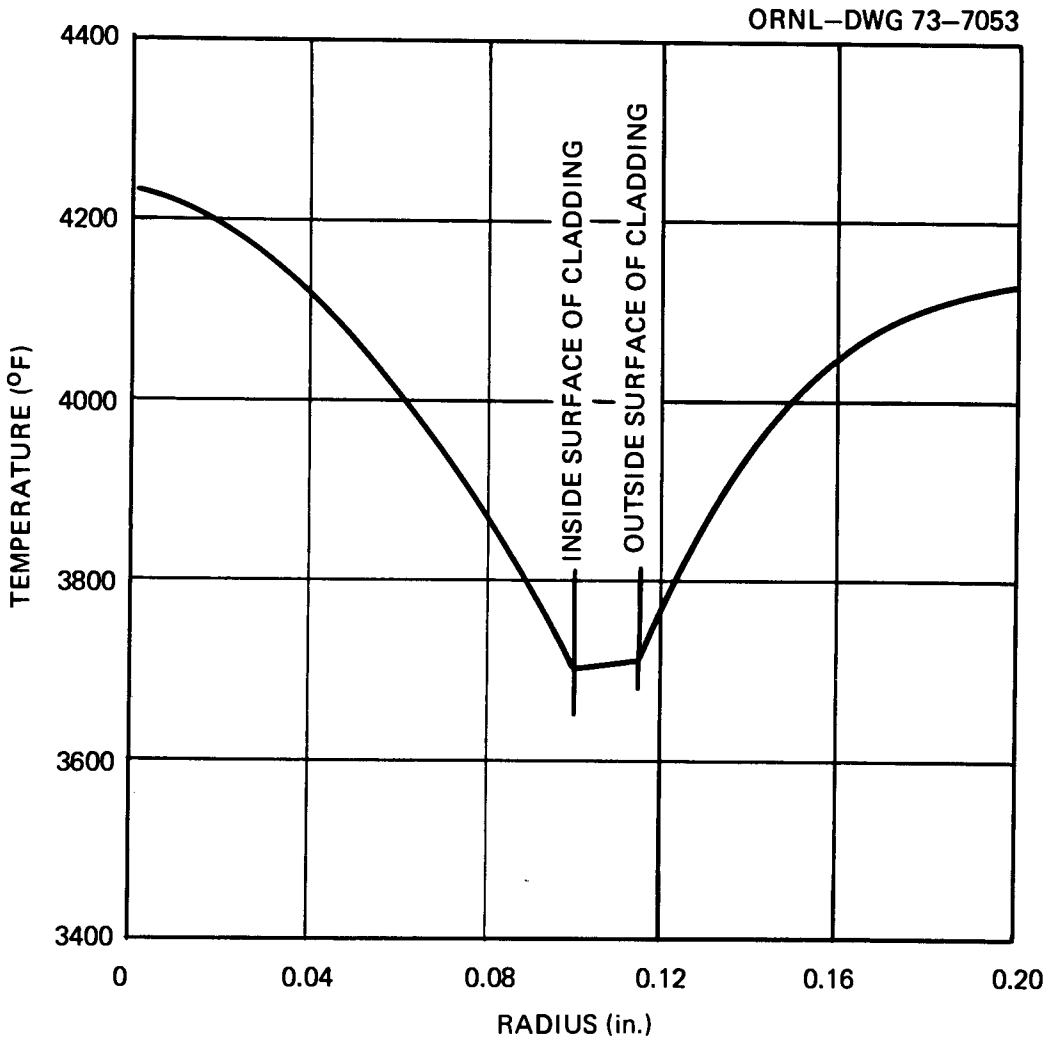

Fig. 34. Radial temperature distribution in fuel and blockage for heat-generating planar blockage 0.25 in. thick and infinite radius.

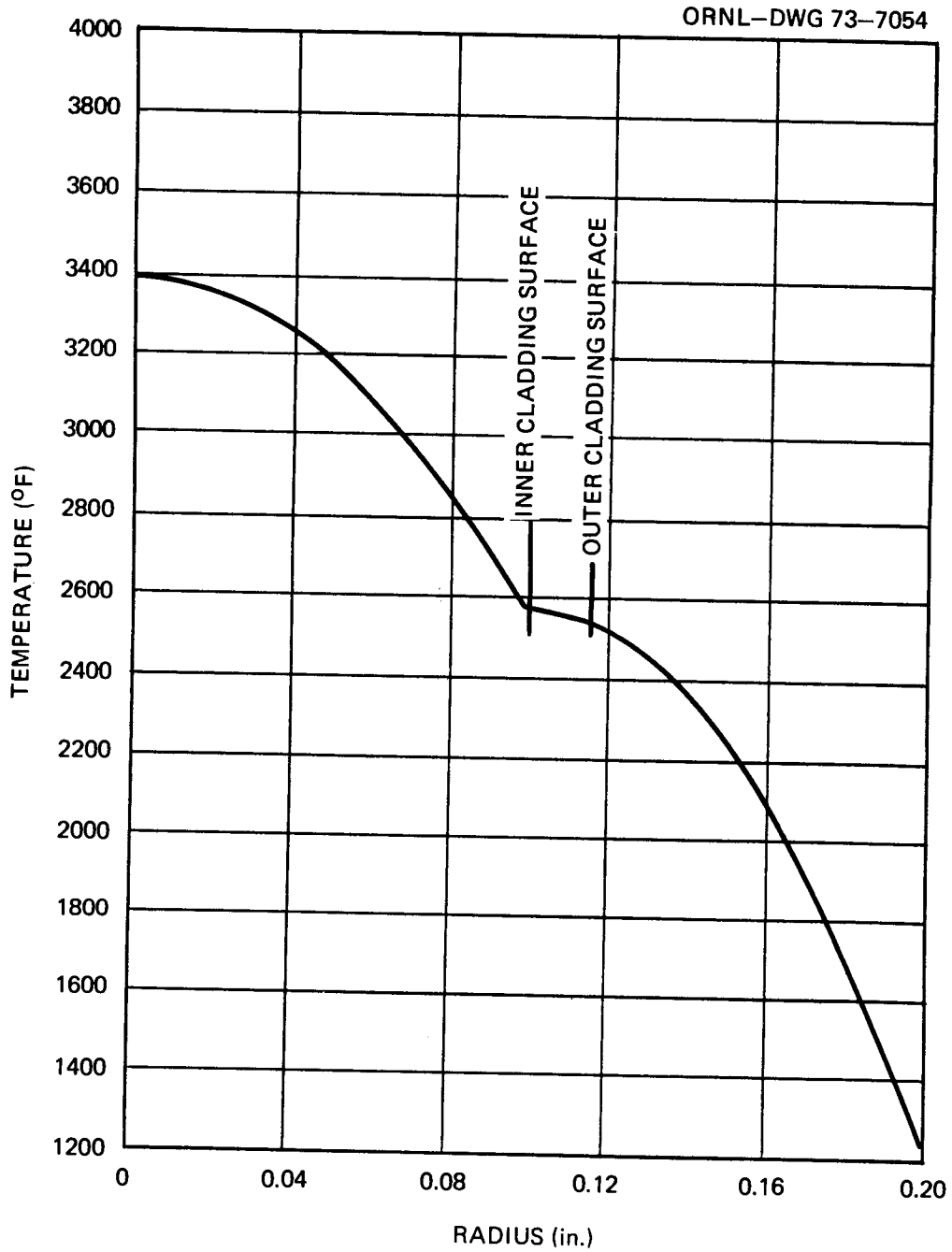

Fig. 35. Radial temperature distribution in fuel and blockage for heat-generating planar blockage 0.25 in. thick and 0.20 in. radius.

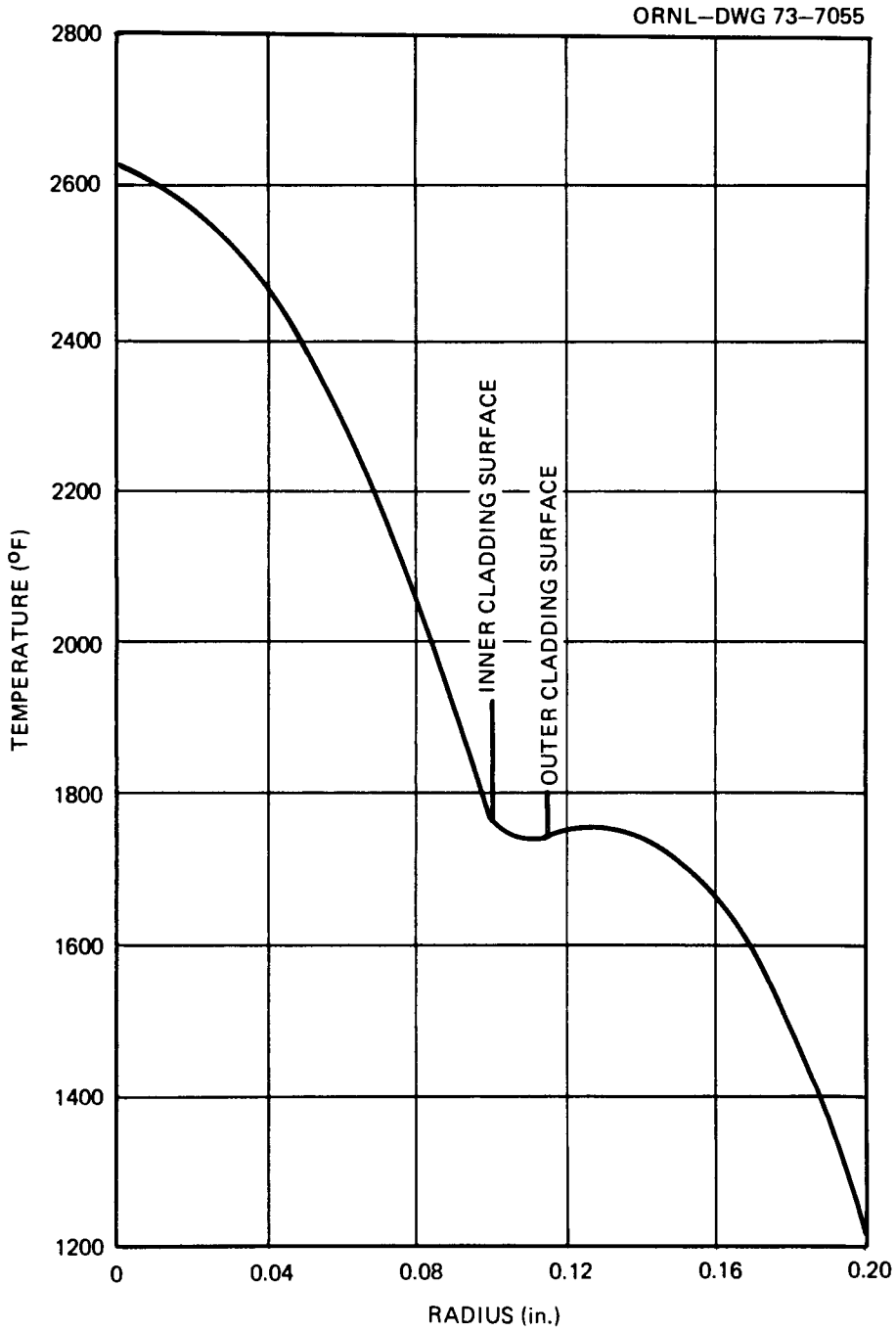

Fig. 36. Radial temperature distribution in fuel and blockage for heat-generating planar blockage 0.125 in. thick and 0.20 in. radius.

A 19-rod bundle is enclosed in a Lucite shroud of hexagonal cross section. One rod is an A-nickel tube that is resistance heated to achieve heat fluxes of $\sim 5 \times 10^5$ Btu hr^{-1} ft^{-2}, yielding water film temperature differences of ~140°F; the remaining 18 rods are constructed of Lucite. The heated rod may be positioned at either the central or a corner position in the bundle.

Demineralized water is circulated through the test section by a 500-gpm centrifugal pump, and a shedding-vortex flowmeter is used to determine the flow rate. Flow blockages in the test section are simulated by inserting Plexiglas blockage plates in the bundle to block a specific number of flow subchannels.

Six thermocouples at each of three axial stations measure the bulk water temperature in subchannels near the central (heated) rod. A traversing thermocouple assembly inside the A-nickel tube measures the inner wall temperatures at any desired axial or circumferential position. Local heat transfer coefficients are calculable from the measured film temperature differentials and heat flux.

The Lucite shroud assembly containing the 19-rod bundle is 54 in. long and has an external cross section of 6 by 6.5 in. Attached to the lower (upstream) end of the shroud is a 30-in.-long, 5-in.-diam stainless steel tee containing a flow redistribution sieve plate and a 3-in.-long Lucite transition piece to change the flow cross section from circular to hexagonal. The upper (downstream) end of the shroud has a similar tee that is 12 in. long.

The characteristics of the system and maximum experimental conditions achievable are summarized in Table 8.

Table 8. Characteristics of the triple-scale FFM water mockup

System characteristics
Number of rods, 19
OD of rods, 0.682 in.
ID of A-nickel rod, 0.650 in.
Heated length, 36 in.
Pitch/diameter ratio, 1.24
Bundle length, 54 in.
Entry length, 18 in.
Heater power at heat flux of 5×10^5 Btu hr^{-1} ft^{-2}, 81.5 kW
Distance across opposing flats in hexagonal shroud, 3.944 in.
Maximum normal flow rate, 490 gpm
Equivalent diameter with full wire wraps, 0.38 in.
Equivalent diameter with $\frac{1}{2}$ thickness outer wire wraps, 0.32 in.
Spacer wire diameter, 0.165 in.
Spacer wire pitch, 36 in.
Operating characteristics
Maximum heat flux, 5×10^5 Btu hr^{-1} ft^{-2}
Mean bundle velocity at maximum flow, ~30 ft/sec
Maximum N_{Re}, $\sim 10^5$
Maximum flow rate, 490 gpm
Normal range of bulk temp., 20–32°C

5.2 Hot-Water Injection Tests

By injecting hot water at known locations in the tube bundle, some information may be obtained on the nature of the mixing process in the bundle. Because of the special nature of these tests a brief

description of the equipment and procedure will be given here together with some results for the unblocked reference bundle before describing results of blockage tests.

5.2.1. Experimental procedure. Hot water is injected through two 0.143-in.-ID injector tubes located on either side of the helical spacer wire on the central rod, 17 in. above the bundle base. Demineralized water is steam heated in a shell-and-tube heat exchanger and then flows upward through a $^3/_8$-in.-OD copper tube located inside a 0.682-in.-OD copper tube (replacing the 0.682-in. copper bar lower power connection to the A-nickel heater tube). A Chromel-Alumel thermocouple is used to measure the temperature of the injection water immediately before it leaves the injection tubes. The injection flow is essentially parallel to the central rod at the point of injection, and isokinetic injection is approximated by adjusting the injection flow rate, as indicated by a rotameter, to obtain an average velocity of injection equal to the bundle mean velocity. The injection flow rate is ~5% of the calculated flow rate in the six central subchannels, or 0.26% of the total flow rate. In tests with injection ratios of 1.27 and 0.77 times the calculated isokinetic injection ratio, the effect of increasing the injection ratio was to increase the temperature difference measured at a particular location, as was expected. However, normalizing the measured Δt by dividing by the maximum measured Δt (Δt_{max}) yields axial temperature profiles that are very similar. Thus, it is felt that a small departure from isokinetic injection has a minimal effect on the normalized test results.

A traversing thermocouple assembly is used to measure the temperature of the inside wall of the 16-mil-thick central A-nickel tube at any desired axial position downstream of the injection plane. Eighteen bulk water temperature thermocouples are used to measure the fluid temperature in the bundle. By measuring the difference in temperature between the inside wall of the central tube at positions adjacent to each of the six central subchannels and the bulk water temperature at the bundle inlet, the axial temperature profiles of each subchannel are experimentally determined.

Hot-water injection tests with the reference bundle are described in Table 9. As indicated in the footnotes, tests were made with the injector located at three different positions relative to the spacer wire: on the leading side, on the trailing side, and 180° around the tube from the spacer wire.

5.2.2 Results of hot-water injection tests for the unblocked bundle. The axial temperature profiles of the six central subchannels as determined in test 46, in which the hot water was injected near the interface of subchannels 1 and 2 on the leading side of the helical spacer wire, are shown in Fig. 37. In this figure, temperature difference has been normalized by the maximum measured Δt. This procedure was found to yield similar curves for tests 41 to 46; hence Fig. 37 is representative of all results obtained at average velocities from 5.2 to 28 ft/sec, or N_{Re} from 1.6 to 8.3 $\times$ 10^4.

Initial peaks in temperature occurred in subchannel 2 at 3 and 6.5 in. above the injector tube outlet. A secondary rise in temperature in subchannel 2 at 16.5 in. above the injection plane is coincident with the appearance of the spacer wire for rod 3 into this subchannel. The peaks which occur in the temperature profile of each subchannel are spaced approximately 6 in. apart, and the spacer wire spirals through an angle of 60° for each 6 in. of height. The decrease in the magnitude of the temperature peaks with increasing elevation above the injection plane are qualitatively indicative of the degree of mixing caused by the helical wire-wrap spacer.

In order to determine the effect of injector location on the temperature profile, tests 47 to 49 were made with injection near the trailing edge of the spacer wire instead of at the leading edge. Results for test 47 are shown in Fig. 38. Comparison of the results of tests 46 and 47 (made under nearly identical conditions) shows that, in general, there is a great degree of similarity between the results. However, some differences in detail are apparent; for instance, there is a considerable difference between the profiles for subchannels 1 and 2 in the region 1.5 to ~4.5 in. above the injection plane. This difference may be explained by observing that the injected tracer water passes completely through subchannel 1 in a

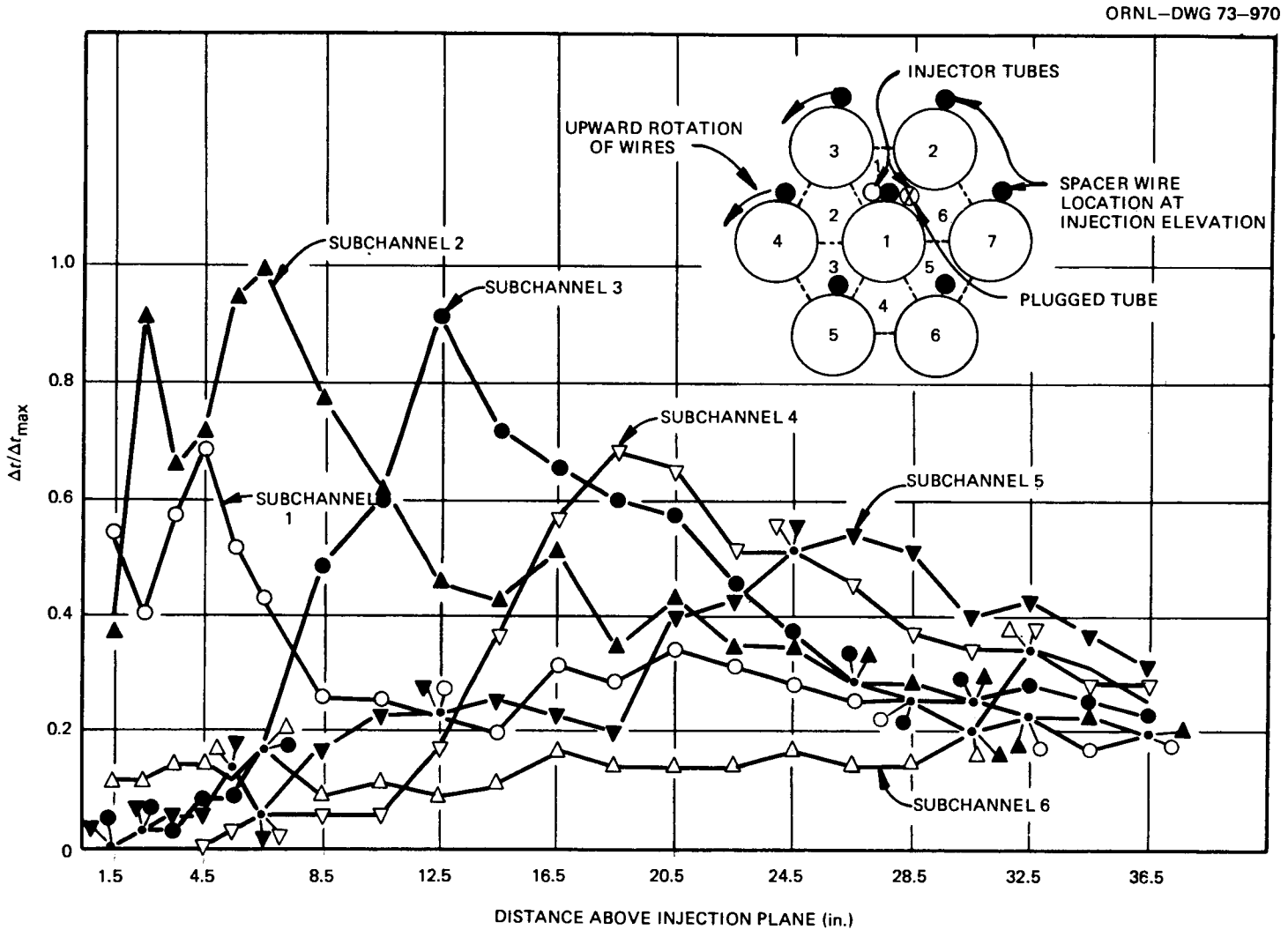

Fig. 37. Central subchannel axial temperature profiles for hot-water injection. Test 46.

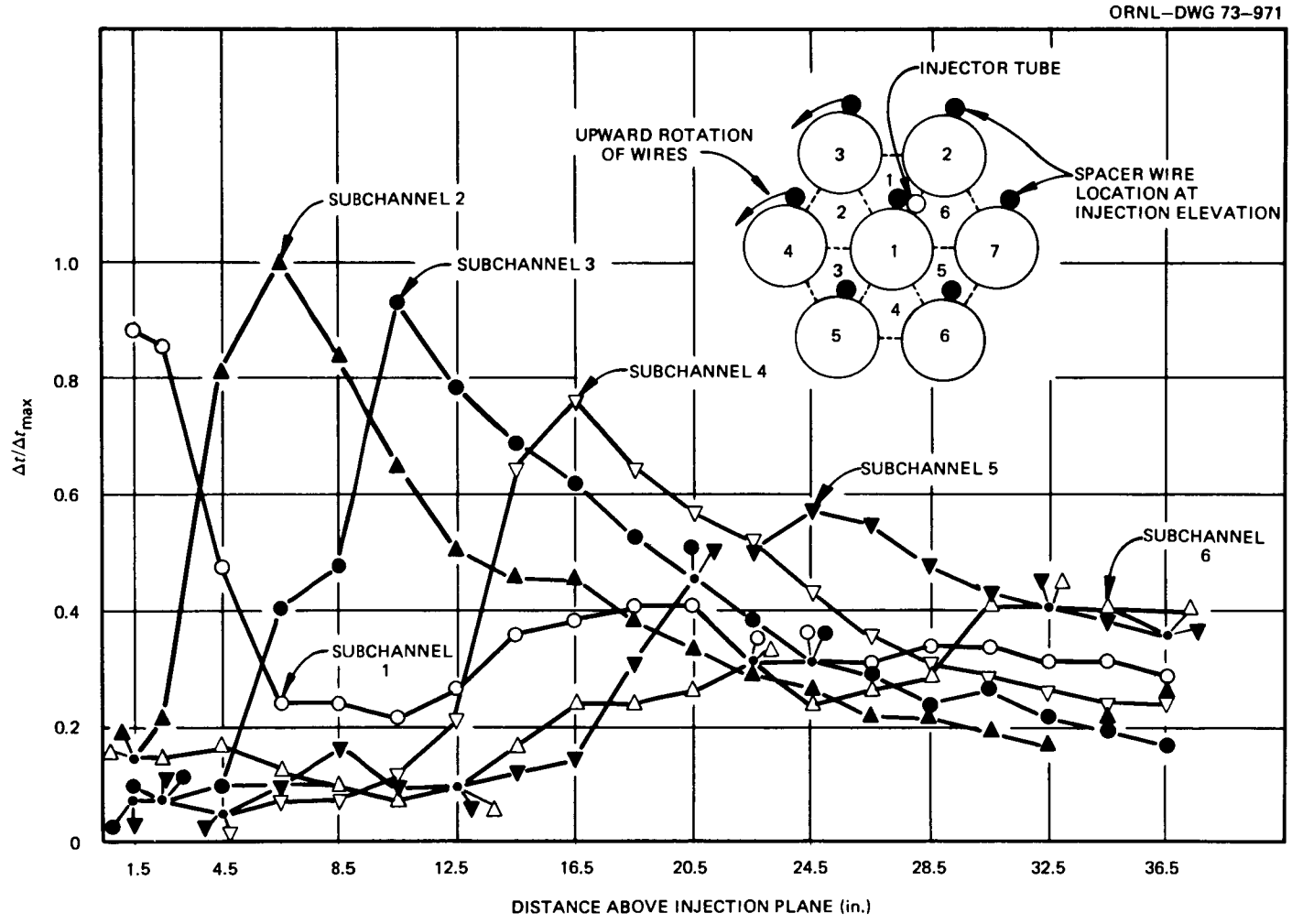

Fig. 38. Central subchannel temperature profiles for hot-water injection. Test 47.

Table 9. Tests with triple-scale water mockup with hot-water injection and nominal (unblocked) reference tube bundle

Test No.[a]	Average velocity (ft/sec)	N_{Re}	t_{inj} (°C)	Δt_{max} (°C)
		$\times 10^4$		
40	9.39	2.7	76	5.5
41	28.0	8.3	86	5.6
42	18.0	5.3	83	6.5
43	17.9	5.5	82	4.9
44	5.18	1.8	71	4.4
45	5.26	1.6	71	7.8
46	9.32	2.6	69	3.5
47	9.37	2.6	73	4.2
48	23.4	6.4	84	4.8
49	17.9	4.9	82	4.5
50	9.41	2.7	76	3.0
51	17.7	5.1	82	4.4
52	23.0	6.8	83	4.9

[a]In tests 40 to 46, hot water was injected near the interface of channels 1 and 2 on the leading side of helical spacer wires. In tests 47 to 49, hot water was injected on trailing side of helical spacer wire. In tests 50 to 52, hot water was injected at a position 180° from spacer wire.

counterclockwise direction when the injection occurs from the trailing injection tube, while, when injection occurs from the leading tube (test 46), the hot fluid is near the interface of subchannels 1 and 2.

Another difference between the results of tests 46 and 47 is that the peaks in the temperature profiles for each subchannel, except 1 and 2, occur ~2 in. closer to the injection plane in test 47. This difference was noted in each of the three tests conducted with the injection occurring behind the spacer wire; the reason is not yet fully understood.

Tests 50 to 52 were made with the injection system rotated 180° around the central tube from the spacer wire location at that level. The normalized axial temperature distributions for the central subchannels as determined in test 51 are shown in Fig. 39. The effect of the hot water is seen to reach a maximum 2.5 in. downstream of the injection plane in subchannel 4. In the first few inches downstream of the injector tube, the spacer wires on rods 5 and 6 are the dominant influence on the flow of the injected water, with the wire on rod 5 moving out of the zone of the influence and that of rod 6 moving into it. Figure 39 shows that a relatively small peak in temperature occurred in subchannel 3 4.5 to 6.5 in. downstream of the injector outlet, indicating that the injected hot water had a tendency to follow the spacer wire of rod 5 into subchannel 3. However, the major effect of the injected water in the first 16.5 in. is seen to be in subchannel 4.

As the spacer wire on the central rod moves into subchannel 4, it forces the tracer water into subchannel 5, where a relative maximum in temperature difference occurs at 18.5 in. Since the wire wrap is on a 36-in. pitch, all the spacer wires have advanced counterclockwise 180° at the 18-in. level. The profile for subchannel 6 shows a very small peak 32.5 in. downstream of the injection plane. This is also attributed to the spacer wire on the central rod forcing a portion of the warmer water from subchannel 5 into subchannel 6. There was no measurable temperature increase in subchannels 1 and 2.

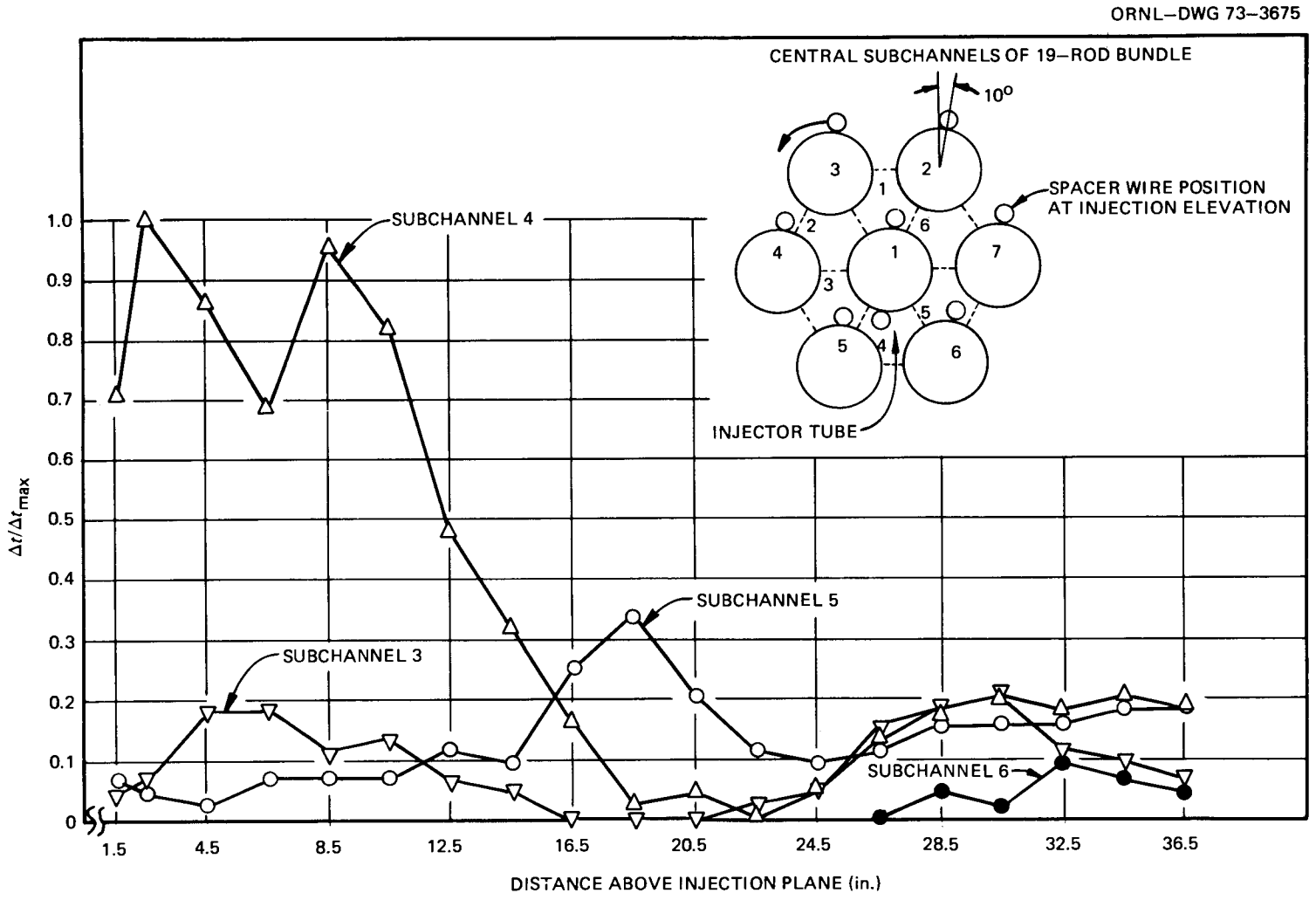

Fig. 39. Normalized axial temperature profiles for hot-water injection. Test 51.

The temperature profiles determined in tests 40 to 46 were compared with theoretically predicted profiles generated with the ORRIBLE code. Since ORRIBLE, in its present state, is capable of calculating only the bulk fluid temperatures in a given subchannel, the effect of any lateral temperature gradient in a given subchannel cannot be represented. Therefore, the input temperature which was used for the injection subchannel was the calculated bulk temperature resulting from the instantaneous mixing of the injected water with the fluid in that subchannel alone. The remaining subchannels were assumed isothermal at the injection plane. The axial temperature profiles predicted with ORRIBLE, using parameters given in Table 10, are shown in Fig. 40 together with profiles from test 46; for comparison, all ORRIBLE results were normalized to the maximum temperature calculated for subchannel 2. In general, the peak in the calculated profiles occurred roughly at the same location as observed experimentally; however, the magnitudes of the peaks were in rather poor agreement.

Table 10. Parameters used in ORRIBLE code calculation of axial temperature profiles with hot-water injection

Turbulent cross flow factor	0
Diversion cross flow factor	0.6
Sweeping cross flow factor	1.0
Edge-gap sweeping cross flow factor	1.5
Angle of influence for edge-gap sweeping	120°
Fanning friction factor	0.005

5.2.3 Results of hot-water injection tests for a 24-channel inlet blockage. Tests 36*a–c* (see Table 13 in Sect. 5.4) were hot-water injection tests made with a 24-subchannel symmetrical heated-zone blockage plate; typical results for test 36*b* (20.8 ft/sec) are shown in Fig. 41. In contrast to the results for tests 40 to 49, the maximum temperature was observed in subchannel 1. However, the maximum temperatures in subchannels 2, 3, and 4 on the blockage plate tests occurred near where they were observed in tests 40 to 49. Since the maximum temperatures in subchannels 5 and 6 in tests 40 to 49 occurred downstream of where the blockage plate was located in tests 36*a–c*, it was not expected that the results for these subchannels would be comparable. Not surprisingly, little temperature rise was observed in the region 6 in. (16 equivalent diameters) downstream of the blockage plate. This might indicate that flow mixing occurs in the recirculation zone behind the blockage plate.

5.3 Inlet Blockage Tests

Twelve tests were made with inlet blockage plates, three with 10 subchannels blocked (asymmetrical blockage), four with 6 subchannels blocked, and five with 24 subchannels blocked. The conditions for these tests are given in Table 11.

Results of tests with both the 6- and 10-subchannel blockage plates indicated that such blockages have little effect on the velocity structure in the heated zone (which begins 46 equivalent diameters downstream of the blockage plate).

With the 24-subchannel blockage plate, heat transfer coefficients for the central (heated) tube were calculated from temperatures measured at three axial stations (S1, S2, and S3) that are 21, 39, and 51 in., respectively, above the bundle base (55, 101, and 132 equivalent diameters). These heat transfer

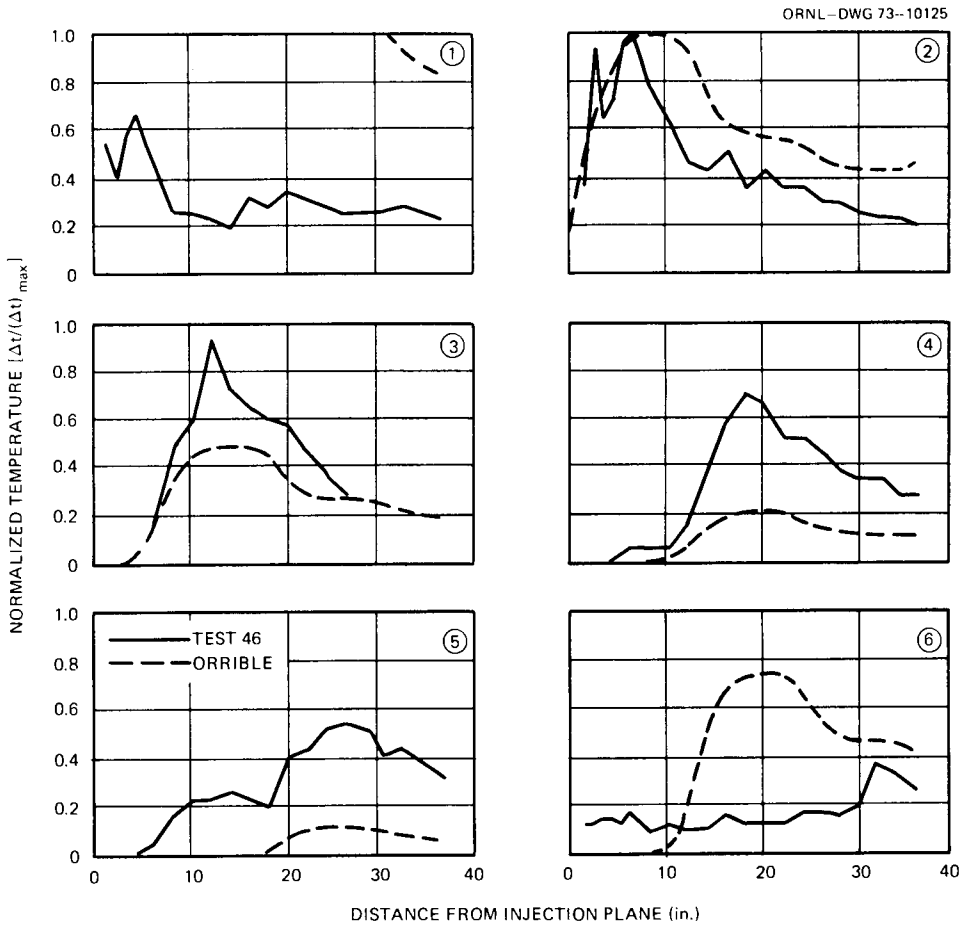

Fig. 40. Comparison of axial temperature profiles experimentally determined by hot-water injection and calculated with the ORRIBLE code. Numbers on graphs refer to subchannels shown in Fig. 6.

Table 11. Tests with triple-scale water mockup with an inlet blockage

Test No.[a]	Number of channels blocked	Average velocity (ft/sec)	N_{Re}	Heat flux [Btu hr^{-1} ft^{-2} $(°F)^{-1}$]
			$\times 10^4$	$\times 10^4$
8	10	26.7	10.1	51.2
9	10	6.1	2.2	24.4
10	10	3.1	1.1	16.1
13	6	26.2	9.42	51.2
14	6	5.7	2.0	21.3
15	6	3.4	1.2	15.8
16	6	5.9	2.2	21.3
23	24	3.0	1.1	12.4
24	24	5.9	2.2	19.5
25	24	25.3	9.4	54.7
26	24	15.2	5.6	40.0
27	24	15.1	5.6	40.0

[a]Tests 8 to 10 were with an asymmetrical inlet blockage; all other tests were with a symmetrical blockage.

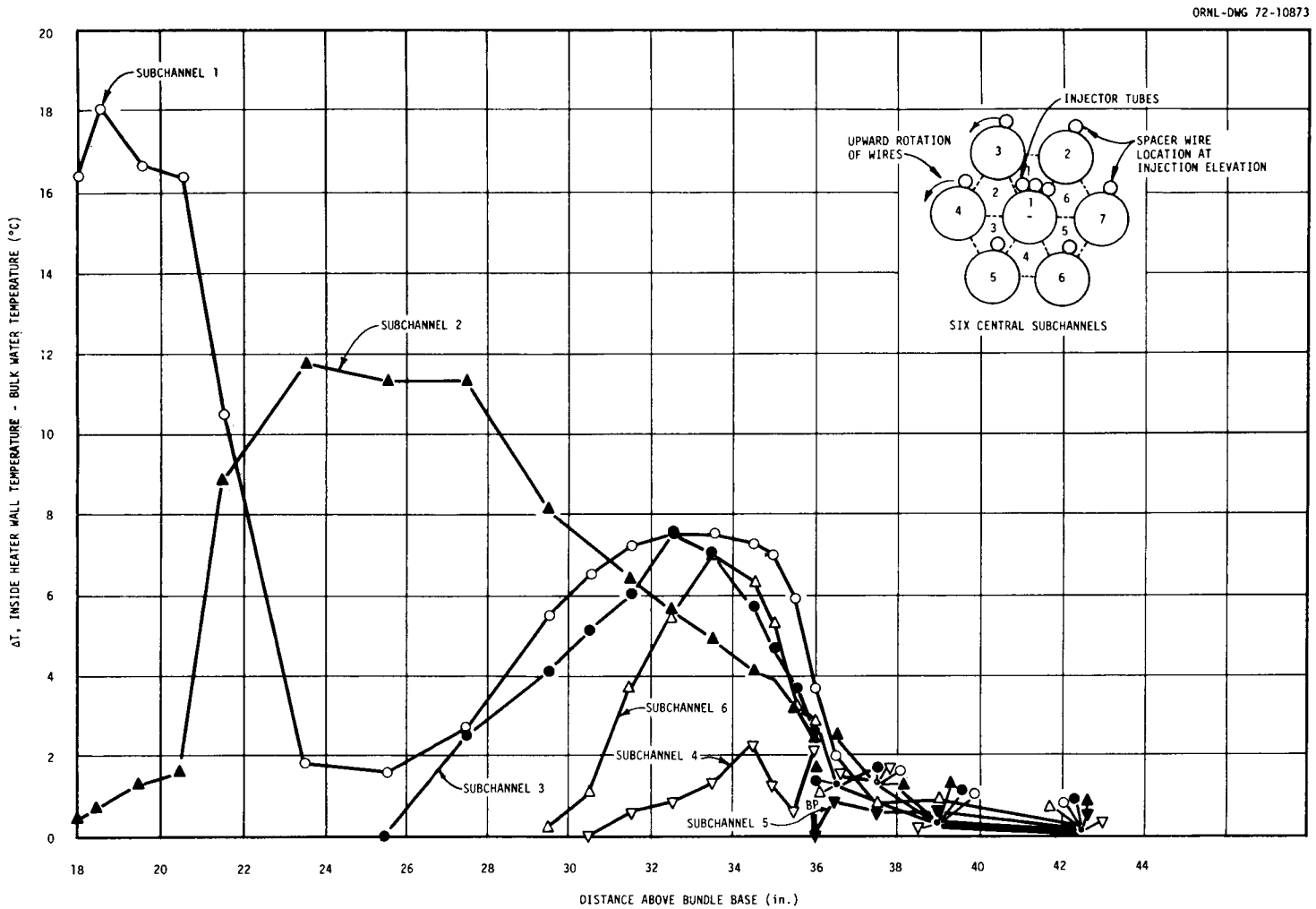

Fig. 41. Central subchannel axial temperature profiles for hot-water injection. Test 36*b*.

coefficients were then used to calculate velocities from the relations

$$Nu = 0.0180 Re^{0.83} Pr^{0.5} , \quad (1)$$

where the numerical coefficient was determined for the water mockup reference bundle with no blockage assuming parallel flow (i.e., no twist in the flow due to the wire wrap and no cross mixing and no secondary or reverse flows in the bundle). Equation (1) can be converted to a more convenient form for calculating velocities by rearrangement to

$$V = 0.0512 D_e^{0.205} F_{pp} h^{1.205} , \quad (2)$$

where

V = parallel flow velocity (ft/sec),

D_e = equivalent diameter (in.),

h = local heat transfer coefficient [Btu hr^{-1} ft^{-2} $(°F)^{-1}$],

F_{pp} = physical property factor
$= (\mu/\rho) k^{1.205} Pr^{0.603}$,

where

μ = viscosity (lb_m hr^{-1} ft^{-1}),

ρ = density (lb_m/ft^3),

k = thermal conductivity [Btu hr^{-1} ft^{-1} $(°F)^{-1}$],

Pr = Prandtl number (dimensionless).

Inferred velocities were calculated for the three different stations along the heated tube (S1, S2, and S3) for the 24-subchannel symmetrical inlet blockage for runs 23 to 27, Fig. 42. The ratios of the mean velocity inferred for the six central channels surrounding the heater rod to the mean bundle velocity are given in Table 12. Apparently, the disturbance to the flow caused by the 24-subchannel symmetrical inlet blockage (which blocked ~45% of the net flow area) persisted for over 100 equivalent diameters downstream. Based on subsequent studies it appears that the wake region behind the blockage plate (where recirculation patterns, countercurrent flows, and strong cross flows could exist) did not extend to the start of the heated zone and that the phenomenon illustrated in Table 12 represents a rather slow recovery of flow to the reference bundle conditions.

Table 12. Inferred velocity ratios downstream of 24-subchannel symmetrical inlet blockage plate

Test No.	Mean velocity (ft/sec)	Ratio of inferred velocity to mean bundle velocity		
		$L = 55 D_e$	$L = 101 D_e$	$L = 132 D_e$
23	3.0	0.89	0.96	0.96
24	5.9	0.78	0.84	0.93
25	25.3	0.90	0.86	0.99
26	15.2	0.86	0.80	0.97
27	15.1	0.87	0.83	0.99
Av		0.86	0.86	0.97

Note: L = number of equivalent diameters downstream of blockage plate.

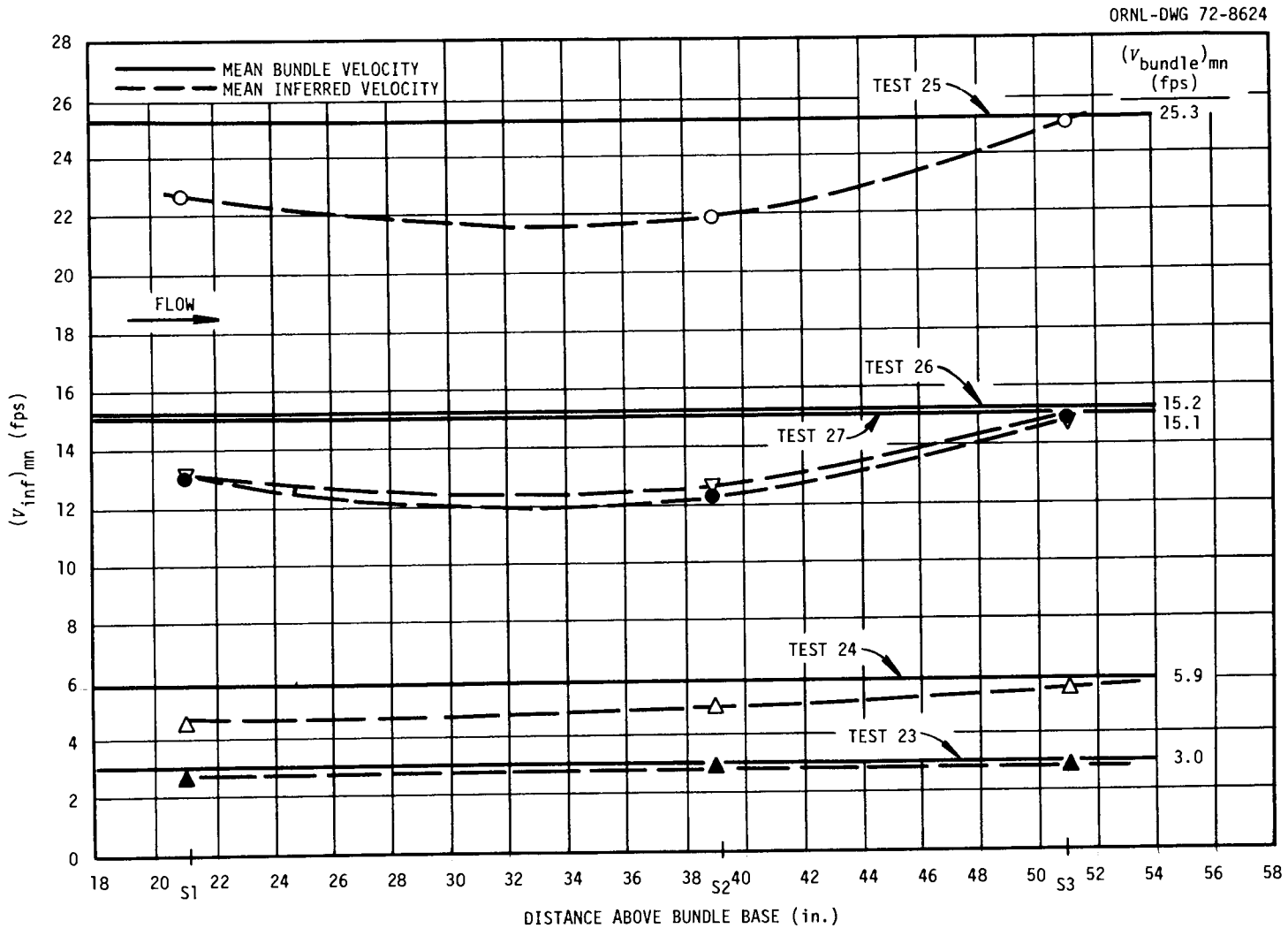

Fig. 42. Variation in mean inferred velocity with length for triple-scale FFM water mockup with 24-subchannel symmetrical inlet blockage plate.

5.4 Heated-Zone Blockage Tests

Two general types of heated-zone blockage plates (BP) have been used in tests with the triple-scale water mockup: symmetrical heated-zone blockage plates with the central rod heated and edge-channel blockage plates with the corner rod heated.

In some tests the local temperature of the single heated tube was measured; in other tests the temperature field at the surface of the metal tube was mapped downstream of a source of hot water; in other tests, flow visualization studies were made by injecting either small air bubbles or dye into the system; and in some edge channel blockage tests, the decay of a pulse of salt solution (injected downstream of the blockage plate) was followed by conductivity probes. Experimental conditions in these tests included mean velocities from 3 to 28 ft/sec, heater tube heat fluxes from 0.8 to 17 X 10^4 Btu hr^{-1} ft^{-2} $(°F)^{-1}$, and inlet bulk temperatures from 16 to 32°C. Conditions for each of these tests are summarized in Tables 13 and 14. The results of the tests with two different blockage types will be discussed separately.

5.4.1 Symmetrical heated-zone blockage. *Six-subchannel blockage.* In these tests local temperatures were measured at six different radial positions at only a few different positions above and below the blockage plate. In light of the complex variation in temperature along the tube found in subsequent 24-subchannel blockage tests and because only two tests were conducted with the 6-subchannel blockages, discussion of these tests will be deferred to a subsequent report.

Twenty-four-subchannel blockage. In tests 28 to 32, temperature scans were made along the inside of the central heated tube at six different circumferential positions at each distance from the blockage plate. There was considerable circumferential variation in local values of the heat transfer coefficient calculated from these measured temperatures as illustrated in Fig. 43. Aside from the marked variation in heat transfer coefficient in the vicinity of the blockage plate, it is notable that local maxima and minima sometimes occurred at almost the same distance from the blockage plate and that the six-point planar average tended to smooth out the extremes while still indicating the complexity of the variation of local heat transfer

Table 13. Tests with triple-scale water mockup with a symmetrical heated-zone blockage

Test No.	Number of channels blocked	Average velocity (ft/sec)	N_{Re}	Heat flux [Btu hr^{-1} ft^{-2} $(°F)^{-1}$]	Temperature ratio			Comments
					h_1/h_{-15}	h_{max}/h_{-15}	h_{15}/h_{-15}	
			× 10^4	× 10^4				
21	6	6.7	2.69	1.9	0.59	NA[a]	1.05	Heated rod temp. scan
22	6	14.2	5.26	3.0	0.80	NA	0.80	Heated rod temp. scan
28	24	3.1	1.1	7.6	1.05	1.60	0.93	Heated rod temp. scan
29	24	5.9	2.2	10.7	0.99	1.60	0.93	Heated rod temp. scan
30	24	15.2	5.9	12.7	0.87	1.10	0.77	Heated rod temp. scan
31	24	23.9	9.3	17.0	0.86	1.13	0.78	Heated rod temp. scan
32	24	10.0	3.8	1.3	0.91	1.20	0.83	Heated rod temp. scan
32*b*	24	9.9	3.8	1.3	NA	NA	NA	Air injection
33	24	23.6	8.8	1.8	1.00	1.00	0.73	Controlled leakage
34	24	9.9	3.7	1.3	1.18	1.18	0.75	Controlled leakage
35	24	3.1	1.2	0.8	1.46	1.61	0.97	Controlled leakage
36*a*	24	9.4	3.0	0	NA	NA	NA	Hot-water injection
36*b*	24	20.8	7.9	0	NA	NA	NA	Hot-water injection
36*c*	24	3.0	1.1	0	NA	NA	NA	Hot-water injection

[a]NA = not available.

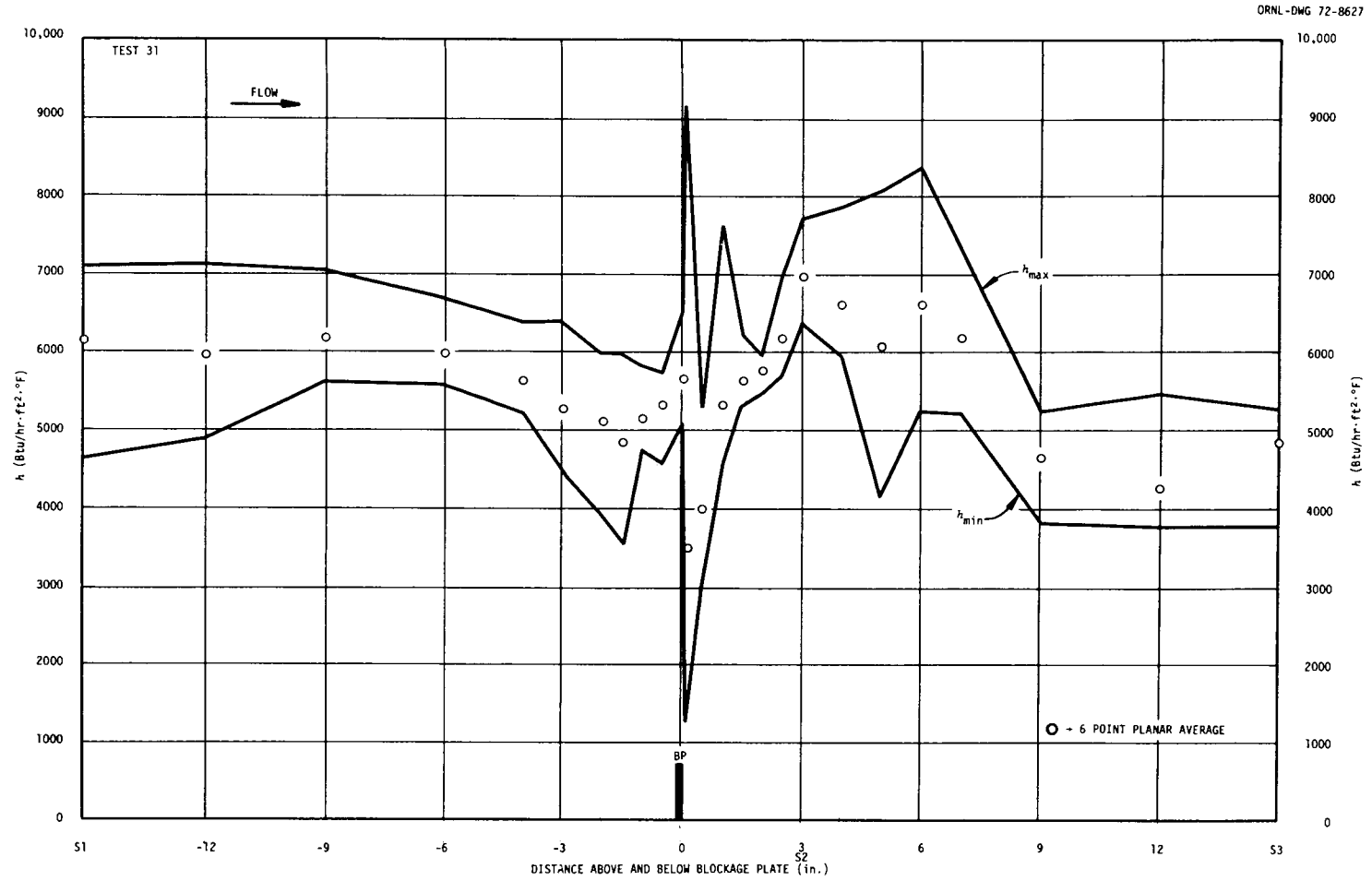

Fig. 43. Axial variation of maximum, average, and minimum heat transfer coefficient for test 31 in triple-scale FFM water mockup with 24-subchannel symmetrical internal blockage plate.

Table 14. Tests with triple-scale water mockup in which there was a heated-zone edge blockage

Test No.	Number of channels blocked	Average velocity (ft/sec)	N_{Re}	Heat flux [Btu hr^{-1} ft^{-2} $(°F)^{-1}$]	Temperature ratio		Comments
					h_1/h_{-8}	h_{24}/h_{-8}	
			x 10^4	x 10^4			
57*a*	14	9.9	2.6	3.5			
57*b*	14	23.8	7.6	5.6			Slight leak
57*c*	14	4.5	1.1	3.0			Slight leak
57*d*	14	9.7	2.5	3.5			Slight leak
58*a*	14	4.7	1.2	4.3	0.50	0.64	
58*b*	14	10.0	3.0	4.4	0.42	0.72	
58*c*	14	20.0	4.9	5.9	0.34	0.68	
58*d*	14	10.0	2.5	4.9			
59	14	10.0	2.6	4.9			
60	14	28.1	9.4	6.8			
61	14	9.5	2.4	5.4			Slight leak
62	14	10.3	2.6	7.5			Substantial leak

coefficient. In contrast to the variations shown in Fig. 43, in tests with the reference bundle configuration the maximum value of the heat transfer coefficient was 5 to 15% greater than the average while the minimum value was 15 to 30% smaller than the average.

The wide range in circumferential variation in local wall temperatures is further illustrated in Fig. 44 using results from the vicinity of the blockage plate for test 31 (23.9 ft/sec) and test 29 (5.9 ft/sec). The greatest range in circumferential variation was observed within $\frac{1}{8}$ in. of the blockage plate; in contrast, measurements made only slightly farther away ($\pm\frac{1}{2}$ in. from the blockage plate) showed a range of values within the range of circumferential variation expected from the unblocked reference bundle results.

The effect of average velocity on the axial variation of the planar-average heat transfer coefficient with the 24-subchannel symmetrical heated-zone blockage is illustrated in Fig. 45. Common features exhibited by the results over the entire velocity range include (1) the planar-average heat transfer coefficient h decreases slowly in the flow direction to a level ~3 in. upstream of the blockage-plate (BP) center, following which it passes through a small peak ~$\frac{1}{2}$in. upstream of the BP center; (2) h then decreases sharply, reaching a minimum $\frac{1}{8}$ in. downstream of the BP center ($\frac{1}{16}$ in. downstream of the BP trailing face); (3) h then increases, attaining a maximum value ~5 to 6 in. downstream of the BP center, after which it decreases to a value approaching that of an unblocked bundle at station 3, which is ~40 equivalent diameters downstream of the BP. Examination of the heat transfer coefficient ratios given in Table 13 shows that there is a consistent decrease in the ratio h_{15}/h_{-15} (heat transfer coefficient 15 in. downstream of blockage plate/heat transfer coefficient 15 in. upstream of blockage plate) as the velocity increases. If this ratio is taken as a measure of the extent of recovery to fully developed turbulent flow, then at low velocities (~5 ft/sec) recovery is 93% complete, while at high velocities (~24 ft/sec) recovery is only about 75% complete. Somewhat surprisingly, the two results for the six-subchannel blockage are in rather good agreement with the results for the 24-subchannel blockage.

Controlled leakages. In order to determine the effect of controlled leakages on the local heat transfer coefficient downstream of the 24-subchannel symmetrical heated-zone blockage plate, three $\frac{1}{8}$-in.-diam holes spaced ~120° apart were drilled through the blockage plate, allowing a controlled leakage through the plate in the central subchannels. Tests 33, 34, and 35 were conducted with test conditions nominally the

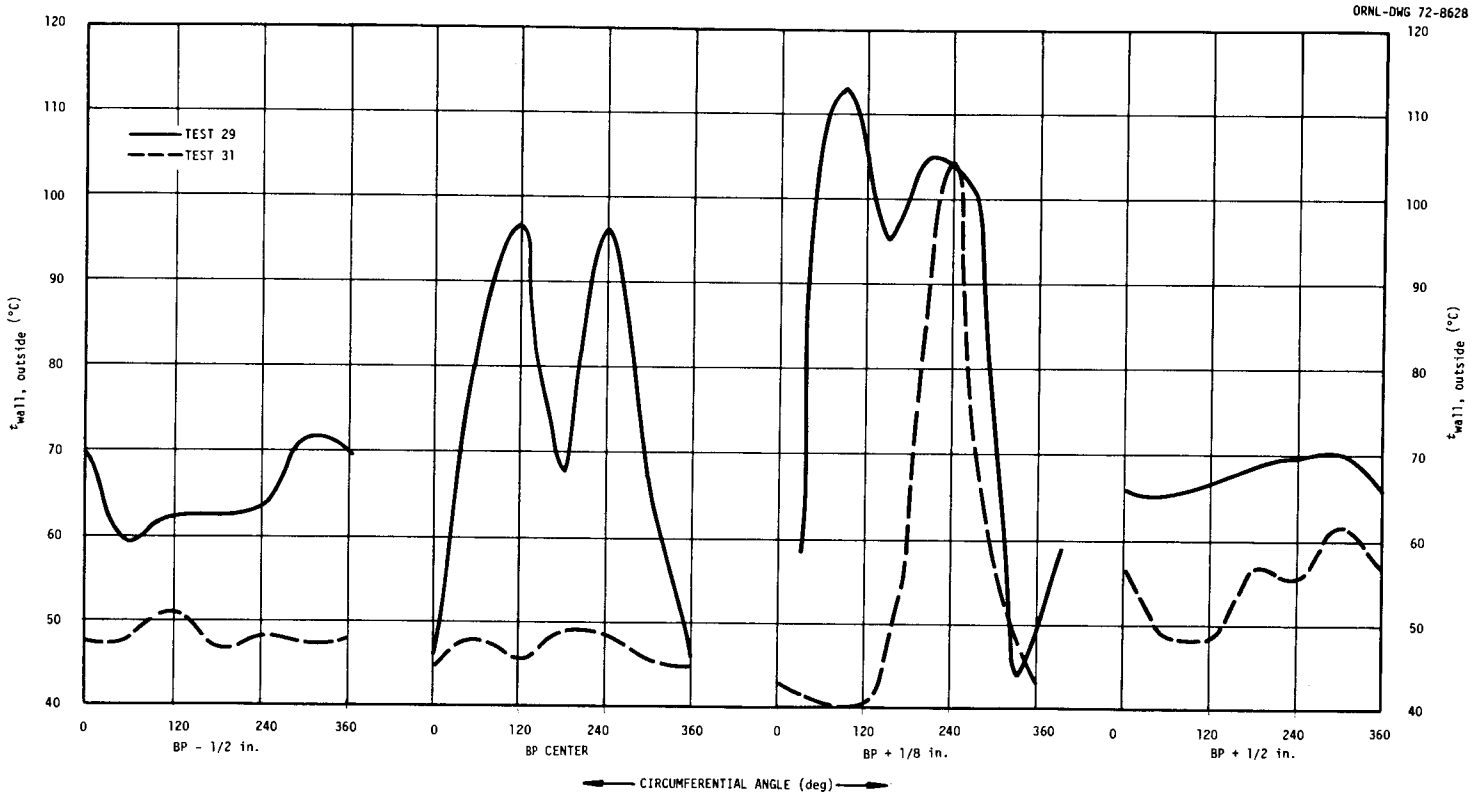

Fig. 44. Circumferential variation of heater outer wall temperature at four axial stations for tests 29 and 31 in triple-scale FFM water mockup with 24-subchannel symmetrical internal blockage plate.

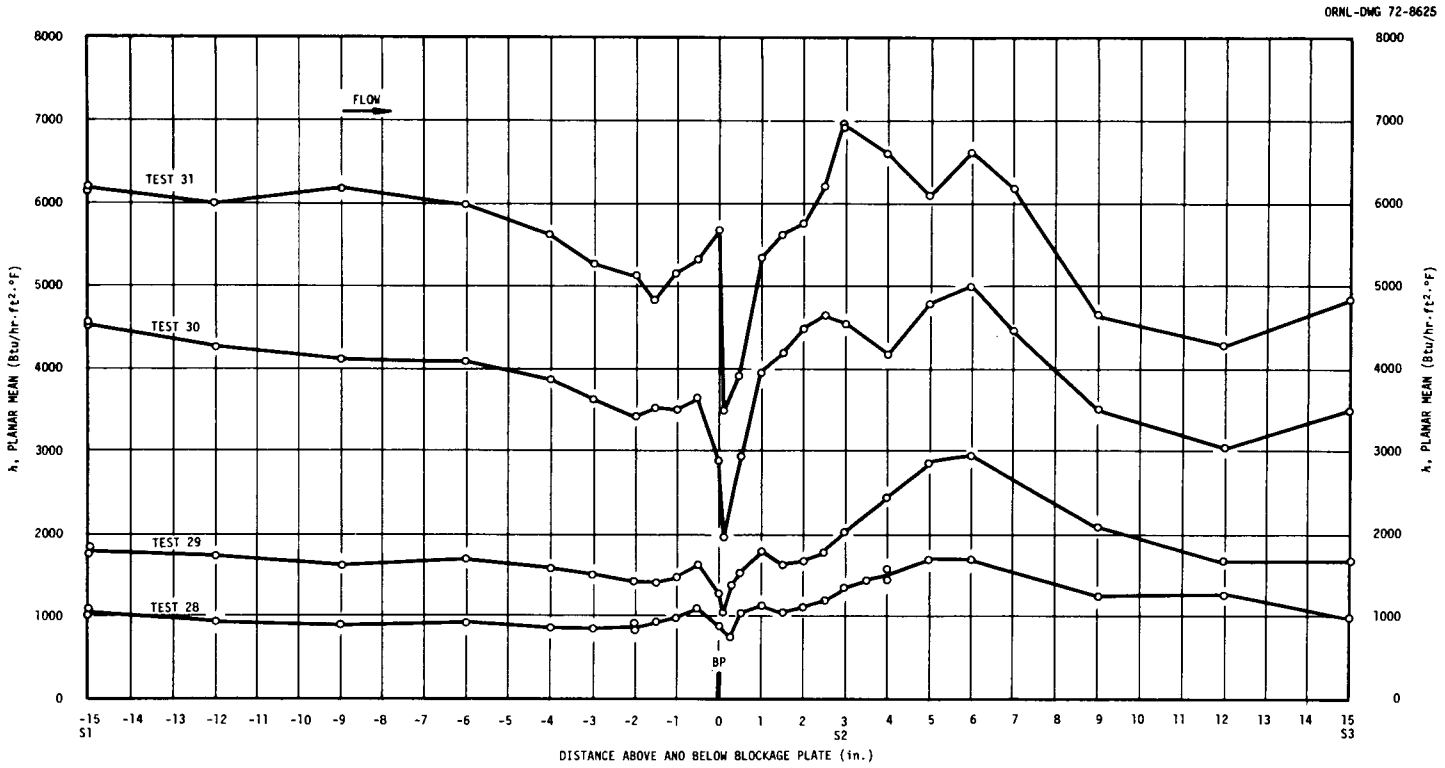

Fig. 45. Axial variation of plane-average heat transfer coefficient for triple-scale FFM water mockup with 24-subchannel symmetrical internal blockage plate.

same as those for tests 31, 32, and 28 respectively. The effect of the controlled leakage was an enhancement of $\bar{h}$ in the region from ~1½ to 6 in. downstream of the BPC, as shown in Fig. 46. The leakage had little effect on the results for distances downstream of the blockage plate greater than 6 in. (~16 equivalent diameters).

5.4.2 Edge-channel blockages. For these tests, the spacing between the 12 peripheral rods of the 19-rod bundle and the walls of the hexagonal duct was half the normal distance of 0.165 in. To accomplish this, the walls of the Plexiglas duct were lined with 85-mil-thick Plexiglas shims, the nickel heater tube was installed in a corner of the rod bundle, and a Plexiglas rod was installed as the center rod of the bundle. The spacer wire on each of the outer rods was machined flat at each position corresponding to a point of contact with a duct wall. This was done so that the spacing distance between the outer rods and the duct walls was 80 mils, while the normal spacing distance of 0.165 in. between rods was maintained.

A ¼-in.-thick heated-zone edge blockage plate was installed in the rod bundle, with the blockage plate center (BPC) located 9 in. from the start of the heated length, or 27 in. above the bundle base. The plate blocked 14 subchannels, or one-third of the total flow area. With the blockage plate located at this position, the wire wrap on the heater rod was in contact with the channel side walls from 5½ to 13 in. downstream of the blockage plate. This means that channel-to-channel cross flow on the periphery of the bundle was possible both upstream of the blockage plate and for 5½ in. downstream of the blockage plate.

Test conditions for the runs conducted with the edge blockage plate are given in Table 14.

At the high flow rate of test 57*b* a slight leak occurred through the blockage plate. Since the effects of a small amount of leakage were not known, testing was continued, and tests 57*c* and *d* were conducted with the slight leakage. The test section was disassembled, and the leakage was repaired prior to conducting tests 58*a*–*c*. A slight leak again developed in test 61, and this leak was deliberately enlarged before the start of test 62. The effects of this leakage are discussed later.

As part of the flow visualization studies, air was injected into the test section ~2 in. upstream of the bundle base, and the flow patterns induced by the blockage plate were observed. Figures 47–49 show the patterns observed during tests 58*a*–*c* respectively. Also shown on these figures is a plot of the local heat transfer coefficients experimentally determined for subchannels 4 and 5 of the heater tube, which are the subchannels directly facing the two walls of the corner where the observations were made. The flow patterns shown are on the same linear scale that was used to plot the heat transfer data. The heated rod is shown crosshatched, and the beginning of the contact of the spacer wire with the channel walls is indicated by a solid star on the spacer wire.

Observation of the flow patterns was largely limited to the flow channels between the periphery of the bundle and the housing side walls, since little could be seen of flow patterns on the interior of the tube bundle. In general, five main types of flow were observed in the vicinity of the blockage plate:

1. recirculating eddies,
2. cross flow parallel to the channel walls,
3. cross flow into or out of the interior of the bundle,
4. flow countercurrent to the bulk flow in the region downstream of the blockage plate,
5. transfer of fluid from the wake "bubble" to the main stream at the outer edge of the wake bubble.

In test 58*a* (4.66 ft/sec), flows 2 and 3 were observed upstream of the blockage plate; downstream of the plate, countercurrent flow on one side of the spacer wire apparently drove a recirculating eddy on the other side of the spacer wire. Type 3 flow was also observed at the outer edge of both sides of the wake bubble.

In test 58*b* (10.0 ft/sec), flow upstream of the blockage plate was little different from the previous test, but downstream of the plate there were two large regions of recirculation. In addition, countercurrent flow

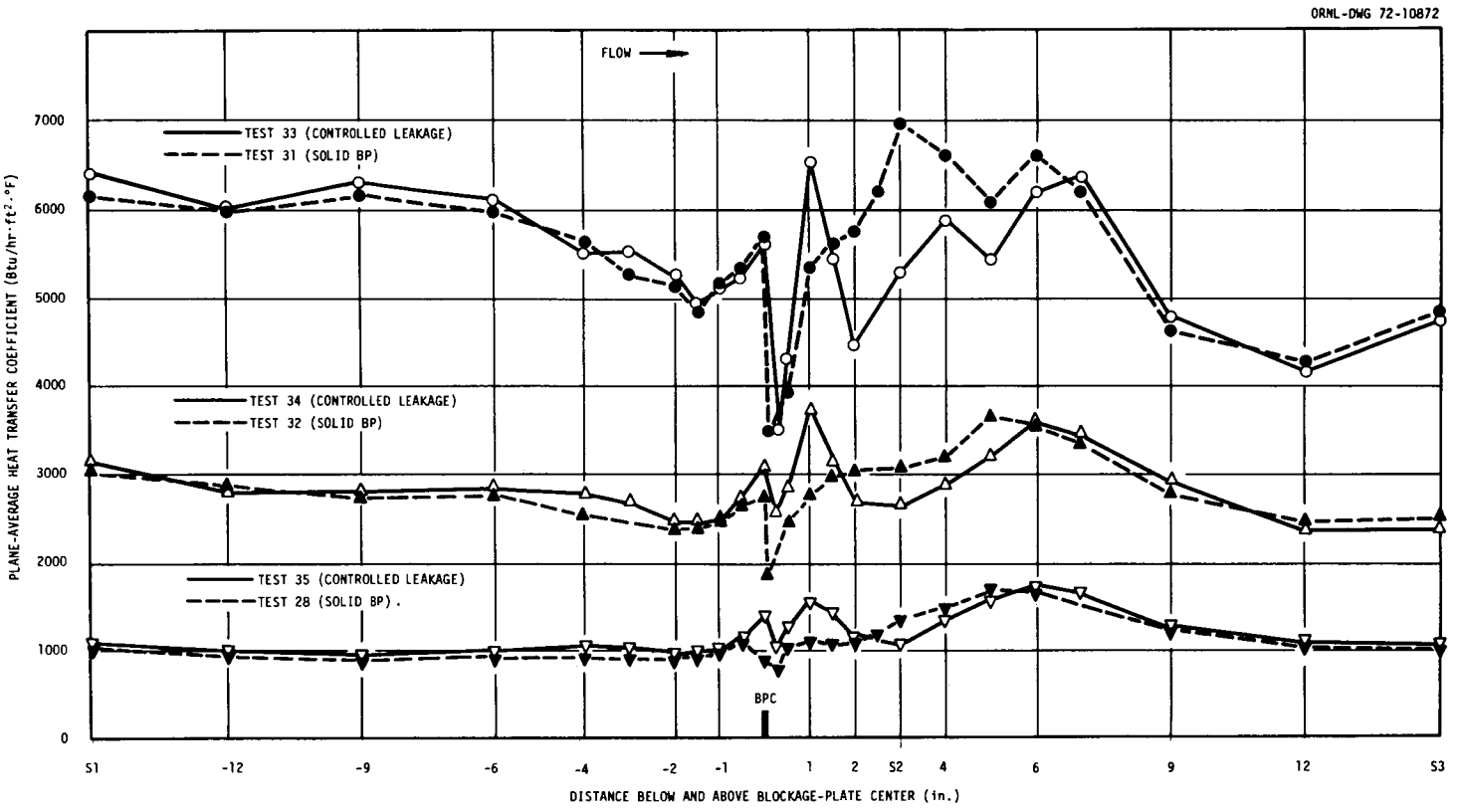

Fig. 46. Comparison of heat transfer coefficient for 24-subchannel internal blockage plate with and without controlled leakage.

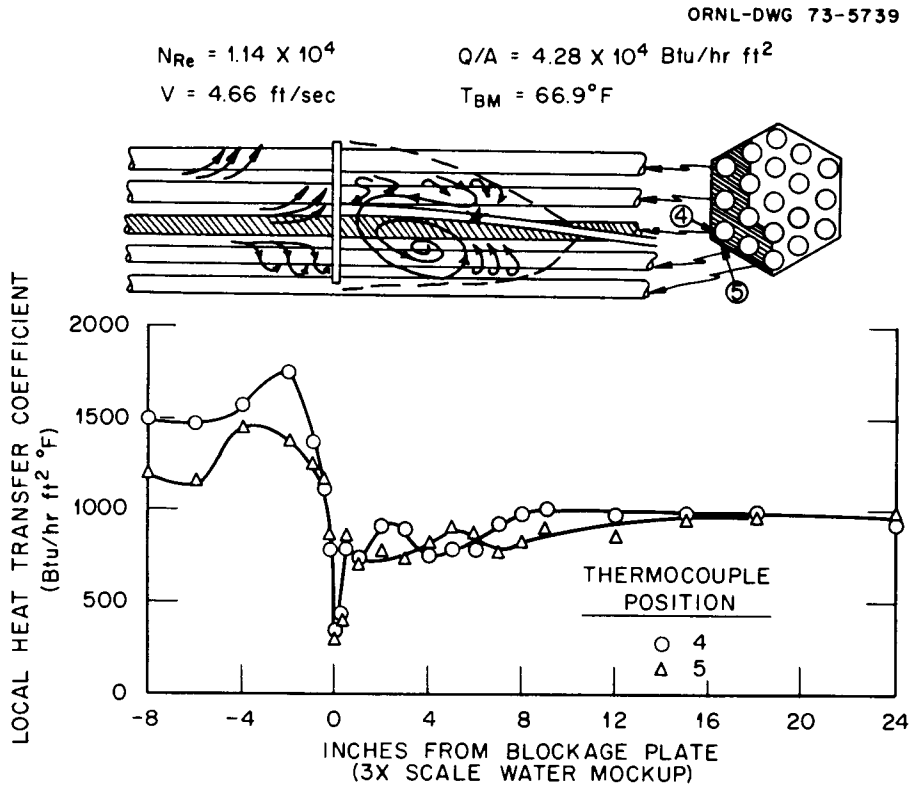

Fig. 47. Local heat transfer coefficients and flow patterns with an edge blockage plate in the FFM water mockup. Test 58*a*.

was observed downstream of the location where the wire spacer contacted the wall, and some type 5 flow was observed on one side of the wake bubble.

In test 58*c* (20.0 ft/sec), flow upstream of the blockage plate was again similar to that of previous tests except that two small (weak) recirculating regions developed. The flow pattern downstream of the plate was similar to that observed at 10.0 ft/sec except that recirculating and countercurrent flows appeared to be stronger; that is, at 10 ft/sec the countercurrent flow started about 8 in. downstream of the blockage plate, while at 20 ft/sec it started about 10 in. downstream.

The most dominant feature of the local heat transfer measurements is the pronounced decrease in the coefficient downstream of the blockage plate and its slow recovery. The following table gives ratios of heat transfer coefficient downstream of the plate (h_1 and h_{24} are heat transfer coefficients measured 1 and 24 in. downstream of the blockage plate respectively) to the heat transfer coefficient 8 in. upstream from the plate (h_{-8}).

N_{Re} x 10^4	Velocity (ft/sec)	h_1/h_{-8}	h_{24}/h_{-8}
1.14	4.66	0.50	0.64
3.04	10.0	0.42	0.72
4.95	20.0	0.34	0.68
9.40	28.1	0.23	0.65

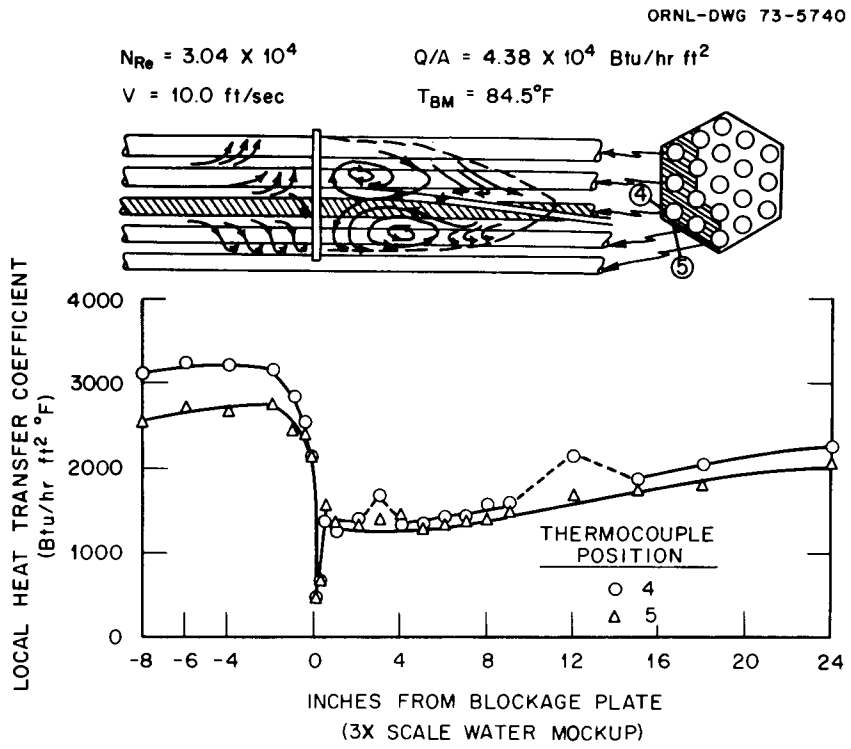

Fig. 48. Local heat transfer coefficients and flow patterns with an edge blockage plate in the FFM water mockup. Test 58*b*.

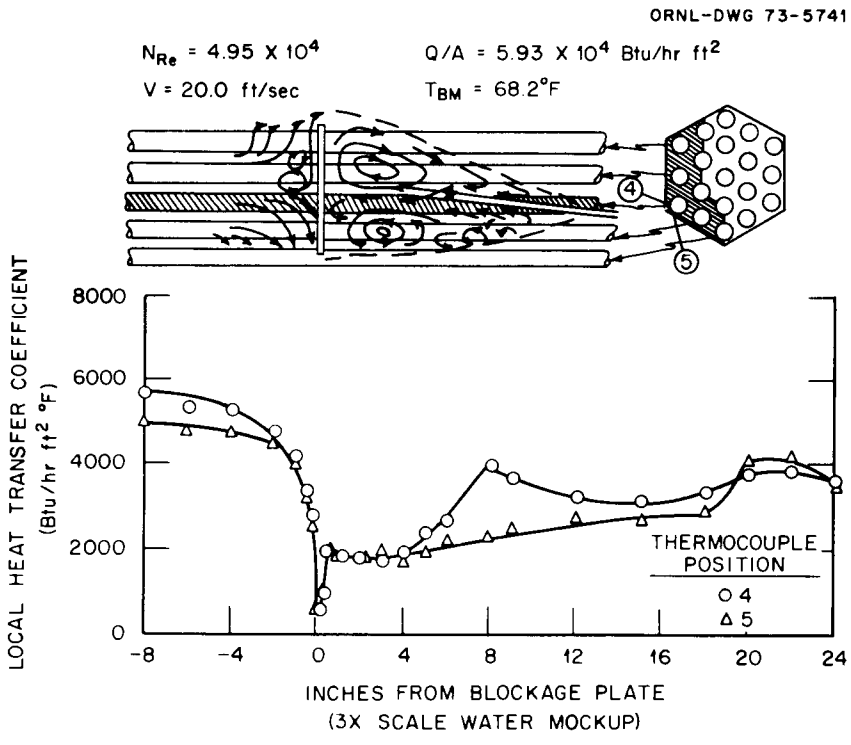

Fig. 49. Local heat transfer coefficients and flow patterns with an edge blockage plate in the FFM water mockup. Test 58*c*.

As velocity increases, the effect of the blockage plate on the heat transfer coefficient within 1 in. of the blockage plate is markedly increased; however, at 24 in. downstream from the blockage plate the heat transfer coefficient had recovered to 64 to 72% of the original value with no clear-cut trend.

At the end of test 60, a slight leak developed between the blockage plate and the channel wall ~1½ tube diameters from the center line of the heated corner tube. For the next test, this leak was deliberately enlarged by forcing the plate away from the channel wall with a machine screw. Although the Silastic sealer compound had pulled loose from the blockage plate for this test, it still remained fixed to the plate on the side toward the heated tube, so that the jet was diverted away from the heated tube. Flow visualization studies clearly showed the jet, but apparently it was not strong enough to completely destroy the eddy regions or the countercurrent flow observed in previous tests with no leaks.

In general, two different trends were observed for the variation of heat transfer coefficient with distance from the blockage plate. These trends are illustrated in Fig. 50; for comparison, results are also included from a no-leak test (test 58*d*) at the same Reynolds number. Subchannels 1, 2, and 6 all showed a pronounced peak in the heat transfer coefficient directly beneath the blockage plate. Since a machine screw was used in test 62 to hold the blockage plate away from the channel wall, it is believed that the screw also

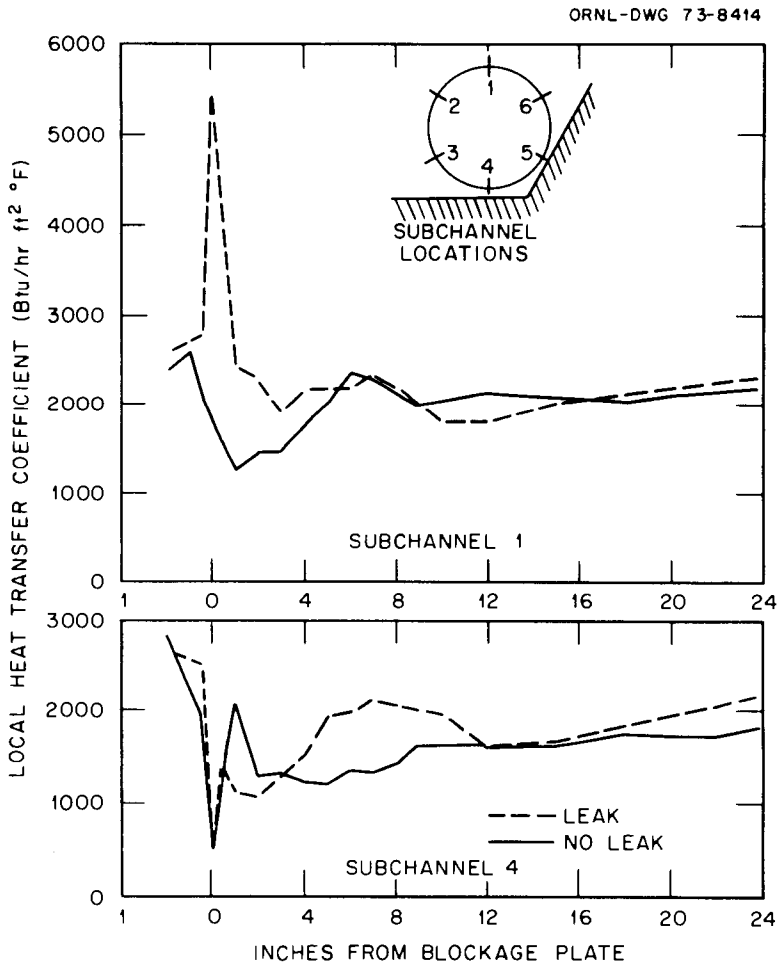

Fig. 50. Effect of a leak between the channel walls and the blockage plate on the local heat transfer coefficient.

forced the blockage plate away from the heated tube at subchannels 1, 2, and 6. However, the heat transfer coefficient for subchannels 3, 4, and 5 showed a substantial increase about 6 to 8 in. downstream of the blockage plate, which is believed to be due to the primary leak between the channel wall and the blockage plate. It is notable that from about 12 in. downstream of the blockage plate there is little evidence for any effect of the leak on the heat transfer coefficient.

5.5 Discussion of Water Mockup Results

Heat transfer in turbulent flow of water is almost entirely by convection processes, whereas with liquid metals the high thermal conductivity of the liquid metal is frequently controlling. This is illustrated in Fig. 51, which shows calculated values (from Dwyer[31]) of Nusselt number for heat transfer to liquid metals flowing in line through unbaffled tube bundles for a fluid with a Prandtl number of 0.004 and a P/D of

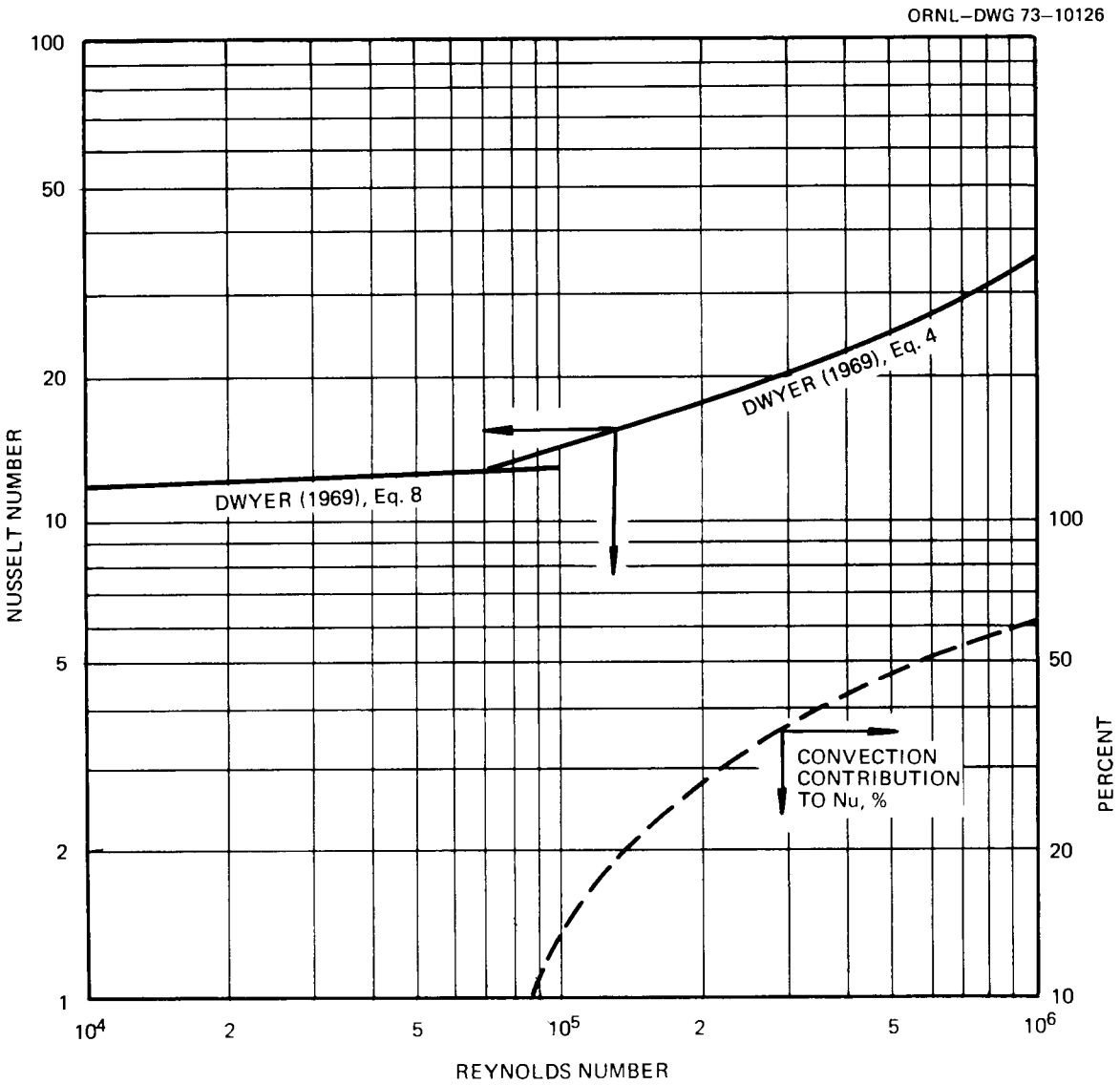

Fig. 51. Heat transfer to liquid metals flowing in-line through unbaffled rod bundles. Dwyer. $P/D = 1.24$, $N_{Pr} = 0.004$.

1.24. In this case the so-called molecular-conduction regime extends to a Reynolds number of 70,000, considerably higher than for flow through pipes or annuli. At a Reynolds number of 1.2×10^5, the contribution of convection to the liquid-metal Nusselt number is only about 18% of the total.

In discussing the relationship between water mockup results and results obtained with sodium in tube bundles, it is convenient to divide flow downstream of the blockage into two regions: (1) the near-wake region, where eddies, countercurrent, and cross flows may exist; and (2) the far-wake region, where flow is parallel or nearly parallel to the rods. It is only in the latter region that Eqs. (1) and (2) can be used to correlate data and infer velocities.

In order to establish a base line for evaluation of far-wake blockage results, reference bundle results are shown plotted in Fig. 52 as

$$j = \mathrm{St}\,\mathrm{Pr}^{2/3} = \left(\frac{h}{C_p G}\right)\mathrm{Pr}^{2/3} \tag{3}$$

vs Reynolds number. The solid line labeled "McAdams (tubes)" represents results for flow inside tubes of fluids with Prandlt number greater than ~1. The dashed line is the recommended value of Kays[32] for unbaffled tube bundles, and the solid upper line represents the present reference bundle results. Apparently, the wire wraps increase convective heat transfer by ~23%. From the results in Fig. 51 (and

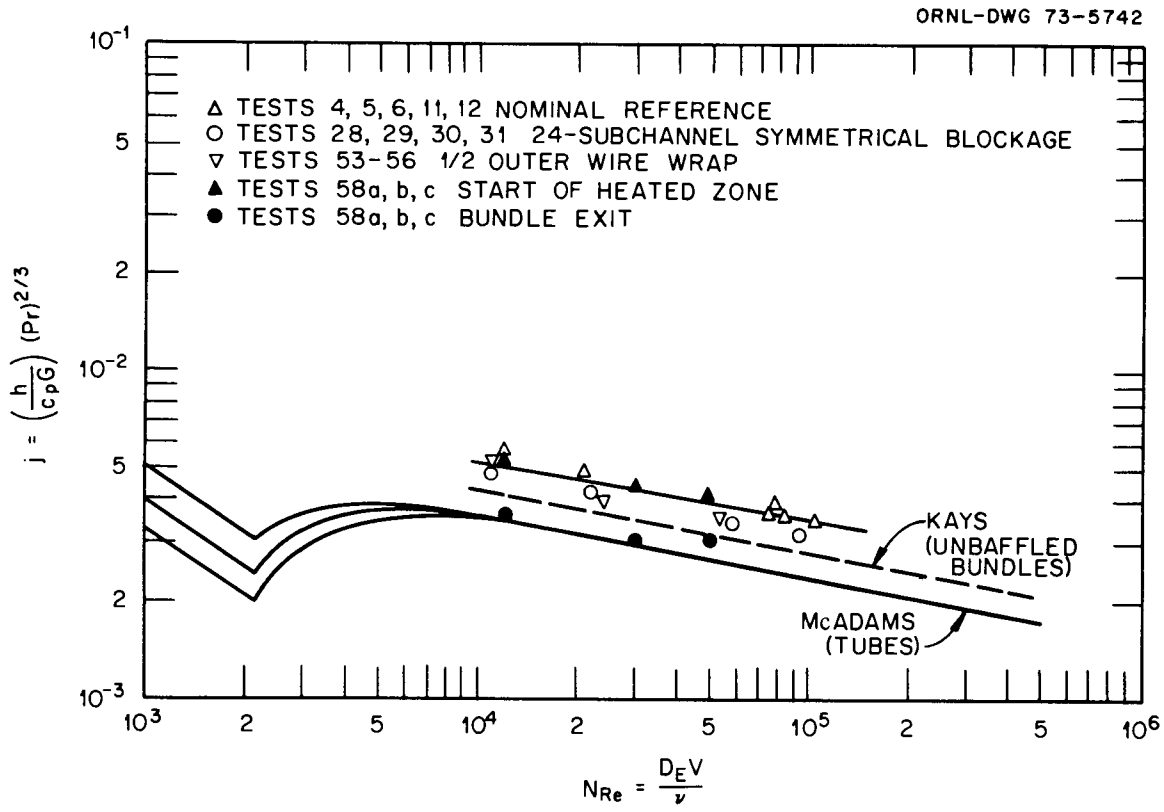

Fig. 52. *j* factors for single heated rod tests in the FFM water mockup.

assuming that molecular conduction and convection can be separated in liquid-metal heat transfer), the 23% increase in convective heat transfer by wire wraps in the water system would amount to only a 4% increase in a liquid-metal system at a Reynolds number of 1.2×10^5.

Also shown in Fig. 52 (solid points) are results from the edge blockage tests for the local heat transfer coefficients at the start of the heated zone and the bundle exit. The good agreement of the results from the start of the heated zone with the reference bundle data indicates that the disturbance from the blockage plate was not propagated an appreciable distance upstream. However, the values of the local heat transfer coefficients at the end of the heated zone were about 70% of that found at the bundle entrance (as pointed out previously). This indicates (based on the results of Fig. 51) that in a liquid-metal system with an edge blockage similar to that used in test 58 the exit heat transfer coefficient may be only 5% less than the entrance coefficient.

So far there are insufficient data to draw any conclusions about the hot-water injection tests with the reference bundle configuration (Figs. 37–39). The surprising fact is that there was little difference in results for (1) nonisokinetic injection, (2) injection along either the leading edge or the trailing edge of the spacer wire, and (3) different Reynolds numbers. However, there was a marked difference between the results just mentioned and results obtained with the injector rotated 180° from the spacer wire. One possible explanation is that the fluid in the vicinity of a spacer wire is conducted along the spacer wire and undergoes mixing to a different extent than fluid in a subchannel which contains no spacer wire.

There are insufficient results to make an extrapolation to larger bundles. However, the limited data on 6- and 24-subchannel blockages with a central heater rod suggest that a difference in the blockage plate size has little gross effect on the heat transfer coefficient along the central rod in the far-wake region. If this is true, it has interesting implications for the mechanism responsible for the slow recovery in the far-wake region. There is a further implication that even in a 19-tube bundle the central tube is so "far" from the channel walls that there is little problem in extrapolating the far-wake effects of a symmetrical central subchannel blockage in larger bundles.

As yet there are insufficient data to assess even in a preliminary fashion the effect of the near-wake region on the liquid-metal heat transfer coefficients. Examination of Figs. 47 and 48 show only relatively minor variations in the heat transfer coefficient which might be identified with some of the flow patterns observed in the test. However, in Fig. 49, there is a relatively large increase in the heat transfer coefficient at position 4 which apparently coincides with a region of strong countercurrent flow. In order to further elucidate phenomena occurring in the near-wake region, tests have been initiated in which a pulse of salt solution is injected into the near-wake region downstream of the edge blockage plate and the decay of the salt solution followed with conductivity probes. Preliminary analysis of the first results indicates that $35 < \tau U/d < 45$, where τ is the mean life of salt tracer in the bubble, U is the velocity approaching the blockage plate, and d is twice the largest dimension (normal to the channel wall) of the blockage plate. Further analysis is required to relate these results to temperature rise in the region downstream of a blockage plate in liquid-metal systems.

6. CONCLUSIONS

1. Blockages at the inlet of the fuel rod bundles caused by a single piece of material small enough to pass through the FFTF inlet flow paths will have little effect on temperatures internal to the fuel subassembly. Experiments were performed with 19-rod bundles in the FFM having identical configuration and heat flux as the FFTF with solid blockages of 13 and 24 channels at the inlet of the rod bundle with 3 in. of unheated zone between the blockage and the start of the heated zones. The effects of 13-channel

blockages were barely discernible. The internal temperatures were elevated as a consequence of 24-channel blockages, but they did not exceed the exit temperature for a normal unblocked subassembly. The effect on the 24-channel blockage results of the nearness of the channel walls in the 19-pin experimental assembly and the manner in which it relates to the full-size FFTF 217-pin subassembly are not known. On the other hand, the FFTF has a 6-in. unheated inlet zone, and the longer length would allow more mixing and reestablishment of flow before entering the heated zone. From this standpoint the experimental results are conservative.

If an inlet blockage can be caused by a gradual buildup of many small pieces, it may be possible, but unlikely, to generate a solid blockage of continually greater size. Therefore, the critical size of the blockage (where the blockage is either intolerable or detectable) will be determined in future investigations.

2. It has been experimentally established that an internal blockage of six subchannels of non-heat-generating material (stainless steel) 0.25 in. long is tolerable but is not detectable with present FFTF subchannel instrumentation. However, the exit temperature distribution is distorted sufficiently that detection might be possible in future reactors with exit multiple thermocouple correlation techniques. Heat transfer in the recirculation zone downstream of the blockage is adequate for this case.

3. Calculations indicate that a long (>0.5 in.) heat-generating blockage of a single subchannel is tolerable, but a blockage of two adjacent channels is not. Also, a ring blockage of stainless steel 0.25 in. thick and of infinite radius (no radial heat loss) is barely tolerable. A ring blockage of heat-generating material of 0.20 in. radius must be less than 0.125 in. long to be acceptable.

4. Analysis of simple representations of flow in a recirculation zone indicates that the internal fluid temperatures will depend strongly on blockage size.

5. Experiments with the FFM water mockup simulator with 19-rod bundles indicate that strong recirculation exists behind 6- and 24-channel internal blockages centered about the central rod and behind edge-channel blockage comprising one-third of the total flow area of the bundle. Heat transfer coefficients dropped to a third of the free stream value for the (most severe) edge-channel case. It is expected that the analogous assembly for the 19-rod FFM sodium experiment (which will be performed in FY 1974) will not experience excessive temperatures as a consequence of this type of edge blockage.

In the near future, the FFM program will be directed toward determining maximum permissible blockage size (of various shapes and leakages) coupled with the development of detectability techniques. The eventual desired result is that plant safety philosophy be freed from consideration of "credibility" and be based on detection prior to the attainment of some known damage limit. Experimental confirmation of maximum allowable internal blockage size is not yet available. However, present experimental results for all blockages tested indicate that blockages of these sizes will not create excessive temperatures in the bundle assembly.

REFERENCES

1. J. L. Wantland, *ORRIBLE – a Computer Program for Flow and Temperature Distribution in LMFBR Fuel Rod Bundles,* ORNL-TM-3516 (October 1971).
2. W. D. Turner and J. S. Crowell, *Notes on HEATING – an IBM-360 Heat Conduction Program,* CTC-INF-980, Computing Technology Center (Nov. 21, 1969).
3. W. D. Turner and M. Siman-Tov, *HEATING 3 – an IBM 360 Heat Conduction Program,* ORNL-TM-3208 (February 1971).
4. E. H. Novendstern, WARD, personal communication to M. H. Fontana, ORNL, February 1971.

5. M. Grolmes, referenced in J. Van Erp et al., "Protection against Local Core Accidents in Liquid Metal Fast Breeder Reactors," *Nucl. Eng. Des.* **15**, 441–47 (1971).
6. P. D. Richardson, "Heat and Mass Transfer in Turbulent Separated Flows," *Chem. Eng. Sci.* **18**, 149–55 (1963).
7. T. Carmody, "Establishment of the Wake behind a Disk," *Trans. ASME, J. Basic Eng.*, 869–82 (December 1964).
8. R. A. Seban, "Heat Transfer to the Turbulent Separated Flow of Air Downstream of a Step in the Surface of a Plate," *Trans. ASME, J. Heat Transfer*, 259–64 (May 1964).
9. D. E. Abbott and S. J. Kline, "Experimental Investigation of Subsonic Turbulent Flow over Single and Double Backward Facing Steps," *Trans. ASME, J. Basic Eng.*, 317–25 (September 1962).
10. R. J. Goldstein et al., "Laminar Separation, Reattachment, and Transition of the Flow over a Downstream Facing Step," *Trans. ASME, J. Basic Eng.*, 732–41 (December 1970).
11. M. Aire and H. Rouse, "Experiments on Two-Dimensional Flow over a Normal Wall," *J. Fluid Mech.* **1**, 129–41 (1956).
12. M. C. Good and P. N. Joubert, "The Form Drags of Two-Dimensional Bluff Plates Immersed in Turbulent Boundary Layers," *J. Fluid Mech.* **31** (Pt. 3), 547–82 (1968).
13. J. W. Mitchell, "Base Heat Transfer in Two-Dimensional Subsonic Fully Separated Flows," *Trans. ASME, J. Heat Transfer*, 342–48 (November 1971).
14. T. L. Shaw, "Effect of Side Walls on Flow past Bluff Bodies," *J. Hydraulics Div., Proc. ASCE*, 65–79 (January 1971).
15. P. K. Chang, *Separation of Flow*, Pergamon, Oxford, 1970.
16. J. Zoubek and J. Graham, "Local Blockage Effects on LMFBR Cladding," *Trans. ANS* **14**(2), 747 (October 1971).
17. A. A. Bishop, J. Graham, and J. Zoubek, "Hydrodynamic Characteristics of a Wake behind a Fuel Assembly Local Flow Blockage," *Trans. ANS* **14**(2), 748 (October 1971).
18. J. B. Van Erp and T. C. Chawla, "Experimental Study of Coolant Crossflow and Subchannel Flow Blockage on a Simulated LMFBR Sub-Assembly," *Trans. ANS* **14**(2), 764 (October 1971).
19. W. Gambill, *ORNL Nuclear Safety Research and Development Program Bimonthly Reports*, Wm. B. Cottrell, ed. (e.g., January–February 1972, ORNL-TM-3738).
20. D. Kirsch and K. Schleisiek, "Flow and Temperature Distributions around Local Coolant Blockages in Sodium-Cooled Fuel Elements," 1971 International Heat Transfer Seminar, Trogir, Yugoslavia, Sept. 6–11, 1971.
21. K. Gast, "Local Boiling in Rod Bundles," 1971 International Heat Transfer Seminar, Trogir, Yugoslavia, Sept. 6–11, 1971.
22. V. Steifel, *Comparison of Measured and Calculated Mass Flow Distribution in Partially Blocked Flow Channels,"* TM-IN-481, Eidgenoess. Inst. fuer Reactorforschung (Sept. 13, 1971).
23. H. J. Teague, "Cooling Failure in a Subassembly," chap. 2 in F. R. Farmer, *An Appreciation of Fast Reactor Safety*, AHSB(S) R188 (1970).
24. P. Basmer, D. Kirsch, and G. F. Schultheiss, *Phenomenological Investigations into Flow Distribution behind Local Coolant Channel Blockages in Rod Bundles*, KFK-1548, Karlsruhe Nuclear Research Center (January 1972).
25. M. H. Fontana and R. E. MacPherson, *Work Plan for LMFBR Fuel Failure Mockup Program*, ORNL-TM-3902 (April 1973).
26. A. G. Grindell and R. E. MacPherson (Comps.), *Final System Design Description of the Failed Fuel Mockup (FFM) of the Liquid-Metal Fast Breeder Reactor*, ORNL-TM-3656 (September 1972).
27. M. H. Fontana et al., *Temperature Distribution in the Duct Wall and at the Exit of a 19-Rod Simulated LMFBR Fuel Assembly (FFM Bundle 2A)*, ORNL-4852 (April 1973).
28. M. H. Fontana et al., *Temperature Distribution in a 19-Rod Simulated LMFBR Fuel Assembly in a Hexagonal Duct (Fuel Failure Mockup Bundle 2A) – Record of Experimental Data*, ORNL-TM-4113 (September 1973).
29. M. H. Fontana, *LMFBR Safety and Core Systems Programs Progress Report for January–February 1973*, ORNL-TM-4148 (June 1973).

30. R. M. Roidt and Y. S. Tang, "Air Flow Measurements on a Simulated LMFBR Seven-Rod Bundle, Part II, Measurement of Velocities Downstream of Blocked Subchannels," Westinghouse Scientific Paper 72-7E9-MIXIN-P1, Jan. 17, 1972.
31. O. E. Dwyer, *Nucl. Eng. Des.* **10**, 3–20 (1969).
32. W. M. Kays, *Convective Heat Transfer,* p. 184, McGraw-Hill, New York, 1966.

Appendix

DERIVATION OF HEAT BALANCE EQUATIONS FOR THE IDEALIZED RECIRCULATING FLOW MODEL

In two-dimensional geometry, heat balances may be made by allowing finite nodes to exchange heat with four neighboring adjacent nodes as shown below.

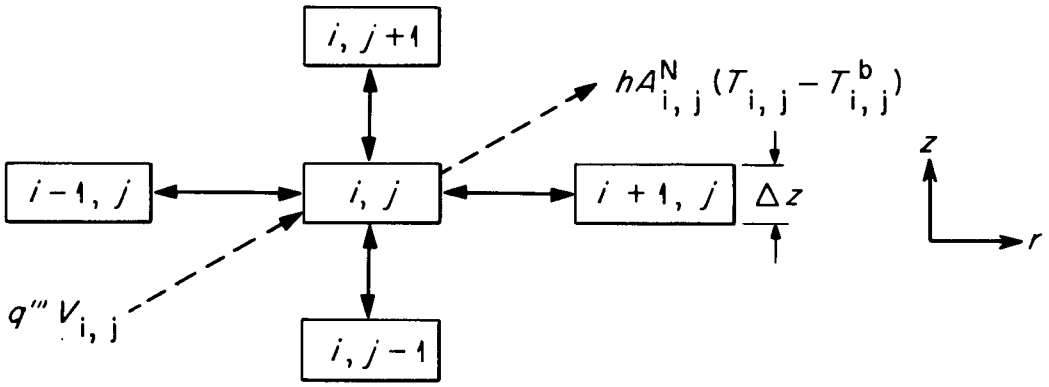

Three mechanisms are assumed for the transfer of heat between nodes:

1. Molecular conduction,

$$_{i-1,j}q^{k}_{i,j} = [2\pi k\ \Delta z/\ln\ (r_{i,j}/r_{i-1,j})]\,(T_{i-1,j} - T_{i,j})$$
$$\equiv K^{r}_{i-1,j}(T_{i-1,j} - T_{i,j})\ .$$

2. Mass convection,

$$_{i-1,j}q^{c}_{i,j} \equiv {}_{i-1,j}\,\omega_{i,j}\,C_p\,T_{i-1,j}\ .$$

3. Turbulent mass exchange

$$_{i,j+1}\,q^{t}_{i,j} = {}_{i,j+1}\,\omega^{t}_{i,j}\,C_p(T_{i,j+1} - T_{i,j})\ ,$$

where

$$_{i,j+1}\,\omega^{t}_{i,j} \equiv C_T(\omega_{i,j+1} + \omega_i)\ ,$$

and C_T is defined as a turbulent transfer coefficient. Heat is added to each internal node i, j by internal generation at a rate of $q'''V_{i,j}$. If a node is one of the outer boundary nodes, heat is transferred to a main stream flow at a rate of

$$q^{h}_{i,j} \equiv hA^{N}_{i,j}(T_{i,j} - T^{b}_{i,j})\ .$$

Making a heat balance for node i, j, expanding, and dividing by $\rho V_{i,j} C_p$ gives

$$\frac{dT_{i,j}}{d\theta} = -T_{i,j}\left(\sum_1^4 \omega_{i,j}^o + \sum_1^2 K^r + \sum_1^2 K^z + hA_{i,j}^N/C_p + \sum_1^4 \omega_{i,j}^T\right)\Big/\rho V_{i,j}$$

$$+ T_{i,j+1}({}_{i,j+1}\omega_{i,j} + K_{i,j+1}^z + {}_{i,j+1}\omega_{i,j}^t)/\rho V_{i,j}$$

$$+ T_{i,j-1}({}_{i,j-1}\omega_{i,j} + K_{i,j-1}^z + {}_{i,j-1}\omega_{i,j}^t)/\rho V_{i,j}$$

$$+ T_{i-1,j}({}_{i-1,j}\omega_{i,j} + K_{i-1,j}^z + {}_{i-1,j}\omega_{i,j}^t)/\rho V_{i,j}$$

$$+ T_{i+1,j}({}_{i+1,j}\omega_{i,j} + K_{i+1,j}^r + {}_{i+1,j}\omega_{i,j}^t)/\rho V_{i,j}$$

$$+ q'''/\rho C_p + hA_{i,j}^N T_{i,j}^b/\rho V_{i,j} C_p \qquad \text{(A.1)}$$

An equation similar to Eq. (A.1) can be written for each node within the cell. Appropriate terms are set equal to zero to account for adiabatic surfaces, no flow exchange between nodes, or if a node is not a cooled boundary.

Nomenclature

$A_{i,j}^N$	Normal surface area of a boundary node exposed to external cooling
C_p	Specific heat
h	Boundary heat transfer film coefficient
k	Thermal conductivity
K^r	Conductance coefficient in radial geometry
K^z	Conductance coefficient in axial direction
r	Radial coordinate
$T_{i,j}$	Temperature of node i, j
$T_{i,j}^b$	Boundary temperature to which boundary node i, j is exposed
q'''	Volumetric internal heat-generation rate
$V_{i,j}$	Volume of node i, j
z	Axial coordinate
ρ	Density
${}_{i-1,j}\omega_{i,j}$	Mass convected from node $i-1, j$ into node i, j
$\omega_{i,j}^o$	Net outflow of mass from node i, j
${}_{i-1,j}\omega_{i,j}^t$	Turbulent mass exchange between node $i-1, j$ and node i, j
θ	Time coordinate

ORNL-TM-4324
UC-79p, -79e

INTERNAL DISTRIBUTION

1. N. J. Ackerman
2. S. E. Beall
3. M. Bender
4. R. H. Bryan
5. D. L. Clark
6. Wm. B. Cottrell
7. F. L. Culler, Jr.
8–17. M. H. Fontana
18. D. N. Fry
19. P. A. Gnadt
20. A. G. Grindell
21. W. O. Harms
22. T. S. Kress
23. R. Kryter
24. R. N. Lyon
25. R. E. MacPherson
26. H. C. McCurdy
27. L. C. Oakes
28. R. B. Parker
29. L. F. Parsly
30. P. Patriarca
31. M. W. Rosenthal
32. T. H. Row
33. R. Saxe
34. Myrtleen Sheldon
35. I. Spiewak
36. D. G. Thomas
37. D. B. Trauger
38. J. L. Wantland
39. A. M. Weinberg
40–41. Central Research Library
42. ORNL – Y-12 Technical Library
Document Reference Section
43–48. Laboratory Records Department
49. Laboratory Records, ORNL R. C.

EXTERNAL DISTRIBUTION

50–51. Director, USAEC, Division of Reactor Research and Development, Washington, D.C. 20545
52. USAEC-RDT Senior Site Representative, Oak Ridge National Laboratory, P. O. Box X, Oak Ridge, Tennessee 37830
53. Research and Technical Support Division, USAEC, Oak Ridge Operations Office, P. O. Box E, Oak Ridge, Tennessee 37830
54–310. For distribution as shown in TID-4500 under category UC-79p and UC-79e, Liquid Metal Fast Breeder Reactors (Safety and Reactor Core Systems)